Università degli studi di Parma

Facoltà di Scienze MM.FF.NN.

Corso di Laurea Specialistica in

Scienza e Tecnologia dei Materiali Innovativi

Interazione tra antibiotici macrolidi e membrane modello

Interaction between macrolide antibiotics and model membranes

Relatore

Prof. Luigi CRISTOFOLINI

Candidato

Agostino ROMEO

Correlatore

Prof. Pietro CICUTA

Anno Accademico 2009/2010

Contents

List of Figures

List of Tables

Riassunto

In questo lavoro si è studiata l'interazione di antibiotici macrolidi con dei modelli di membrana fosfolipidica. Lo studio dell'interazione di farmaci con membrane biologiche permette di ottenere informazioni sui meccanismi di azione dei farmaci, nonchè sui loro effetti sull'organizzazione molecolare, fluidità e permeabilità delle membrane. La modificazione delle proprietà meccaniche delle membrane per effetto dei farmaci può influenzare processi biologici connessi, ad esempio, all'endocitosi, di estrema rilevanza in tutti gli organsmi viventi.

Gli antibiotici studiati sono Aivlosin, Azitromicina e Claritromicina. I fosfolipidi utilizzati sono 1,2-dioleoyl-sn-glycero-3-phosphocholine (DOPC) e 1,2-dipalmitoyl-sn-glycero-3-phosphocholine (DPPC).

Si è investigato l'effetto del farmaco sulla stabilità di alcune forme di ag-

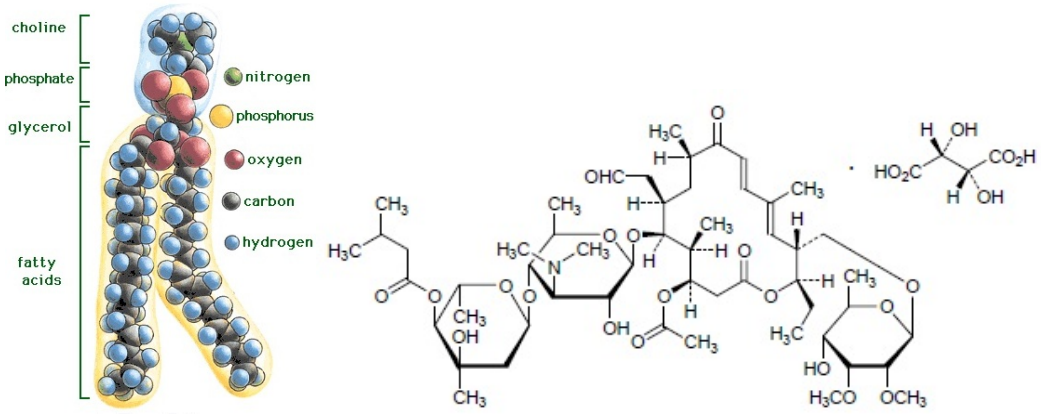

Figure 1: *Pannello sinistro: struttura generale di un fosfolipide [12]. Pannello destro: molecola del farmaco Aivlosin [57].*

gregazione dei fosfolipidi (vescicole unilamellari giganti, GUV e monostrati di Langmuir) nonchè gli effetti di tali farmaci sulle proprietà meccaniche quali il modulo di compressibilità, di bending, di shear.
Le principali tecniche utilizzate sono la microscopia in fluorescenza e a contrasto di fase e la reometria di scorrimento interfacciale su monostrato di Langmuir.

Distribuzioni di taglia di GUV

GUV di DOPC, con diametri compresi tra i pochi μm e le decine di μm, sono state preparate mediante il metodo di elettroformazione.
Le immagini, ottenute mediante microscopia in fluorescenza (figura 2), sono state analizzate per ricavare informazioni sulle distribuzioni di taglia delle vescicole in assenza ed in presenza del farmaco.

Nell'analisi delle distribuzioni di taglia delle vescicole due concentrazioni (50 μM e 150 μM) sono state studiate per ogni farmaco. Le GUV sono state incubate in soluzione contenente ciascun farmaco con tempi di incubazione variabili da qualche ora ad un massimo di 50 ore. Le distribuzioni di taglia sono state descritte con un andamento esponenziale, i cui parametri caratter-

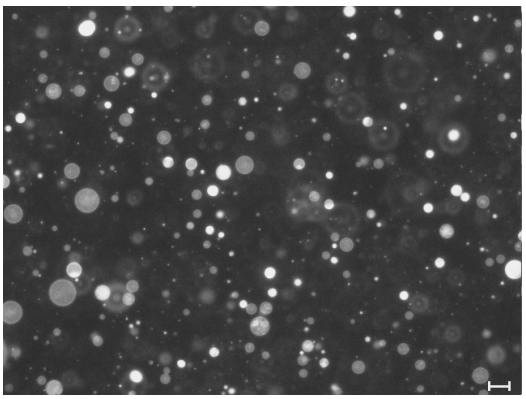

Figure 2: *L'immagine, registrata mediante microscopia in fluorescenza, mostra le GUV. Barra: 20 μm.*

	R_0 (μm)
Control	7.8 $\pm$0.4
Aivlosin 50 μM	7.9 $\pm$0.6
Aivlosin 150 μM	8.0 $\pm$0.4
Azitromicina 50 μM	6.1 $\pm$0.3
Azitromicina 150 μM	6.2 $\pm$0.5
Claritromicina 50 μM	6.3 $\pm$0.2
Claritromicina 150 μM	5.0 $\pm$0.4

Table 1: *Raggi medi ottenuti fittando le distribuzioni di taglia delle GUV con una funzione esponenziale.*

istici (il raggio medio caratteristico di ciascuna distribuzione) sono mostrati in tabella 1. Alle concentrazioni studiate, il farmaco Aivlosin ha mostrato di non modificare apprezzabilmente la distribuzione di taglia delle GUV. Al contrario, sia Azitromicina che Claritromicina hanno influenzato tali distribuzioni, inducendo la riduzione del numero di GUV su tutto l'intervallo di dimensioni accessibile con la tecnica utilizzata (3 - 20 μm). L'effetto dell'Azitromicina è risultato saturare a 50 μM, mentre Claritromicina ad alta concentrazione ha indotto un ulteriore riduzione del numero di vescicole rilevate.
Effetti rilevanti sulle GUV sono stati riscontrati con Aivlosin a concentrazioni molto elevate (800 μM e 4 mM). In tali condizioni è stata osservata la formazione di cluster di materiale fosfolipidico (costituito sia da piccole vescicole sia, probabilmente, da multistrati fosfolipidici riarrangiati) intorno a vescicole di dimensioni normali. La variazione della permeabilità di membrana è stata occasionalmente riscontrata in alcune vescicole.

Flickering di GUV

Le fluttuazioni delle pareti fosfolipidiche (flickering) di DOPC-GUV sono state studiate per ottenere informazioni sulla flessibilità delle loro membrane

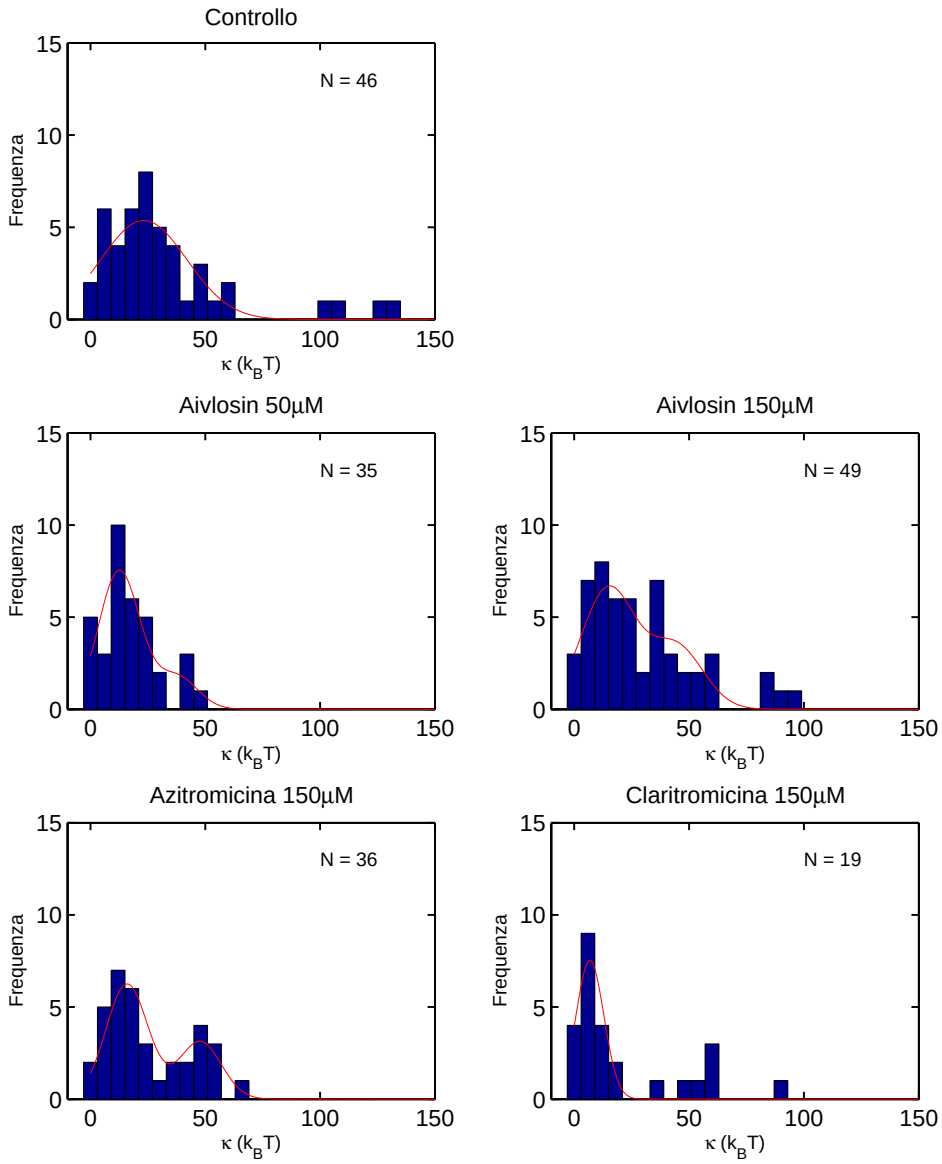

Figure 3: *Distribuzioni di modulo di bending di DOPC-GUV. In ordinata è presente il numero di vescicole che hanno esibito lo stesso modulo di bending. In rosso sono visibili i fit con cui sono stati ricavati i valori medi di κ per ogni campione. Nell'inserto viene indicato il numero totale di vescicole analizzate per ciascun campione.*

e su come questa può essere influenzata dall'interazione con i farmaci. Da questo studio è stato ricavato il modulo di bending per le GUV non trattate

con farmaci (23.2 k_bT), in ottimo accordo con la letteratura. Tutti gli antibiotici studiati hanno indotto un abbassamento di tale modulo. Aivlosin (50 μM e 150 μM) e Azitromicina (150 μM) hanno causato una abbassamento di κ di pari entità (40%), con saturazione dell'Aivlosin già a 50 μM. Claritromicina (150 μM) ha mostrato un effetto anche più marcato (70%).
Nelle distribuzioni di κ di alcuni campioni (Azitromicina e Aivlosin) si nota la presenza di picchi distinti centrati su valori multipli del κ fondamentale, associabili a vescicole multilamellari (figura 3).

Reologia di monostrati fosfolipidici

Film fosfolipidici di Langmuir sono stati preparati a partire da DPPC.
In primo luogo, isoterme Π-A sono state misurate sui monostrati in presenza e in assenza di Aivlosin e Claritromicina (figura 4). Esse hanno mostrato che le fasi caratteristiche di un monostrato fosfolipidico (gas, liquido-espanso, liquido-compresso, solido) permangono anche dopo l'effetto dei farmaci. Aivlosin ha indotto un abbassamento della pressione di collasso, mentre Claritromicina ha mostrato un aumento dell'area limite della fase liquido-compatta. Il modulo di compressibilità calcolato dalle isoterme ha mostrato un ridotto effetto di Claritromicina; al contrario, Aivlosin ha indotto un incremento del modulo di compressibilità (figura 4, inserto).
Il monostrato di DPPC ha mostrato un comportamento visco-elastico, ben descritto dal modello di Maxwell (sull'intero range di frequenze analizzato). E' stato ipotizzato di poter generalizzare il principio di sovrapposizione tempo-temperatura al caso tempo-pressione superficiale (sulla base di considerazioni simili a quelle su cui si basa la teoria del volume escluso per la transizione vetrosa). Tale ipotesi consiste nel traslare lungo l'asse delle frequenze in plot log-log dati ottenuti a differenti temperature, sovrapponendoli a quelli relativi ad una temperatura di riferimento: fattori di traslazione dipendenti dalla temperatura vengono applicati a tutti i dati. Il risultato di questa procedura

viene definito master curve. Questo metodo è stato applicato allo studio del modulo di scorrimento viscoso G^* dei monostrati: questo ha permesso di avere accesso ad un intervallo di frequenze più ampio di quello altrimenti accessibile e di generare le master curves.
Le master curves, nel limite di basse frequenze, sono descritte dal modello Newtoniano, cioè da una modulo di scorrimento viscoso G" proporzionale alla frequenza ovvero da una viscosità bidimensionale η_{2D} indipendente dalla frequenza.

L'analisi di G^* ha mostrato effetti rilevanti da parte di Aivlosin e Claritromicina. In tabella 2 sono riportati i valori di η_{2D}. In particolare, Aivlosin è risultato l'antibiotico con il maggiore effetto sul monostrato, inducendo un grande aumento della sua viscosità. Claritromicina ha mostrato un effetto analogo, seppure meno marcato. Azitromicina, al contrario, non ha mostrato effetti misurabili sulla viscosità del monostrato.
Tempi di rilassamento caratteristici τ e moduli istantanei G_0 sono stati calcolati dal modello di Maxwell applicato alle master curves (tabella 3). I risultati ottenuti hanno permesso di supporre la probabile formazione di complessi farmaco-fosfolipide. τ molto maggiori del controllo sono stati calcolati per il film esposto ad Aivlosin, il che potrebbe essere connesso alla formazione di complessi con dimensioni maggiori rispetto al singolo fosfolipide.

	Controllo (μNs/m)	Aivlosin (μNs/m)	Azitromicina (μNs/m)	Claritromicina (μNs/m)
15 mN/m		149.1 ±10		
20 mN/m		427.0 ±15		
25 mN/m	44.3 ±4	577.8 ±11		45.0 ±4
30 mN/m	81.6 ±7	1141.0 ±7	58.7 ±6	161.0 ±7
35 mN/m	148.5 ±6		116.7 ±6	441.6 ±7
40 mN/m	290.9 ±7		223.3 ±7	1409.9 ±15
45 mN/m	572.1 ±9		445.4 ±9	-
50 mN/m			791.5 ±11	

Table 2: *Viscosità dinamiche dei monostrati di DPPC calcolate mediante il modello di Newton.*

	Controllo	Aivlosin	Azitromicina	Claritromicina
G_0 (mN/m)	5.17	4.42	5.02	13.4
τ (s)	0.014	0.409	0.0097	0.0095

Table 3: *Parametri G_0 and τ calcolati dal modello di Maxwell applicato alle master curves.*

I campioni trattati con farmaci hanno mostrato discrepanze più o meno marcate dal modello di Maxwell (figura 5). Questo potrebbe essere un effetto della formazione dei complessi farmaco-fosfolipide, i quali ridurrebbero l'omogeneità del monostrato rendendo il modello di Maxwell ad un solo tempo caratteristico e un modulo istantaneo non adatto a descrivere tali sistemi. Un modello più generale, che tenga conto di una distribuzione di tempi caratteristici e moduli istantanei, potrebbe permettere una migliore descrizione dei sistemi qui studiati.
L'aumento di area limite nell'isoterma con Claritromicina sembrerebbe avvalorare l'ipotesi della formazione di complessi farmaco-fosfolipide. L'assenza di variazione di area limite nel caso dell'Aivlosin, potrebbe essere dovuta a due effetti contrastanti: oltre all'intercalazione dei complessi nel monostrato

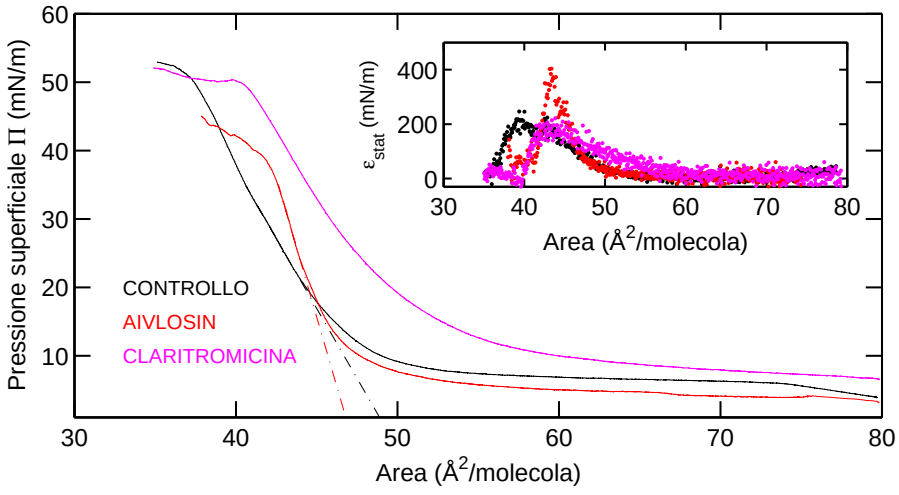

Figure 4: *Isoterme Π-A di monostrato di DPPC in assenza e in presenza di antibiotici. Nell'inserto sono riportati i corrispondenti moduli di compressibilità statici ϵ.*

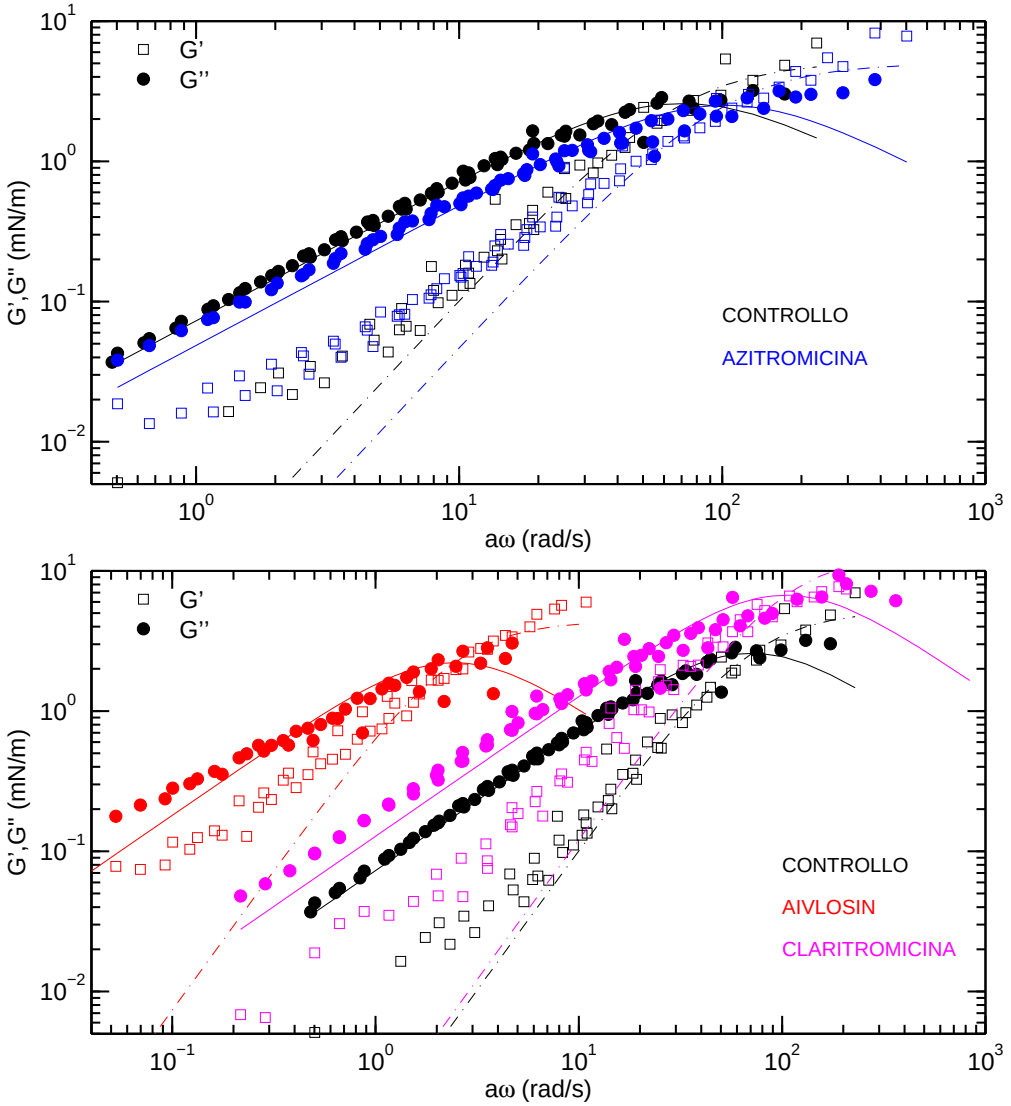

Figure 5: *Master curves di DPPC puro e monostrato esposto ad Azitromicina (pannello alto); master curves di DPPC puro e monostrato esposti a Claritromicina e Azitromicina.*

potrebbe avvenire anche una parziale solubilizzazione di tali complessi nella subfase acquosa. Questo indurrebbe un sequestro parziale dei fosfolipidi dal monostrato, riducendo l'area limite disponibile nel monostrato.

In questo lavoro è stato mostrato che antibiotici macrolidi possono interagire in maniera importante con membrane fosfolipidiche, modificandone numerose proprietà meccaniche (modulo di bending, di compressibilità e di shear). E'

stato ipotizzato che, tra gli antibiotici studiati, Aivlosin sia quello con il maggiore carattere idrofobico.
Ad oggi, la reometria superficiale è una tecnica utilizzata poco comunemente per lo studio di sistemi fosfolipidici modello. Il suo utilizzo in questo lavoro assume, quindi, una particolare rilevanza dal punto di vista dell'innovazione e del progresso nello studio di sistemi fosfolipidici.

Introduction

Artificial phospholipid systems, such as Langmuir monolayers spread on acqueous surfaces, nanometer- or micrometer-sized vesicles and supported bilayers, provide a model system representing particular aspects of essential similarity to the cellular plasma membrane bilayer. These model systems are widely used to investigate the properties of biological membranes and associated processes such as molecular recognition, enzymatic catalysis, cell adhesion and membrane fusion [1][2][3]. In the case of micrometer-sized vesicles, the properties of the membrane and its constituents are directly related to the vesicle shape and size, which can be easily observed by optical microscopy.
Model membranes have also been extensively used in pharmaceutical research on drug-delivery systems and provide assays for studying drug-membrane, lipid-lipid, lipid-protein interactions [4]. Experimental work on artificial membranes has also demonstrated that the membrane properties may be affected strongly by the presence of membrane associated molecules. Examples of membrane properties that can be affected by drug-membrane interactions include the conformation of acyl groups, the membrane surface and thickness, the phase transition temperature, the membrane potential, hydration of head groups and the membrane fusion properties [5].

The main goal of this work is to investigate the effect of macrolide antibiotics on model lipid membranes (tens-of-micron sized vesicles), with particular regard to their size distributions, mechanical properties and thermotropic

behaviour.
In this work three different macrolide antibiotics are studied. Physico-chemical properties of one, Azithromycin, have already been studied and many works are available in literature. It was used here to compare our results with literature. The others two, Avilosin and Clarithromycin, have not been object of research studies on artificial membranes, and represent interesting substances for investigation.
The first part of the present work was carried out in the Biological and Soft Systems (BSS) group at the Cavendish Laboratory, Cambridge, UK, under the supervision of Dr. Pietro Cicuta, and deals with the mechanical properties of vesicle membranes, and in particular with their bending properties. It consists of an analysis of vesicle membrane fluctuations, performed using a refined contour analysis method and exploiting many results reached in previous works ([6][7][8][9][10]). The effects of Aivlosin, Azythromycin and Clarithromycin on these mechanical properties were studied in comparison with control vesicles not exposed to the drugs.
Studies on size distributions, thermotropic behavior and microfluidics of model membranes were also carried out at Cavendish Laboratory.
The final part of this work was carried out at the Physics Department, University of Parma, under the supervision of Prof. Luigi Cristofolini, and deals with rheologic studies on Langmuir phospholipid monolayers, performed to analyse the effect of macrolide antibiotics on the shear properties of such model membranes.

This thesis is divided into the following chapters.
In Chapter 1 some general aspects about phospholipid membranes are treated, like their structure, thermotropic phases, and model membrane typologies. Results of previous works about the interaction of phospholipid membranes with drugs are presented, as well as a theoretical background on shape fluctuations of vesicles and rheology of phospholipid films.
In Chapter 2 reagents and experimental procedures are presented. A descrip-

tion of the protocol to prepare giant unilamellar vesicles and the experimental procedures (optical microscopy, differential scanning calorimentry, microfluidics, and interfacial stress rheology) used in this work are given. Then the algorithms used to detect the vesicle sizes and contours, and to analyse the ISR data are described.

In Chapter 3 results of analysis are outlined. Size distributions and flickering analysis results are presented in detail, followed from sections with results about calorimetric and microfluidic channels experiments. Finally, rheology of monolayers is also described.

In Chapter 4 experimental results are discussed. A possible mechanism of interaction of the antibiotics with phospholipid model membranes is also proposed.

In Chapter 5 the results obtained here are briefly summarized.

Chapter 1

Physical properties and pharmacology of lipid membranes

1.1 Phospholipids

Phospholipids are a class of lipids and are the main component of all cell membranes, as they can form lipid bilayers.
Most of the phospholipids studied to date consist of two hydrophobic hydrocarbon chains, a glycerol backbone and a hydrophilic headgroup. So a phospholipid molecule can be schematically thought as made of a hydrophilic headgroup and a hydrophobic tail: the result is an amphiphilic molecule [11] (see figure 1.1).

The polar head group contains one or more negatively charged phosphate groups, and may contain other polar groups.
The hydrophobic tail is made up of two fatty acyl chains, usually containing an even number of carbon atoms in biomembranes [11]. The carbon atoms may be saturated (neighboring C atoms are all connected by single bonds) or unsaturated (some neighboring C atoms are connected by double bonds).
Phospholipids are surfactants, compounds that lower the surface tension of a liquid or the interfacial tension between two liquids, or a liquid and a solid because of their amphiphilic nature.

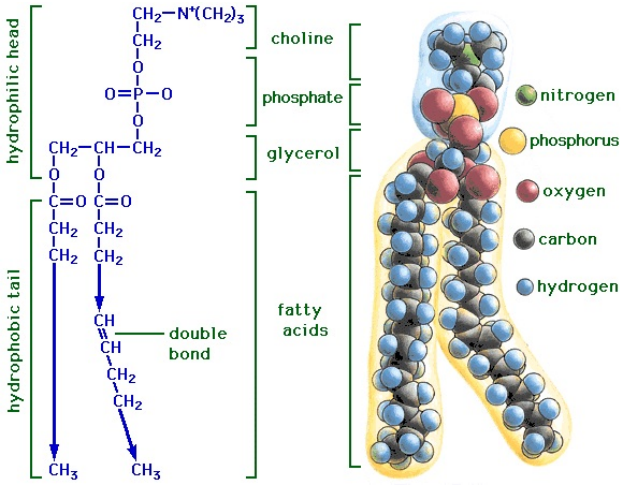

Figure 1.1: *Structure and main characteristics of a typical phospholipid [12].*

Examples of naturally occuring phospholipids include phosphatidylcholine, phosphatidylserine, phosphatidyl- ethanolamine and phosphatidylinositol.
In the present work three different phospholipids are used: 1,2-dioleoyl-sn-glycero-3-phosphocholine (DOPC, a double-unsaturated phospholipid), 1,2-dipalmitoyl-sn-glycero-3-phosphocholine (DPPC, a saturated phospholipid) and 1-palmitoyl-2-oleoyl-sn-glycero-3-phosphoethanolamine (POPE, mono-unsaturated). See figure 1.2.
Some phopholipids are negatively charged (POPS, POPG), but all the phospholipids used in this work are neutral.

1.2 Polymorphic phases of phospholipids

1.2.1 Cell membranes

Amphiphilic lipids are major constituents of cell membranes. These molecules form a fluid phospholipid bilayer with their hydrophilic (polar) heads facing

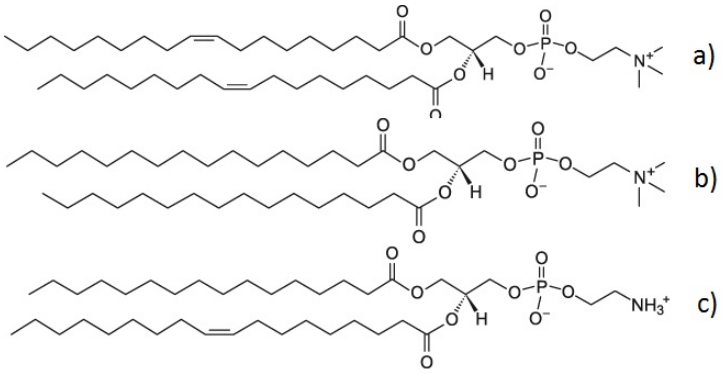

Figure 1.2: *Chemical structures of phospholipids used in this work [13]. a) DOPC, b) DPPC, c) POPE.*

their aqueous surroundings (e.g., the cytosol) and their hydrophobic tails facing each other. Phospholipid molecules can move about in their own leaflet (Fluid Mosaic Model), while migration to the other side of the bilayer, flip-flop process [14], is extremely slow for phospholipids (half-time of several hours [15]) due to a significant energy barrier.

The structural complexity of cell membranes is very high, as they contain a wide variety of biological molecules, primarily phospholipids (thousands of different species are contained in cell membranes) but also proteins, and carbohydrates embedded in and attached to the bilayer (see figure 1.3).

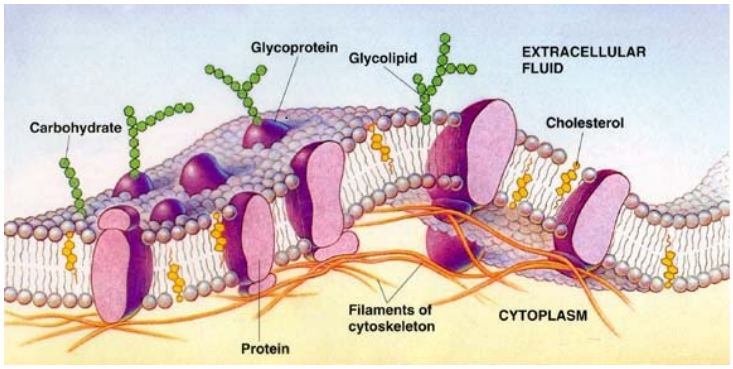

Figure 1.3: *Plasma membrane composition [16].*

1.2.2 Phospholipid aggregates

Phospholipids in polar solvents tend to aggregate forming self-assembled ordered structures [17] with typical lyotropic liquid crystalline symmetries [18]. At high lipid concentrations in water these are predominantly lamellar phases [19] (spherical or cylindrical micelles, or bilayers, figure 1.4).

Micelles

Spherical micelles are aggregates with the hydrophilic "head"' regions in contact with surrounding solvent, and the hydrophobic tail regions sequestered in the micelle centre. Inverse micelles also exist, in which the headgroups are at the centre with the tails extending out; more often these last aggregates show up as a cylindrical phase, called inverted-hexagonal phase H_{II}.
Mixtures of cone shaped (H_{II} phase preferring) phospholipids and inverted cone shaped (micellar) phospholipids can exhibit bilayer structure (see figure 1.5), a structure which is not adopted by either lipid species in isolation [17]. More complex phases also exist (bi-continuous, etc.).

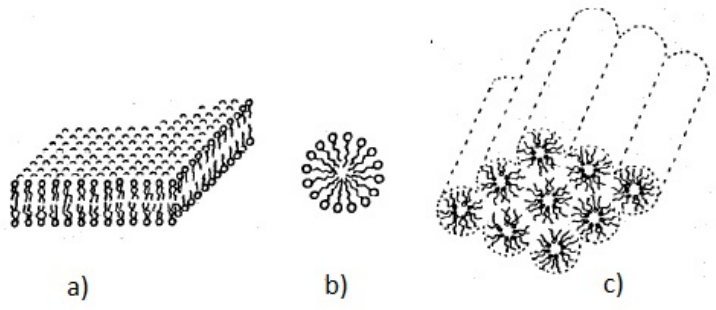

Figure 1.4: *Polymorphic phases available to phospholipids [17]. a) Bilayer, b) Micelle, c) Hexagonal phase. The acqueous pores of the hexagonal phase H_{II} have a diameter which lies in the range of 2 nm or lager.*

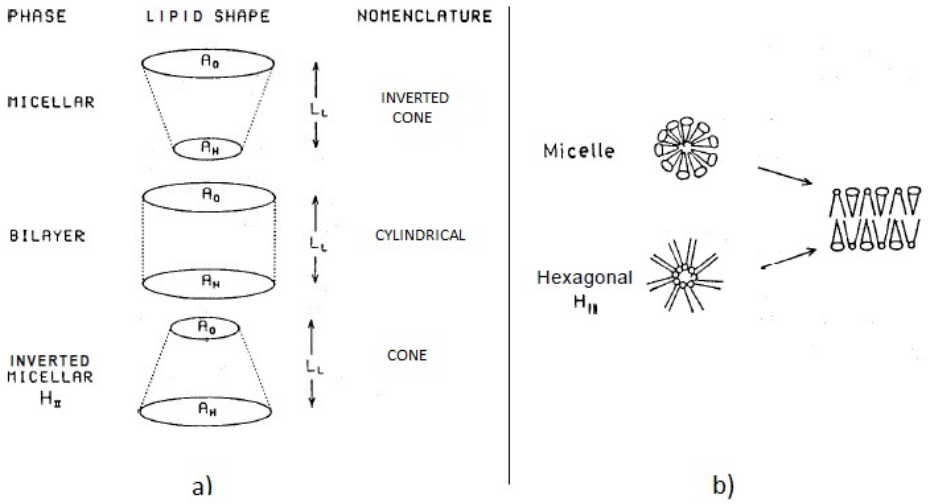

Figure 1.5: *Panel a): shape features exhibited by membrane phospholipids.* A_0 *refers to the area subtended by the polar region, whereas* A_H *refers to the area at the hydrophobic interface. Panel b): complementary effect arising from the shape properties of phospholipids. [17] This is a particular way by which phospholipids form bilayers; they tipically form bilayers because of the hydrophobic effect.*

Bilayers

In general, phospholipids self-assemble into bilayer structure because of the hydrophobic effect, which creates an energetically unfavorable interaction between the hydrophobic lipid tails and the surrounding water. Thus, a lipid bilayer is typically held together by entirely non-covalent forces that do not involve formation of chemical bonds between individual molecules.
In a phospholipid bilayer, the values of surface area per phospholipid molecule usually fall within the range of 65 to 70 Å^2 [20]. The surface area remains almost constant as the lengths of the acyl chains vary; this suggests that the interactions of the phospholipid head groups at the bilayer surfaces predominate in determining the equilibrium configuration of the bilayer [20].

The lipid bilayer is very thin compared to its lateral dimensions. The hydrophilic headgroup is completely hydrated and is typically around 8-9 Å thick. Next, there is an intermediate region which is only partially hydrated. This boundary layer is approximately 3 Å thick. The hydrophobic core of the

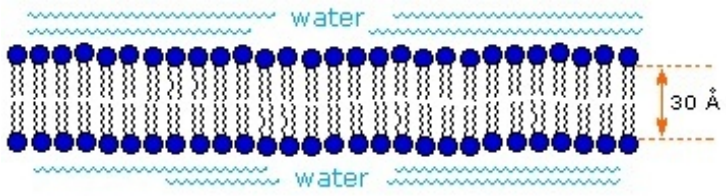

Figure 1.6: *Tipical thickness of hydrophobic bilayer core [23].*

bilayer is typically 3-4 nm thick (see figure 1.6), but this value varies with chain length and chemistry: a linear relation seems to exist between acyl chain length and core thickness [20]. This thickness also varies significantly with temperature, particularly near a phase transition. In fact, many degrees of order can exist in a lipid bilayer, from liquid phases to different crystalline packings (see section 1.4).

1.3 Model membranes: vesicles and Langmuir-Blodgett films

1.3.1 Phospholipid vesicles

In excess water bilayers may close up to form vesicles (also called liposomes), consisting of an aqueous core enclosed in one or several phospholipid bilayers [21] [22](see figure 1.7), with size reaching hundreds of μm. Single closed bilayers, forming cell-size liposomes many microns in diameter (larger than about 5μm), are called Giant Unilamellar phospholipid Vesicles (GUVs). Many artificial vesicles exist, classified according to their size: Small Unilamellar Vesicles (SUVs) are typically 10 nm - 1 μm and anything between GUVs and SUVs are called Large Unilamellar Vesicles (LUV).
Vesicles can assume a variety of shapes, that have been described by means several theories: some examples are the theory called area-difference-elasticity

(ADE) model [99][46], the ΔA (Bilayer-Couple) model [98] and the spontaneous curvature (SC) model (used in this work and described in the section 1.6), defined by the energy functional 1.1. Under the experimental conditions used in the current work, the GUVs are generally quasi-spherical.

Several GUV preparation techniques have been developed, such as electroformation [24] (see section 2.2.1), the hydration method [27][28], chemically induced vesiculation from biological cells [29][30], membrane perturbation effect by the protein molecule [31], and emulsification using a microchannel [32]. Spontaneous swelling (swelling stacks of lipid bilayers in excess water [25][26]) is similar to electroformation but no AC field is used.

GUVs, with a diameter of 10 μm or more, have the size of biological cells and constitute useful model systems for studying real cell membranes. Their low membrane curvature better mimics flat domains of the plasma membranes than conventional small vesicles exhibiting a higher curvature.

They also present the advantage of being visible with an optical microscope. Thus, their shape and shape modifications can be easily followed, in contrast to SUVs and LUVs, which can only be observed by electron microscopy.

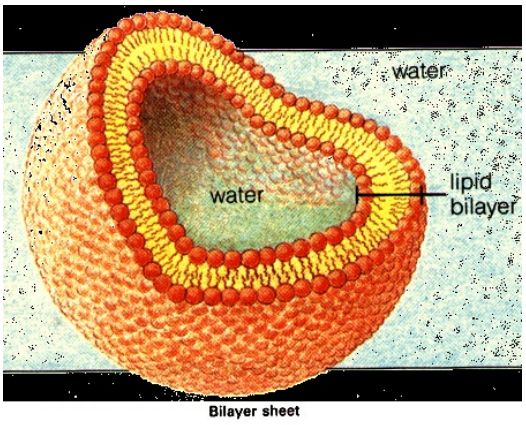

Figure 1.7: *Liposome cross-section [33].*

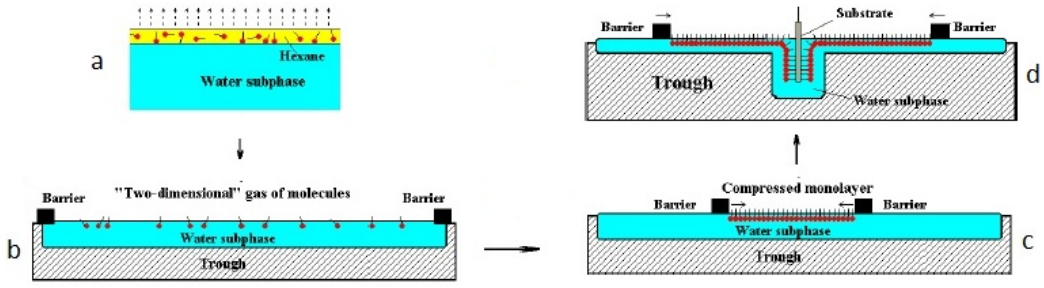

Figure 1.8: *a: amphiphilic substances, dissolved in a volatile and water-insoluble solvent, can be spread on water surface; b: the solution covers the available area and the solvent evaporation leaves a monolayer; c: the available surface area of the monolayer is reduced by a barrier system, leading to a 2D-solid; d: LB film deposition. [34]*

1.3.2 Langmuir and Langmuir-Blodgett films

Amphiphilic molecules can be deposited onto solid substrates as thin films of a thickness up to few nanometers (i.e., single layers of amphiphilic molecules). Techniques used for preparing these systems are Langmuir-Blodgett (LB) and Langmuir-Schaefer (LS) deposition.

Many amphiphilic substances insoluble in water can, dissolved in a volatile and water-insoluble solvent, easily be spread on a water surface to form an insoluble monolayer (Langmuir film) at the air/water interface (figure 1.8 a). The amphiphilic nature of the surfactants dictates the orientation of the molecules at the interface (air/water or oil/water) in such a way that the polar head group is immersed in the water and that the long hydrocarbon chain is pointing towards air. The solution spreads rapidly to cover the available area. As the solvent evaporates, a monolayer is formed (figure 1.8 b). To form a stable monolayer there should be more than 12 hydrocarbons or groups in the chain. If the chain is shorter the amphiphiles on the water surface tend to dissolve in the subphase.

If the available surface area of the monolayer is reduced by a barrier system, molecules start to exert a repulsive effect on each other (figure 1.8 c): the monolayer undergoes phase transitions, passing through several different phases. Such phase transitions can be monitored by measuring Π-A isotherms

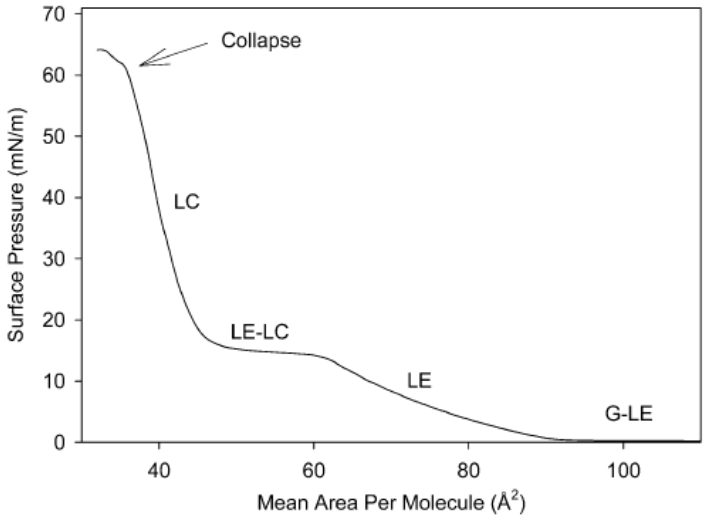

Figure 1.9: *Typical* Π-*A isotherm of a phospholipid. G: gas phase; LE: liquid-expanded phase; LC: liquid-condensed phase (LC here contains both solid and liquid-expanded phases described in text); G-LE: coexistence of G and LE phases; LE-LC: coexistence of LE and LC phases.*[35]

(figure 1.9). The area of the monolayer is varied by moving a barrier across the water surface. The surface tension is determined by suspending a plate of a material that is completely wetted by water, and measuring the downward force on it. The surface pressure Π is the difference between the surface tension of pure water and the surface tension of monolayer-covered water.
The very dilute monolayer is well described as a two-dimensional gas. With decreasing area per molecule (increasing surface pressure), the monolayer proceeds into the liquid expanded phase (denoted LE or L1). In this phase, as in the gas phase, the heads of the molecules are translationally disordered and the chains are conformationally disordered [36]. Further compression of the monolayer gives rise to a liquid condensed phase (LC). Upon further compression a "solid" state is reached. The monolayer possesses the same degree of translational order in both the last two regions of the isotherm: x-ray-diffraction studies showed that the hydrocarbon chains of the molecules are aligned parallel to each other in both sections of the isotherm; differences rise in the orientation of the chains, which are either tilted with respect to

the water surface or perpendicular to it [36]. The monolayer is relatively easily compressible in the tilted state, where decrease of the surface area can be accomodated by decreasing the tilt angle. In the untitled state, the distance between close-packed vertical molecules determines the areal density, and so such phases are much less compressible. The two "condensed" regions of the isotherms can also be distinguished by calling them tilted condensed and untitled condensed. Further compression induces the film to collapse, forming a three-dimensional structure (of poor experimental reproducibility). The pressure corresponding to the equilibrium between the solid and the collapsed monolayer is called collapse pressure.
The deposition of this film on a solid substrate can be carried out by successive dipping of a vertical substrate up and down through a compressed at the air-water interface; simultaneously the surface pressure is kept constant by a computer controlled feedback system (figure 1.8 d). In this way multilayer structures (LB films), of up to hundreds of layers thick, can be produced by repeated dipping.
On the other hand, the deposition of LS films can be achieved by repeatedly touching the surface of the compressed monolayer on the water subphase by an almost horizontal solid substrate.

1.4 Phase transitions in lipid bilayers

The phase behaviour of lipid bilayers is largely determined by the strength of the attractive Van der Waals interactions between adjacent lipid molecules. The interaction area is larger in longer tailed lipids: this increases the strength of this interaction, and consequently decreases the lipid mobility. Thus, at a given temperature, a short-tailed lipid will be more fluid than an otherwise identical long-tailed phospholipid [38].
Transition temperature can also be affected by the degree of unsaturation of

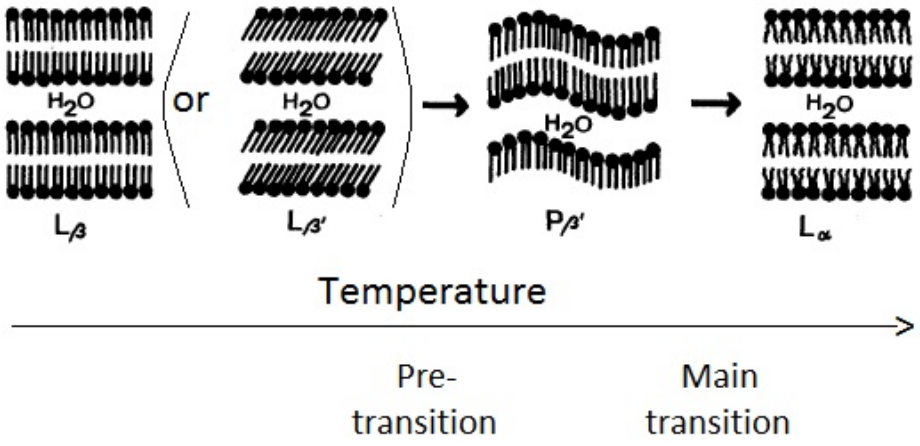

Figure 1.10: *Phase transitions in lipid bilayers [43].*

the lipid tails. An unsaturated double bond can produce a kink in the alkane chain creating extra free space within the bilayer which allows additional flexibility in the adjacent chains.
At a given temperature a lipid bilayer can exist in either liquid or gel (solid) phases. In both phases the lipid molecules are prevented from flip-flopping across the bilayer, but in liquid phase bilayers a given lipid will undergo a random walk, exchanging locations with its neighbor millions of times a second [39]. Unlike liquid phase bilayers, the phospholipids in a gel phase bilayer are locked in place.

A large number of intermediate, metastable, and transient lamellar gel structures can be adopted by different phospholipids [40]. Four lamellar phases have been recognized in saturated phosphatidylcholines: a liquid−crystalline phase, L_α, and phases with ordered hydrocarbon chain arrangements designated ripple phase, P_β [41], gel phase, L_β and $L_{\beta'}$, and 'subgel' or crystal phase, L_c (see figure 1.10, L_c not shown). Ripples are formed at intermediate temperatures between the gel phase L_β and the liquidcrystal phase L_α of saturated phosphatidylcholines. The low-temperature ordered phase L_c is a more highly ordered crystalline form than the gel phase.
A new low-temperature subgel phase with convex-concave deformations, des-

ignated P_{cc}, has been observed in some phosphatidylcholines [42].
Often, phase behaviour is dominated by the main $L_\beta - L_\alpha$ (gel-fluid, L_β stands for the generic gel phase) transition, associated with the melting of the lipid hydrocarbon chains. In DPPC, for example, the main transition occurs at 41°C, while the pre-transition $L_\beta - P_\beta$ occurs at 35°C [44]. In DOPC, instead, the main transition occurs at -18°C [45]. POPE shows the main transition at 25°C [13].
The liquid-crystal phase L_α is the biologically most relevant membrane phase as the living cell membranes are made of phospholipids in this phase.

1.5 Interactions of drugs with model membranes

Many drugs with different chemical structures and pharmacological effects are known to bind to membrane lipids and to alter physical properties. Typical examples include anesthetics [47][48], steroids [49], anti-psychotic drugs [50], as well as anti-cancer [51], anti-bacterial [52], anti-viral agents and antibiotics like aminoglycosides [53] or macrolides (Azithromycin) [54].
The biological activity and/or toxicity of many drugs is known to directly depend on their interaction with biological membranes [4].

1.5.1 Drugs: Aivlosin, Azithromicyn, Clarithromycin

In the present work macrolide antibiotics are studied. Macrolides are a group of drugs (included in antibacterial and antiviral agents) characterized by the presence of a macrolide ring, a large macrocyclic lactone ring (14-, 15-, or 16-membered) to which one or more deoxy sugars may be attached. Macrolide antibiotics prevent bacteria from growing. They work by blocking the protein synthesis of bacteria by interfering with their ribosomal subunits [55].

Three macrolide antibiotics are studied here: Aivlosin, Azithromycin and Clarithromycin. In the following they are briefly described.
Aivlosin (3-acetyl-4 isovaleryltylosin) is an innovative drug, licensed to treat diseases in pigs (Porcine Proliferative Enteropathy, Swine Dysentery and Enzootic Pneumonia) and poultry (Mycoplasma Pneumonia, Necrotic Enteritis). Throughout this report, Aivlosin refers to the active ingredient Tylvalosin. Aivlosin was available in the tartrate form as granules, with molecular weight 1192.3 (figure 1.11). The salt form used in this work is easily soluble in water. The non-salt form of Aivlosin, instead, shows a high hydrophobicity: tha major contribution to this property could be due to the isovaleryl group [56].
Aivlosin is rapidly absorbed and concentrates in target tissues, particularly the lung and gut. It is very clinically efficient as it achieves peak therapeutic levels in blood plasma within two hours of administration [57].
Aivlosin was chosen in this work for its innovativeness, its low cost and because, at high concentrations, it seems to have both antibiotic and antiviral effects [58]. In fact, it could eventually be used for treating a large number of viruses including PRRS (Porcine reproductive and respiratory syndrome) virus, Influenza virus, Hepatitis C virus, Ebola virus, SARS CoV, Coxsackie B3 and B5 virus, other than for simultaneously treatment of bacterial and viral infections.
Some side effects of Aivlosin presented in animals. Maternotoxic effects have been observed in rodents at concentrations of 400 mg for Kg of body weight. In mice, a slight decrease in fetal weight has been found at concentrations that do not cause maternotoxic effects [59].

Azithromycin is an azalide (antibiotics containing a nitrogen in the macrolide ring) and one of the world's best-selling antibiotics, sold in the USA under the name Zithromax. In humans, it is used to treat many different types of infections caused by bacteria, such as respiratory infections, skin infections, ear infections, and sexually transmitted diseases [60].

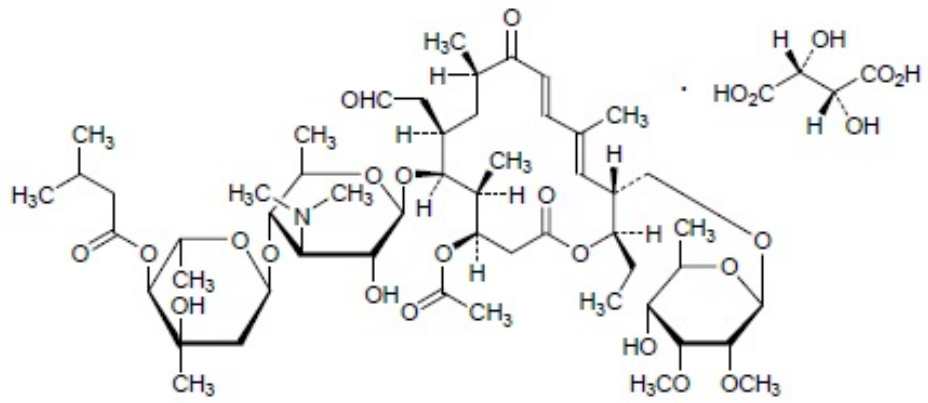

Figure 1.11: *Aivlosin structural formula [57].*

Azithromycin has the chemical name (2R,3S,4R,5R,8R, 10R,11R,12S,13S,14R)-13-[(2,6-dideoxy-3-C-methyl-3-O- methyl-α-L-ribo-hexopyranosyl)oxy]-2-ethyl-3,4,10-trihydroxy-3,5,6,8,10, 12,14-heptamethyl-11-[[3,4,6-trideoxy-3-(dimethylamino)-β-D-xylo-hexopyranosyl]oxy]-1-oxa-6-azacyclopentadecan-15-one (figure 1.12). Azithromycin, as the dihydrate, is a white crystalline powder with a molecular formula of $C_{38}H_{72}N_2O_{12} \cdot 2H_2O$ and a molecular weight of 785.02.

Azithromycin is derived from Erythromycin; however, it differs chemically from Erythromycin in that a methyl-substituted nitrogen atom is incorporated into the lactone ring. It is sparingly soluble in water, but it can be dissolved in acid solutions (e.g., 0.1 M HCl).

Azithromycin is generally well tolerated. The most common side effects are diarrhea or loose stools, nausea, abdominal pain, and vomiting which may occur in fewer than one in twenty persons who receive Azithromycin. Rare side effects include abnormal liver tests, allergic reactions, and nervousness [61].

Azithromycin was chosen as control because it is well known in literature, as many studies have already been carried out using it on biological systems.

Clarithromycin is a macrolide antibiotic chemically related to Erythromycin

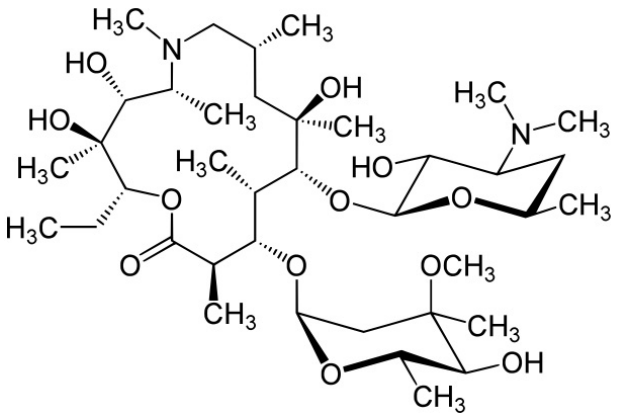

Figure 1.12: *Azithromycin structural formula [62].*

and Azithromycin. Chemically, it is 6-0-methylerythromycin. The molecular formula is $C_{38}H_{69}NO_{13}$, and the molecular weight is 748.0 (figure 1.13).
It is used to treat pharyngitis, tonsillitis, acute maxillary sinusitis, acute bacterial exacerbation of chronic bronchitis, pneumonia, skin and skin structure infections [63].
Possible side effects from Clarithromycin may include: nausea, vomiting, diarrhea, abdominal pain [64].
Clarithromycin is a white to off-white crystalline powder, practically insoluble in pure water (as well as Azithromycin) but soluble at low pH.
Clarithromycin was chosen in this work because of its hydrophobicity and high solubility at low pH. These characteristics make it a very effective drug against viruses. A possible mechanism of action against viruses is the following: when viruses enter in cells they are enclosed in small lipid vesicles (liposomes); as the pH inside the liposomes is lower than outside, the solubility of Clarithromycin would be favoured in the liposome, where it could fight back the virus at local much higher than normal concentrations. It is possible that this mechanism is analogous to that of Aivlosin [58].
Moreover, Clarithromycin has a very similar structure to that of Azithromycin, and along with other drugs of the Macrolide family can represent a valid check of the different effects between them on lipid systems.

All the antibiotics introduced are weak bases: while they can move across the membrane readily in the uncharged form, in the protonated form they will be trapped in the low pH aqueous compartment inside the endosome.

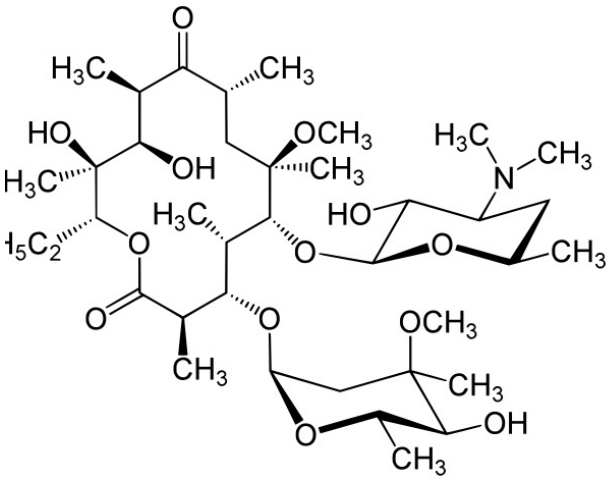

Figure 1.13: *Clarithromycin structural formula [65].*

1.5.2 Effect of Azithromycin on lipid bilayers

Lipid:lipid interactions and mechanical properties of membranes can be affected by incorporation of molecules which perturbs the lipid packing. Many previous studies on Azithromycin effectively showed that this macrolide antibiotic can affect the physical properties of the lipid membranes.
The effect of Azithromycin on molecular organization, membrane fluidity and permeability in lipid mixtures of DPPC:DOPC, DPPE:DOPC, Sphingomyelin:DOPC, and Sphingomyelin:Cholesterol:DOPC has been investigated [67] (DPPE is dipalmitoylphosphatidyletanolamine).
These mixtures exhibit well defined phase separation. Atomic Force Microscopy (AFM) revealed that Azithromycin perturbed lateral phase separation, indicating a perturbation of membrane organization in lateral domains. Azithromycin did not alter the permeability of lipid vesicles, but it increased

the fluidity at the hydrophilic/hydrophobic interface in DPPC:DOPC and DPPE:DOPC bilayers.

More specific studies on mechanisms of interaction between Azithromycin and phospholipids have been perfomed.
Azithromycin was found to bind to lipid model membranes and interact with the polar head groups of phospholipids, decreasing their motional (both orientational and translational) freedom [68]. Thus, the position of Azithromycin is probably near the polar head and the interface, in the upper 10 carbons of the acyl chain.
Fa et al. (2007) [69] investigated the effect of Azithromycin on size distributions and elastic properties of DOPC-GUVs.
GUVs prepared by electroformation showed an initial spherical shape reaching diameters of up to 50 μm. Addition of 50 μM Azithromycin preferentially destabilized membranes with the lowest curvature (largest vesicles were irreversibly lost with the concomitant increase of smallest vesicles).
The amplitude of thermal fluctuations of a bilayer is related to its bending modulus (κ; see section 1.6); the apparent area compressibility modulus K_{app} characterizes the energy necessary for the increase of bilayer surface area. Azithromycin addition was found to enhance lipid membrane fluctuations reducing both the required energy for thermal fluctuations and the stress to stretch the bilayer. Molecular modeling confirmed that Azithromycin induces a modification in the DOPC organization at the interface of phospholipid bilayers. Structurally, this modification consists in an increased mean surface occupied by each phospholipid molecule in presence of Azithromycin (see figure 1.14).
Calorimetric studies on DOPC and DPPC multilamellar dispersions showed that for high Azithromycin content, thermal transitions are markedly reduced (the height of the transition peaks is reduced). The enthalpy variation associated with the transition also decreases [70]. These effects may be due to an increase of the available space between hydrophobic chains after insertion of

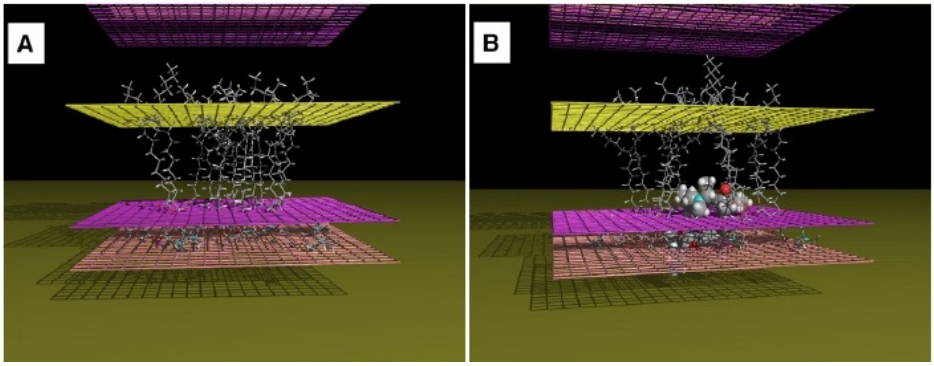

Figure 1.14: *Assembly of DOPC alone (A) or combined with azithromycin (B) inserted in the membrane. Yellow plane= bilayer centre (z=0); magenta plane=phospholipid acyl chain/polar headgroup interface at z=13.5 Å from the centre; pink plane=phospholipid:water interface (z=18 Å). Azithromycin is represented in CPK (CoreyPaulingKaltum) mode. [69].*

azithromycin in phospholipids, allowing an enhancement of their mobility.

1.6 Thermal fluctuations of fluid membranes

By the end of the 19th century, the "flickering" phenomenon of fluid membranes had already been observed in red blood cells. The first quantitative study of this phenomenon was made only in 1975 by Brochard and Lennon [71]: they described thermally driven equilibrium shape fluctuations of Red Blood Cells (RBCs), due to the conformational flexibility of the membranes. It has been proposed that flickering in real cells serves biological functions, for example enabling the cells to tune their adhesion to surfaces and thus control frictional resistance to flow [77]. In particular, RBCs are an interesting system to study in relation to membrane thermal fluctuations. Their fluctuations are connected to their mechanics and quantifying their mechanics is important in gaining new insights into the etiology of a number of human deseases [71][72]. In the healthy individual, these cells withstand repeated, large-amplitude mechanical deformations as they circulate through

the microvasculature. Certain pathological conditions cause changes in both RBC equilibrium shape and mechanics. For example, the cell's morphological transitions from discocyte(DC, normal shape) to echinocyte (EC, spiculated shape) to spherocyte (SC, nearly spherical) are accompanied by changes in RBCs mechanics. Diffraction phase microscopy (DPM) [73] and stabilized Hilbert phase microscopy (sHPM) [74] studies revealed that during these transitions an enhancement of elastic constant and tension occurs: the increased stiffness of some morphological RBC forms must be due to chemical changes in the lipid bilayer and structural changes in the spectrin network tethered to it.

Fluid phospholipid membranes in water are classically described as fluctuating 2-dimensional sheets. The out-of-plane fluctuations, also called undulations, can be induced by thermal motions. Their amplitude can be large enough to be visible in an optical microscope, and is mostly controlled by curvature elasticity and lateral tension of the membrane [71][75][76][7]. Their elastic energy depends on two main parameters: the bending modulus κ and the effective tension σ [6]. The former is defined as a constant which determines how the energy depends on the mean curvature of the membrane; the latter represents an energy that couples to the area of the bilayer surface.
Over the last three decades giant vesicles have been a popular system for measuring κ through these fluctuations, since the size of GUVs is suitable for direct observation using light microscopy.
Several single-cell techniques, for research purposes, have been used to measure the mechanical properties of vesicles: micropipette aspiration [78], stretching by optical tweezers [79], deformation in microfluidic channels [80], analysis of shape flickering [81][82], tether formation [83], and deformation under electric fields [84].

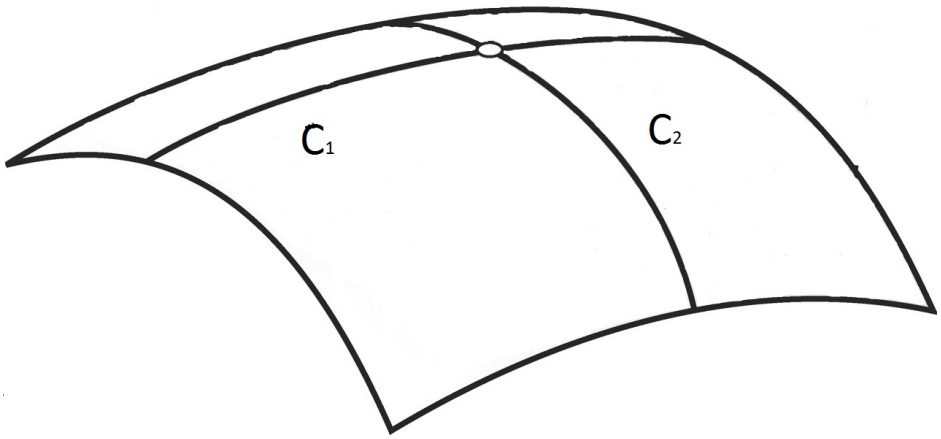

Figure 1.15: *Example of principal surface curvatures, c_1 and c_2*

1.6.1 The Helfrich Hamiltonian

Membrane elasticity has been traditionally studied using the Helfrich Hamiltonian [6]. This phenomenological Hamiltonian relates the curvature elastic energy to the local principle curvatures of the membrane c_1 and c_2 (see figure 1.15), and has the following form [85]:

$$F = \int_A \left[\sigma + \frac{1}{2}\kappa(J - 2c_0)^2 + \bar{\kappa}K\right] dS, \tag{1.1}$$

where $J = c_1 + c_2$ and $K = c_1 \cdot c_2$ are the total and Gaussian curvatures respectively, c_0 is the spontaneous curvature, σ is the surface tension, κ is the bending modulus, and $\bar{\kappa}$ is the saddle-splay modulus. The integration in Eq.(1.1) is carried out over the whole surface of the membrane.

The Helfrich Hamiltonian is derived by assuming that the local curvatures are small, and the free energy can be expanded to second order in J and to first order in K. It, therefore, involves four phenomenological parameters: c_0, and the three elastic coefficients σ, κ, and $\bar{\kappa}$ whose values depend on the area density of the amphiphiles. The spontaneous curvature c_0 is, in general, nonzero whenever the two sides of the membrane are unequal. There may be differences in lipid concentration and composition or in the aqueous media

facing an otherwise symmetric bilayer (monolayers are asymmetric by definition). The sum of curvatures, $c_l + c_2$, and the Gaussian curvature $c_1 \cdot c_2$ are associated with different elastic moduli, κ and $\bar{\kappa}$.
We can ignore terms containing the Gaussian curvature as its integral depends only on the genus of the (closed) surface. The Helfrich Hamiltonian for this system is:

$$F = \int_A \Big[\sigma + 2\kappa(H^2 - 2c_0H)\Big]dS - P\int_V dV, \tag{1.2}$$

where $H = J/2$ is the mean curvature, and P is a uniform pressure difference between the two sides of the membrane.
The volume integral in Eq. (1.2) is contained to account for the conservation of volume in the vesicle [86]. For fluctuations with very short wavelength, this volume integral is equivalent to having a constant constraining potential proportional to σ.
The theoretical and experimental methods for determining the elastic coefficients of interfaces can be classified into equilibrium (or mechanical) methods and fluctuation methods. In the equilibrium approach one extracts the elastic coefficients by comparing the free energies of two equilibrium surfaces with different curvatures. In the fluctuation approach, on the other hand, the Helfrich Hamiltonian is used to calculate the free energy cost due to a thermal fluctuation that changes the local curvature from its equilibrium value. The elastic coefficients are derived from the mean-square amplitudes of the fluctuations.
In the following the fluctuation approach is applied.

1.6.2 The planar approximation

In optical microscopy experiments only fluctuations in the equatorial plane of the vesicle can be measured. The flickering analysis is then made assuming

the vesicle spherical surface as planar; only a linear section of this surface is taken, that corresponds to the equatorial perimeter of the vesicle. The oscillations on this closed curve are analysed, and this is what is called the *planar approximation* [9].

Vesicle thermal fluctuation spectra in spherical geometry were calculated in previous work [87]. As we are not interested in the static shape of the vesicle but only in its fluctuations, we choose to work with the equations valid for a planar membrane. The errors due to curvature and closed topology of the membrane are important only for the first modes.

Let us consider a fluctuating planar continuous membrane, of lateral size L. If the average height of the plane is small compared to the lateral size of the fluctuation, such a fluid membrane can be completely described by out of plane displacements $h(\vec{r}) = h(x, y)$ from a horizontal (x,y)-plane (Monge parametrization).

The energy cost due to both stretching and bending in Eq.(1.2) can be written as [10]:

$$F = \int_A \left[\frac{1}{2}\sigma(\nabla h)^2 + \frac{1}{2}\kappa(\nabla^2 h)^2\right] dxdy. \tag{1.3}$$

The displacement $h(\vec{r})$ can be decomposed into Fourier modes. For a square membrane of area $A = L$ x L we have, with periodic boundary conditions, in terms of complex waves,

$$h(\vec{r}) = \sum_{\vec{q}} h_{\vec{q}} e^{i\vec{q}\vec{r}}, \tag{1.4}$$

where $q = \frac{2\pi}{L}(m, n)$, m and n (the mode numbers) being natural numbers.

For large mode number m (i.e., for short wavelengths), the fluctuation modes can be assumed to be continuous: this allows the replacement of the summations with integrals, that are evaluable analytically.

Eq.(1.4) becomes:

$$h(\vec{r}) = \frac{L^2}{(2\pi)^2} \int h_{\vec{q}} e^{i\vec{q}\vec{r}} d\vec{q}, \tag{1.5}$$

$$h_{\vec{q}} = \frac{1}{(L^2)} \int h(\vec{r}) e^{-i\vec{q}\vec{r}} d\vec{r}. \tag{1.6}$$

The expression in Eq.(1.4) can be used to evaluate F in Eq.(1.3).
We find:

$$\nabla h = \sum_{\vec{q}} i\vec{q} h_{\vec{q}} e^{i\vec{q}\vec{r}}, \tag{1.7}$$

$$\nabla^2 h = \sum_{\vec{q}} -\vec{q}^2 h_{\vec{q}} e^{i\vec{q}\vec{r}}. \tag{1.8}$$

We can use these expressions in Eq.(1.3), obtaining:

$$F = \sum_{\vec{q}\vec{q'}} \int \int \Big[\sigma(-\vec{q}\vec{q'} h_{\vec{q}} h_{\vec{q'}} e^{i(\vec{q}+\vec{q'})\vec{r}}) + \kappa(\vec{q}^2 \vec{q'}^2 h_{\vec{q}} h_{\vec{q'}} e^{i(\vec{q}+\vec{q'})\vec{r}})\Big] dxdy. \tag{1.9}$$

The only terms that survive in this integral are those for which

$$\vec{q} + \vec{q'} = 0 \Rightarrow \vec{q} = -\vec{q'}. \tag{1.10}$$

The elastic energy becomes:

$$F = \sum_{\vec{q}} L^2 \Big(\sigma \vec{q}\vec{q} + \kappa(\vec{q}\vec{q})^2\Big) h_{\vec{q}}^2. \tag{1.11}$$

The mean square amplitudes of the modes can be obtained from Eq.(1.11). In fact, according to the equipartition theorem:

$$L^2(\sigma \vec{q}^2 + \kappa \vec{q}^4) < h_{\vec{q}}^2 >= k_B T. \tag{1.12}$$

This gives [7]:

$$< h_{\vec{q}}^2 >= \frac{k_B T}{L^2(\kappa |\vec{q}|^4 + \sigma |\vec{q}|^2)}. \tag{1.13}$$

In optical microscopy experiments there are two fundamental differences with the theory: a) a one dimensional cut of the membrane plane is observable, b) the surface is closed.
a) The vesicle is usually visualised along the vertical axis (from above or

below), focussing on the equatorial plane x,z. The edge is a quasi-circular contour and only the fluctuations of the vesicle in the plane of its equator are observable.

We must project the displacements in Eq.(1.13) onto the equator of the sphere. This is achieved by the Fourier transform of Eq.(1.13) in the y-coordinate, evaluated at the plane $y = 0$ [9]. We then measure:

$$< h(q_x, y = 0)^2 >= \frac{1}{L'} \frac{k_B T}{2\sigma} \Big[\frac{1}{q_x} - \frac{1}{\sqrt{\frac{\sigma}{\kappa} + q_x^2}} \Big], \tag{1.14}$$

where $L' = 2\pi <\mathrm{r}>$ and $<\mathrm{r}>$ is the average radius of the sphere. The mode amplitudes given by the planar approximation of Eq.(1.14) and by the spherical model (see, e.g., [9]) are within 15% of each other for the lowest modes, and converge for the high modes. For bending-dominated fluctuations, $\sigma/q_x^2\kappa \to 0$, the spectrum reduces to [8]:

$$< h(q_x, y = 0)^2 >= \frac{1}{4L'} \frac{k_B T}{\kappa q_x^3}. \tag{1.15}$$

b) Eq.(1.15) describes well the data for quasispherical vesicles in the region between modes 6 and 20, i.e., typically $2 \times 10^5 m^{-1} < q < 1 \times 10^6 m^{-1}$. In quasi-spherical vesicles, modes up to 5 are affected both by membrane tension and membrane overall spherical geometry (there can be a regime where $< h(q_x, y = 0)^2 >\sim q^{-1}$, if tension is non-negligible); modes above 20 can usually not be detected reliably due to the limited optical resolution, their fast relaxation rate and the camera noise [91].

1.6.3 Spherical Harmonics representation

To investigate spherical membranes, we need to define a suitable basis. A reasonable choice is spherical polars and, as most of our work takes place in Fourier Space, the Fourier basis in spherical symmetry consists of spherical

harmonics. These, defined in spherical polar coordinates, can be written as [88]:

$$Y_l^m(\theta,\phi) = (-1)^m \Big[\frac{(2l+1)(l-m)!}{4\pi(l+m)!}\Big]^{1/2} P_l^m(\cos\theta) e^{im\phi}, \tag{1.16}$$

with $m \geq 2$ and $l \geq m$, and where P_l^m is the associated Legendre polynomial of order l and m.
The fluctuations on the surface of a sphere can be written as:

$$h(\theta,\phi) = \sum_{lm} U_{lm} Y_l^m(\theta,\phi). \tag{1.17}$$

We recall that the only experimental available data is the equatorial projection of fluctuations of spherical harmonics. The Fourier transform of the perturbation h around the equator is:

$$h_m = \frac{1}{2\pi}\int_0^{2\pi} h(\theta=\frac{\pi}{2},\phi) e^{-im\phi} d\phi. \tag{1.18}$$

Substituting Eq.(1.16) into Eqs. (1.17) and (1.18) gives:

$$h_m = \sum_l b_{lm} U_{lm}, \tag{1.19}$$

where $b_{lm} = Y_l^m(\frac{\pi}{2}, 0)$.
The variation of elastic energy from an initially spherical surface is the sum of two contributions: a term due to surface tension and a second one due to the bending modulus. The variation to second order in h has the form:

$$\Delta F = \frac{1}{2}\sum_{lm} \frac{U_{lm}^2}{a^2}[(l-1)(l+2)a^2\sigma + (l-1)l(l+1)(l+2)\kappa], \tag{1.20}$$

where a is the radius of the sphere.
Applying the equipartition theorem to the Helfrich Hamiltonian in spherical

harmonics (Eq. (1.20)):

$$\frac{< |U_l|^2 >}{a^2} = \frac{k_B T}{\kappa(l-1)l(l+1)(l+2) + \sigma a^2 (l+2)(l-1)}. \tag{1.21}$$

The projection of these fluctuations onto the equatorial plane gives

$$< |h_m|^2 >= \sum_{l \geq 2} b_{lm}^2 < |U_l|^2 >, \tag{1.22}$$

therefore:

$$\frac{< |h_m|^2 >}{a^2} = k_B T \sum_l \frac{b_{lm}^2}{\kappa(l-1)l(l+1)(l+2) + \sigma a^2 (l+2)(l-1)}. \tag{1.23}$$

1.6.4 Dynamics of membrane fluctuations

What we have studied up to here consists of the static fluctuations of a membrane. The dynamics of the fluctuations can also be studied experimentally. This allows us to obtain further physical parameters, such as the bulk viscosity of the membrane and the surrounding fluid, and perhaps the bulk modulus of the membrane.

The temporal behaviour of the membrane can be studied by means of two approaches: one consists in the study of the dynamics of individual modes; another one is to record the power spectrum of fluctuations at a single point, usually on the vesicle equator.

The time correlation of spatial modes of the membrane is defined as:

$$C_{\vec{q}}(\tau) = C_{lm}(\tau) =< U_{lm}(t) U_{lm}^*(t+\tau) >_t . \tag{1.24}$$

Using the results found in [87] and [89], we expect that the time correlation function will be an exponential decay:

$$C_{lm}(\tau) =< |U_{lm}|^2 > \exp\left(\frac{-\tau}{\tau_{lm}}\right), \tag{1.25}$$

where [90]

$$\tau_{lm} = \frac{a^3 Z(l)}{\kappa(l-1)l(l+1)(l+2) + \sigma a^2(l+2)(l-1)}, \tag{1.26}$$

$$Z(l) = \eta_{int}\frac{(2l+3)(l-1)}{l} + \eta_{ext}\frac{(2l-1)(l+2)}{l+1}. \tag{1.27}$$

The theoretical result of Eq.(1.25) needs to be corrected by projecting onto the equatorial contour to be compared to experiments [91]:

$$C_m(\tau) =< h_m(t)h_m^*(t+\tau) >_t = \sum_l b_{lm}^2 < |U_{lm}|^2 > \exp\left(\frac{-\tau}{\tau_{lm}}\right). \tag{1.28}$$

As discussed in [8], the experimentally observed decay time can be approximated as $\tau_m \simeq 0.8\tau_{mm}$ at long times.
Perturbations like those in Eq. (1.28) decay as the sum over many exponentials. Unfortunately it is hard to develop an approximation for short time scales, since all modes contribute significantly in that regime. This makes the recovery of the decay constant difficult using this approach.

The power spectral density (PSD) is defined as the squared temporal Fourier transform of fluctuations at a single point [10]:

$$G(\omega) = \frac{\mathscr{F}(h(\theta,\phi))\mathscr{F}^*(h(\theta,\phi))}{ps}, \tag{1.29}$$

where p is the number of points sampled, and s is the sampling rate. On a sphere, we can set $\theta = \pi/2$ and $\phi = 0$ without loss of generality. Using the

identity $\sum_m [Y_l^m(\pi/2,0)]^2 = \frac{2l+1}{4\pi}$ we obtain:

$$G(\omega) = \sum_l < |U_l|^2 > \frac{\omega_l}{\omega_l^2 + \omega^2} \frac{2l+1}{2\pi}. \tag{1.30}$$

Using Eqs.(1.21) and (1.26) gives:

$$< |U_l|^2 >= \frac{k_B T a^2 \tau_{lm}}{a^3 Z(l)} = \frac{k_B T \tau_{lm}}{a Z(l)}, \tag{1.31}$$

and, with $\omega_l = 1/\tau_{lm}$, we obtain:

$$G(\omega) = \frac{k_B T}{2\pi a} \sum_l \frac{2l+1}{Z(l)(\omega_l^2 + \omega^2)}. \tag{1.32}$$

In the high frequency, planar approximation, we find:

$$G(\omega) = \frac{k_B T}{12(2\eta^2\kappa)^{1/3}\omega^{5/3}}, \tag{1.33}$$

obtained using a slightly different definition of Z from that used in [10]: our final expression differs from Betz's by a factor of π. Since the expression in Eq. (1.33) must agree with the spherical expression in the high frequency limit, this implies a mistake in this part of the calculation in [10].

In summary, the relevant physics governing the static equilibrium shapes of GUVs is very well understood. On the contrary, many aspects of the dynamics of equilibrium shape fluctuations of the vesicles remain not well explained. The reason of this uncertainty is that the dynamics of fluid membranes involves many more physical factors than the statics. For example, the membrane viscosity (here considered only as a constant parameter) and the bulk modulus couple into these equations in complex ways [89]. In principle, even compression and splay modes, not considered above, can affect the dynamics in some parameter range [89].

1.6.5 Pixellation effects

Experimentally detected fluctuation spectrum is not exactly the same as the real fluctuation spectrum of the vesicle. The discretization of the image into pixels, and the limited sampling frequency which produces effects due to the Nyquist limit, modify the observed fluctuations.
As a model to explain their effects, we take a 1d signal F(x). The camera sampling with pixels of size L gives a pixelated function P(F(x)), which can be defined as:

$$P = S_L \star \delta_L \cdot S_L \star F, \tag{1.34}$$

where $\star$ is the convolution operation, and $\cdot$ represents the usual multiplication. S_L is a top hat function centred on the origin of full width L, and amplitude $1/L$. δ_L is an array of delta functions of spacing L. The rightmost S_L and the δ_L represent the mapping of all the light falling on one pixel in the camera onto a single point. The other S_L represents the mapping of these points back onto pixels on the screen.
P(x) is sampled (discretized in 360 sectors) to give what we actually measure, R(x):

$$R = \delta_b \cdot S_L \star P, \tag{1.35}$$

where the S_L comes from sampling with a pixel sized object, and the δ_b comes from the sampling spacing b which is different from the pixel size L.
Combining Eqs. (1.34) and (1.35) gives:

$$R = \delta_b \cdot S_L \star S_L \star \delta_L \cdot S_L \star F. \tag{1.36}$$

Taking the Fourier transform and using the convolution theorem, we get $\mathcal{R}$ of R:

$$\mathcal{R} = \mathcal{D}_b \star \mathcal{S}_L \cdot \mathcal{S}_L \cdot \mathcal{D}_L \star \mathcal{S}_L \cdot \mathcal{F}. \tag{1.37}$$

where we take the order of the operations from right to left. $\mathcal{D}_b$ is an array of delta functions of spacing $\frac{2\pi}{b}$ and:

$$\mathcal{S}_L = \mathrm{sinc}(\frac{qL}{2}). \tag{1.38}$$

When measuring vesicle flickering, we effectively measure $< \mathcal{R}^2 >$. For a high enough sampling rate, b, we can ignore the effect of the Nyquist frequency: the fluctuation spectrum decays quickly at high mode number, so the Nyquist effect will not contribute much to the amplitude of modes below the Nyquist limit. Thus, we can write:

$$< \mathcal{R}^2 >= \mathrm{sinc}^6(\frac{qL}{2}) < \mathcal{F}^2 > . \tag{1.39}$$

1.7 Interfacial Shear Rheology of phospholipid monolayers

1.7.1 Generalities

Dynamics of insoluble surfactants confined as thin film at the air-water surface is quite different than in the bulk. Rheology of monolayers is very interesting as it can give us information about mechanical properties of the monolayer not accessible with other techniques. In particular, measuring the force necessary to shear the film (at different deformations, γ, and deformation rates, $\dot{\gamma}$) and comparing them at different thermodynamic conditions (temperature, T, and surface pressure, Π) can provide valuable information beyond that obtained with pressure-area isotherms [92].

1.7.2 ISR experiment

In this work an Interfacial Stress Rheology (ISR) equipment was used to study if Aivlosin, Azithromycin and Clarithromycin can affect the shear modulus of phosphatidilcoline Langmuir monolayers. Both DOPC and DPPC were used for these experiments.

ISR experiments were carried out inducing a sinusoidal stress $\sigma(\omega)$ in the monolayer by the oscillations of a magnetic needle floating on the surface, driven by the magnetic field gradient generated by a pair of coils. The resulting shear strain $\gamma(\omega)$, along with its phase shift $\delta(\omega)$ with respect to σ, was measured by tracking the small needle oscillation with a microscope. Two parameters were monitored: the amplitude ratio, AR, defined as the ratio of the amplitude of the needle displacement, γ, to the forcing amplitude, σ, and the phase difference, δ.

The inertial response of the needle was characterized performing a measurement on pure water surface as a function of frequency, in absence of any surface film. The overall frequency behaviour could be modelled as the response of a forced-damped oscillator of mass m, spring constant k and damping constant d, in analogy with [94]:

$$\frac{\gamma}{\sigma} = \frac{1}{\sqrt{(k - m\omega^2)^2 + (\omega d)^2}}, \tag{1.40}$$

and

$$\delta = \arctan(\frac{-\omega d}{k - m\omega^2}). \tag{1.41}$$

Since the only object in motion is the needle, m is the mass of the needle.

The oscillator parameters (previously worked out for the same instrument in [93]) can be determined by performing a fit on the water stress-strain ratio curve. Moreover at high frequency the stressstrain ratio was found [93] to be proportional to ω^2: this allowed one to obtain a current-to-force calibration constant.

The dynamic surface modulus, $G^*(\omega)$, is defined as the proportionality factor

between the stress and the strain:

$$\sigma e^{i\omega t} = G^*(\omega)\gamma e^{i[\omega t - \delta(\omega)]}. \tag{1.42}$$

By rearranging Eq. (1.42) and solving for $G^*(\omega)$ we can directly express the dynamic modulus as a complex number:

$$G^*(\omega) = \frac{\sigma}{\gamma} e^{i\delta(\omega)} = G'(\omega) + iG"(\omega) \tag{1.43}$$

where G'(ω) is the surface storage modulus (elastic part) and G"(ω) is the surface loss modulus (viscous part). The former represents storage of elastic energy, while the latter represents the viscous dissipation of that energy.
When the film is purely elastic $\delta = 0°$, which means that the shear strain follows faster the stress applied. When the film is purely viscous $\delta = 90°$ and the strain follows slowly the stress applied.

1.7.3 Newtonian fluids

Newtonian fluids are characterized by a constant dynamic viscosity, independent from the angular frequency. This implies a linear relation between the viscous shear modulus G" and the angular frequency ω:

$$G" = \eta \cdot \omega. \tag{1.44}$$

The stress versus strain rate curve is, therefore, linear and passes through the origin.

1.7.4 Maxwell model

Even in mainly viscous systems, at high frequencies the elastic response of a material starts to be relevant. In order to study the shear properties of

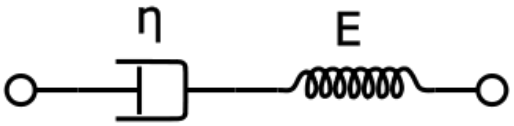

Figure 1.16: *Modeling of the Maxwell model by means of a purely elastic spring and a purely viscous damper connected in series.*

such systems, the Maxwell model can be used. The Maxwell model can be represented by a purely elastic spring and a purely viscous damper connected in series (see figure 1.16).
The components of the dynamic modulus G^* in such model can be written as:

$$G' = G_0 \cdot \frac{(\omega\tau)^2}{1+(\omega\tau)^2} \tag{1.45}$$

and

$$G" = G_0 \cdot \frac{(\omega\tau)}{1+(\omega\tau)^2}, \tag{1.46}$$

where G_0 is the instantaneous modulus and τ the characteristic relaxation time, which corresponds to the crossover time between the two moduli.
For a viscous fluid the storage modulus is much lower than the loss modulus, and it scales with frequency as $G' \propto \omega^2$ (figure 1.17); the loss modulus is linear in frequency, $G" \propto \omega$ as described by the Newtonian model (that is a low-frequency limit of the Maxwell model). The low-frequency region in which these power laws are obeyed is called the *terminal region*.

1.7.5 Time-temperature superposition

In order to achieve broader ranges of frequency, not accessible in a single measurement, time-temperature superposition [95] is often invoked.
This technique consists in shifting data obtained at several temperatures to a common reference temperature. It involves the use of temperature-dependent shift factors for the magnitudes of measured moduli (vertical shift factor) and for frequency (horizontal shift factor) on log-log plots of material functions

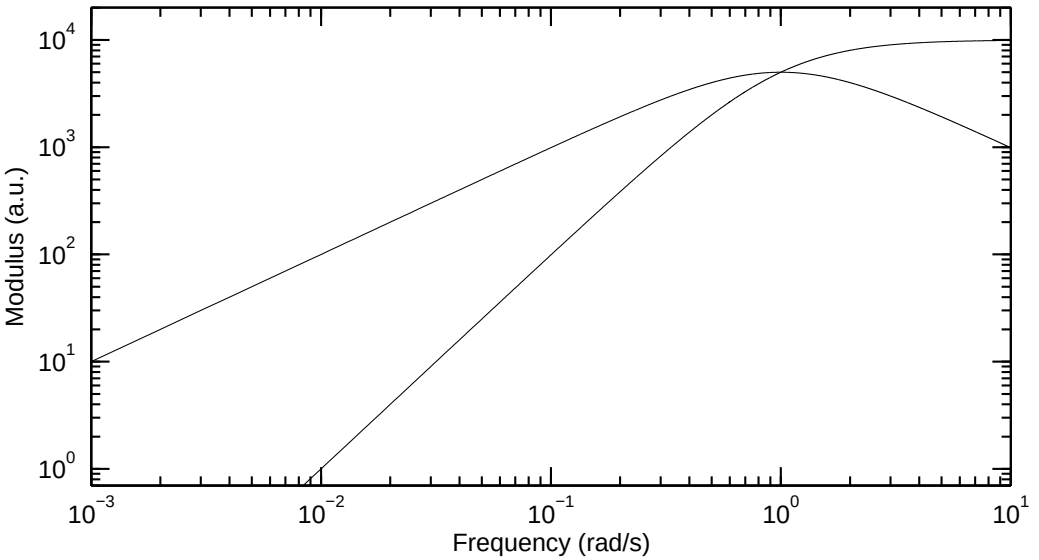

Figure 1.17: *Example of behaviour of viscous G" and elastic G' shear moduli according to Maxwell model. Curves are plotted having crossover between viscous and elastic regime at angular frequency 1 Hz.*

such as the relaxation modulus, the storage and loss moduli, and the creep compliance.

The shift along the modulus axis is often small or negligible. Thus, the functions measured at different temperatures can be superimposed by shifting along the logarithmic frequency axis, with a minor shift along the logarithmic modulus axis, if required. The temperature-dependent horizontal shift factor a multiplies a frequency to yield a reduced value equal to $a\omega$. If time-temperature superposition is obeyed, the use of shift factors will yield a "master curve".

This technique holds for linear polimers (obeying the Rouse model), but also for wider classes of materials, as long as there are no phase transitions or other temperature-dependent structural changes [96].

Chapter 2

Materials and methods

2.1 Materials

DOPC, DPPC and POPE were purchased from Avanti Polar Lipids in 25 mg/ml chloroform solutions. The lipid solutions in chloroform were kept at -20 °C in order to limit the oxidation of phospholipids and the formation of lysolipids.
Stock solution of DOPC was diluted to 3 mg/ml. 1% in weight Texas-Red DHPE (Invitrogen) was added to DOPC for fluorescent imaging.
100 mM sucrose solution and 100 mM and 125 mM glucose solutions (Sigma-Aldrich) were used for vesicles formation and suspension respectively (100 mM glucose solution was used for size distribution analysis, 125 mM glucose solution was used for flickering analysis). Milli-Q water was used.
2-(N-morpholino)ethanesulfonic acid (MES) was purchased from Sigma-Aldrich (P.N. M1317) as 1 M solution.
Aivlosin ($M_w = 1192.3$) was supplied as tartrate salt (provided by Dr David Brown, Dept of Viriology, Cambridge University). Azithromycin ($M_w = 748.98$) and Clarithromycin ($M_w = 747.95$) were purchased from Fluka (SigmaAldrich; P.N. 75199 and C9742, respectively). Since Azithromycin and Clarithromycin are sparingly soluble in water at pH 7.0 [97], but very soluble at acidic pH, two stock 100 mM sucrose solutions were prepared by dissolving

2.99 mg of drug in 10 ml 0.1 M HCl (399.2 mM) and adding 267 μl MES solution (26.7 mM). Further dilution in Milli-Q water before analysis allowed to reach a final pH = 6.3 (by titration with NaOH), concentration of MES 10 mM, and concentration of drug 50 μM or 150 μM. The salt form of Aivlosin also allowed high solubility at not acidic pH, so the same procedure as for Azithromycin and Clarithromycin was followed but without HCl.
Immersion oil (density 1.09 g/cm^3) for microfluidic experiments was purchased from Sigma-Aldrich.

2.2 Experimental Methods

In this section, the protocols used for the experiments discussed in later chapters are described. First, the protocol for the production of GUVs is presented. We next describe microscopy imaging of GUVs followed by tecniques used to prepare and study DOPC monolayers. Finally, Differential Scanning Calorimetry and microfluidics are described.

2.2.1 GUVs preparation: Electroformation method

The classical electroformation technique originally developed by Angelova and Dimitrov [24] and modified by Mathivet et al. [100] was used to prepare the DOPC-GUVs.
A chamber was constructed with a pair of conducting indium tin oxide (ITO)-coated glass microscope slides. For each sample 25 μl of a DOPC solution (3 mg/ml in chloroform, 1% in weight of fluorescent dye) were deposited onto the conductive face of one slide, forming a film as uniform as possible with the tip of pipette. The complete evaporation of the solvent was achieved by vacuum drying overnight.
Two teflon spacers of $\sim$ 0.5 mm were placed between the two slides, with the

conductive faces oriented toward each other. The system was held together with small clips, sealing one aperture with vacuum grease and a stripe of parafilm. An aqueous solution of 100mM sucrose was injected between slides from the still open aperture, then sealing it with a stripe of parafilm.
A power supply generated a low-frequency voltage (10 Hz, 1 V peak to peak). Giant vesicles were obtained in 1.5 hours and then recovered by suction with a pipette.
The main mechanism behind the GUVs formation seems to be the electro-swelling: the lipid film is swelled to increase the curvature of lipid film [102]. The details are not fully understood, but the protocol yields a mostly unilamellar sample as checked in [24] and [101].

2.2.2 Microscopy for size and flickering analysis

Sample preparation

After formation, vesicles were suspended in acqueous solution containing 100 mM sucrose, 10 mM MES buffer solution (pH 6.3) and antibiotic (Aivlosin, Azithromycin or Clarithromycin, earlier 50 μM and then 150 μM for each one). Control vesicles were suspended only in buffered sucrose solution. Seven samples of suspended vesicles (one for each concentration with each drug plus the control sample) were analysed after 5 hours, 1 day and 2 days of incubation.
Just before observation under microscope, vesicle suspensions were mixed with acqueous solution containing 100 mM or 125 mM Glucose (for size distribution and flickering analysis respectively) and 10 mM MES buffer solution. Then the vesicles were carefully transferred into the observation chamber for visualization.
Observation chambers were prepared balancing a cover slip (18 x 18 mm) between two other cover slips, lengthways along a microscope slide. A drop

of optical adhesive (Norland Optical Adhesive 61) was placed under the middle of each free side of the supported cover slip, being careful to leave the supporting cover slips free. The glue was cured under a UV lamp for a few minutes. The supporting cover slips were then removed. More adhesive was added to form a chamber (a space of $\sim$ 1 cm diameter) with two narrow diametrically opposite apertures (1-2 mm) at either end. The glue was cured again, then the sample (vesicles suspension, 40 μl) added using a pipettor before sealing off the ends of the chamber with vacuum seal to avoid evaporation. The final inner thickness of the chamber was of the order of $\sim$ 200 μm.
Glucose and sucrose, classically used for phase contrast microscopy experiments, enhance the contrast of the vesicles because of their differences in refraction index. Due to their slight difference in density, they also drive vesicles towards the bottom of the chamber where they can be easily observed.
The sugar solutions were filtered using a 0.22 μm filter beforehand to remove any particle which could perturb the vesicle analysis.
Since not all lipid initially deposited on the ITO-coated slide becomes organized in giant vesicles, it was not possible to evaluate the exact amount of phospholipid transferred in the observation chambers.

Experimental setup

Vesicles were observed using a Zeiss LSM510 confocal microscope platform, but in conventional imaging. A 10x objective was selected for size analysis and 40x phase objective for flickering analysis.
In vesicle samples, where size analysis was to be performed, a fluorescent dye (Texas-Red DHPE) was added to the lipid solution (1% weight) before electroformation. Texas-Red DHPE, which has an excitation peak at 584 nm, and emission at 608 nm, was found to have no appreciable photobleaching over the experimental timescale of several minutes. Then the vesicles were

imaged with a green-red filter set (Zeiss Filter Set 15, excitation: BP 546/12, emission: LP 590) and a 10x dry objective (Zeiss). The low 10x magnification was used to obtain a large number of vesicles per image, and to give a large depth of focus to image the whole vesicle, rather than just the equator. Epifluorescence was found to give better contrast than bright-field methods: thus, a fluorescence Mercury lamp was used to illuminate the vesicles from the dark background. Three sets of 30 pictures were taken for each sample and averaged to obtain mean behaviours for each time of incubation (5 hours, 1 day, 2 days).
For the thermal fluctuation analysis the image series were recorded in phase contrast on a CCD camera at 60 frames per seconds. With the objective used (40x) the pixel size was of the order of 200 nm. About 300 vesicles were analysed, capturing up to 7000 contours for each of them. The fluctuating membrane contour was detected by an algorithm developed in-house and coded in MatLab (see subsection 2.3.2). Mean values and standard deviations were obtained from the several vesicles analysed.
All measurements were performed at room temperature ($\sim 23°C$).

2.2.3 Interfacial Shear Rheology (ISR)

Instrument description

The design of the instrument follows that described in [93].
A custom Langmuir trough made of Teflon was used for all measurements. The trough sizes were 31 cm x 8.5 cm x 0.7 cm. Two hydrophobic Teflon barriers were moved simmetrically to change the surface concentration of the surfactant molecules at the interface. The surface pressure was monitored using a Wilhelmy balance.
Two solenoid rings (R = 16 cm) were aligned parallel, separated by one ring radius (Helmoltz configuration). The trough was positioned so that the plane

of the air -water surface was aligned with the axis. The coils were used to produce a constant magnetic field that aligned the probe along their axis. The probe used in these experiment was a stainless steel needle (12 mm long, 0.34 mm thick), rinsed in chloroform before each measurement to keep its surface clean. The needle was magnetized to saturation before each experiment with a permanent magnet, and then positioned in a flow cell between the coils, floating at the air-water interface due to surface tension (see figure 2.1). The flow cell was made by two partially submerged glass slides normal to the interface, supported by a thin Teflon block completely submerged in the subphase. The hydrophillic nature of the slides produced a meniscus that aided in aligning the needle along the channel centerline.
The largest part of the magnetic field (tipically 10 G) was uniform and was needed to keep the probe alignment. In addition, a sinusoidal current was added to one of the coils to produce an oscillating field gradient whose effect was to apply a force to the needle. A typical sinusoidal wave of frequency 0.25 Hz and amplitude I=1 mA generates a force of the order of 50 nN on the needle, resulting in a displacement of about 10 μm.
Both this sinusoidal signal and the movement of the barriers were controlled by a Digital Aquisition (DAQ, National Instruments 6036E): its analog outputs were used to drive the trough barriers and to apply the oscillating current to the Helmoltz coils via a set of power amplifiers (BOP36-5 M by Kepco Inc.). The DAQ analog inputs were used to measure the surface pressure and the time-dependent current on the coils.
The displacement of the needle was monitored as function of time by a CCD USB camera equipped with a long focal objective (Mitutoyo MPLAN-APO-10X.).

ISR measurement

The ISR technique was used to show if antibiotics can affect the shear properties of Langmuir films.

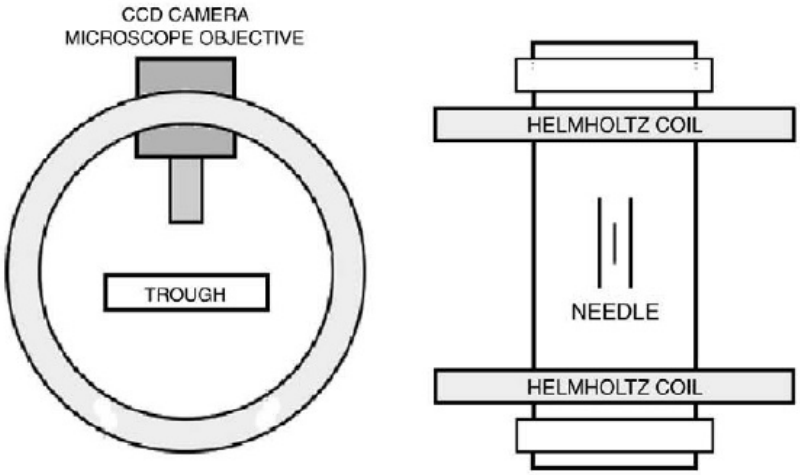

Figure 2.1: *Simplified scheme of the ISR experimental setup (side and top views) [93]. The two partially submerged glass slides of the flow cell are visible next to the needle in the central part of the trough, top view. In the outermost region of the trough the teflon barriers are visible.*

First, a DPPC monolayer was spread onto a clean water surface, and an isotherm Π/area was measured. A range of surface pressures was chosen (25-45 mN/m), so that we ensured the system to be in the 2D-Liquid-Compact phase [36].

For each measurement, a new DPPC monolayer was spread onto a clean water surface, with flow cell already placed in the trough. After evaporation of the solvent, the needle was placed in the trough and compression of the barriers started until the correct surface pressure was reached.

The experiment was performed by applying to the needle a chirp signal, made of a wave train with 15 different frequencies (from 4 Hz to 0.08 Hz, spaced in logarithmic scale) and 10 oscillations for each frequency (see figure 2.2). The time scale of the needle displacement, and so of the film deformation behaviour, was probed according to the model described in section 1.7. The same procedure was followed with a film formed on a 50 μM drug solution in water.

All the measurements were carried out at 22°C, and the temperature was maintained by a Lauda temperature bath to within 0.1°C.

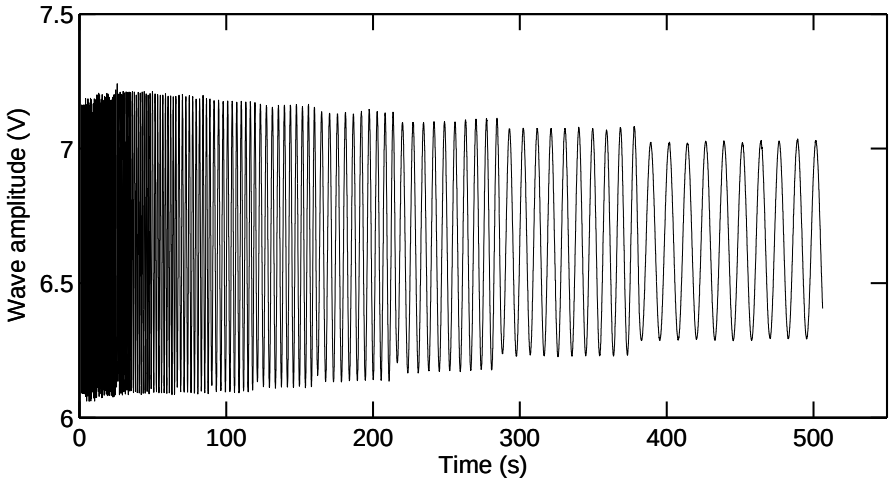

Figure 2.2: *Sinusoidal train - wave applied to the magnetic needle by one of the two coils. Applied frequencies, spaced with logarithmic scale, were (in Hz): 4.00, 3.02, 2.29, 1.73, 1.31, 0.99, 0.75, 0.57, 0.43, 0.32, 0.25, 0.18, 0.14, 0.11, 0.08. The signal is centred on the voltage used by the static coil to keep aligned the needle.*

2.2.4 Differential Scanning Calorimetry (DSC)

Preparation of lipid samples for DSC

DSC can be used to analyse phase transitions of single phospholipids and phospholipid mixtures. The protocol used here follows [103].
Phospholipids (1-2 mg, DOPC, DPPC, POPE) were deposited directly onto DSC aluminium pans in chloroform solution, and solvent was removed under gentle nitrogen flow, before resuspension in 30μl aqueous solution containing 10mM buffer and 5μM, 50μM and 500μM Aivlosin (without drug in case of control sample). After sealing hermetically the pans, the sample was equilibrated for 2 hours at 50°C in the DSC machine itself. The precise structure

of the lipid bilayers produced by this method is unclear. There are probably a mixture of unilamellar and multilamellar vesicles, together with a connected stack of bilayers.

DSC measurements

DSC measurements were performed with a Perkins-Elmer Pyrus I heat conduction machine. Water was used in reference pan.
Temperature range studied with DOPC was -5°C and -35°C (so that liquid-solid water transition was avoided). After equilibration at 50°C, the temperature was decreased to -5°C at high cooling rate (100°C/min), and the following temperature scan was applied to the sample:

1) sample was mantained at -5°C for 2 minutes;

2) it was then cooled to -35°C at 10°C/min rate and mantained for 5 minutes;

3) temperature was increased again to -5°C at 10°C/min.

Thermal steps from 1 to 3 were repeated three times to ensure constancy and good repeatability of the data and to erase the thermal history of the sample.
Due to supercooling phenomenon and in accordance with [104] thermotropic transitions were more accurately evaluated from heating curves. Conseguently, only heating scans have been used throughout this work.

A similar equilibration procedure was followed with DPPC and POPE, but avoiding complete evaporation of solution from the pan was very hard. Probably this was due to their different physical properties in comparison with DOPC (the main transition temperature of the latter is much lower than that of DPPC and DOPC; see section 1.4). Thus, measurements with DPPC and POPE were not performed.

2.2.5 Microfluidics

Device fabrication

Chips containing microfluidic channels (2-3 cm length, $\approx$ 100μm diameter) were kindly manufactured for this experiment by Dr. Debjani Paul (Cavendish Laboratory, University of Cambridge, UK) using the Nanoscience microfabrication facilities.
Devices were prepared by "soft lithography" [105], and the main steps are outlined briefly in the following.
SU-8 lithography was used to make the 'negative' mold of the chip on a clean and hydrophilic glass slide. Polydimethylsiloxane (PDMS) was poured on the SU-8 pattern, heated in oven at 65°C for 1 hour and then peeled off from the glass slide. Holes in the chip were drilled to make reservoirs. Finally, PDMS solid chip was plasma-bonded to a glass cover splip, previously cleaned (as before).
The channel was shaped as a double simmetric-y, as shown in figure 2.3.

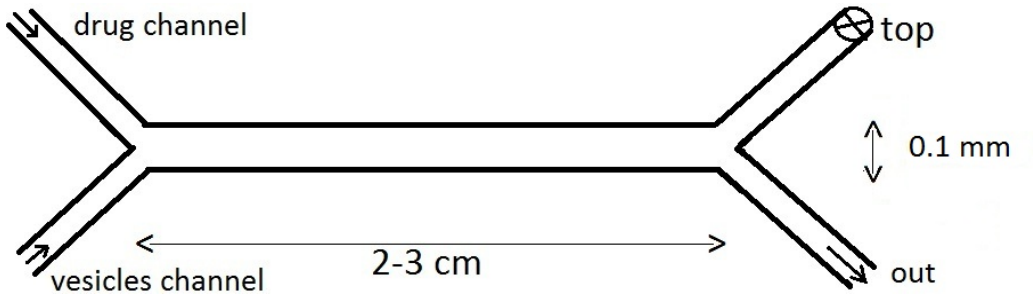

Figure 2.3: *Microfluidic channel in PDMS chip obtained by soft lithography.*

Fluidics and stopped-flow analysis

DOPC-GUVs were used in microfluidic experiments. After electroformation they were poured in an eppendorf (diluted 100 times in 100 mM sucrose, to prevent obstruction of the channel from vesicles), in which the end of the inlet tube was inserted. A 150 μM Clarithromycin solution (in 100 mM sucrose) was poured in a different eppendorf and connected to the device as before.
Fluids were delivered in the channel pulling with a precision syringe pump (Harvard Apparatus, '11' Plus, single syringe) outfitted with a 50ml syringe on the output stream. The silicone tubing (Altec, UK) was 1.50mm bore diameter and 0.50mm wall thickness.
The typical flow rate, determined by the dispense rate of the syringe pump, was 0.001 ml/min. This low flow rate ensures laminar flow of the fluids, that, in turn, prevents vesicles from reacting with drug. The analysis was led in stopped-flow mode: when rapid injection ends, which happens abruptly when the syringe reaches a physical stop, the two fluids begin reacting. This static regime was used to look for the instantaneous effects of the exposition to the drug on vesicles: buddings, for example, can happen on very short timescales, not observable by simple optical microscopy.

Optical detection

In order to observe the flows of vesicles and drug solution inside the channels, an inverted Leica TCS SP5 confocal microscope was used (but in conventional imaging mode). The glass side of the chip was placed down on the stage, facing the microscope objective. A 10x oil immersion objective was used for all measurements. A mercury arc lamp was used as light source and the filter set to make fluorescence measurements. Fluorescence emission was collected using a CCD camera.

2.3 Data analysis

In the next section, the methods of analysis of the imaging data, both in the case of size distribution and flickering experiments will be discussed. Then the analysis of the ISR data will be briefly described.

2.3.1 Size distributions of vesicles

Vesicle size distributions were obtained by computationally segmenting epi-fluorescent images of fluorescent vesicles.
Size analysis of vesicles was performed by means of an in-house program coded in Matlab. A suitable threshold was chosen, and the image was thresholded. The choice of threshold could be automated by scaling the intensity levels of each image. In practice it was found that under identical optical settings, the same threshold could be used for each image. Each bright region in the thresholded image was identified as a vesicle, and the effective diameter was calculated from that of the smallest convex polygon that can contain the region (see figure 2.4). Also, the diameter was calculated from the squareroot of the number of pixels in the region. As there were very few dark pixels inside the vesicles, the convex area was not different from the number of pixels. An eccentricity parameter was initially set for excluding the vesicles, as in [69]. In practice, in the samples studied in this work this was not necessary, because there were no really non-spherical vesicles.
Number and radii of all the vesicles detected in the pictures of a kind of sample were stored. A size distribution (normalized by the number of vesicles detected in each sample) was plotted and constituted the function on which to check the effect of drugs.

In previous works size distributions of lipid vesicles have already been studied [106]. If the spontaneous curvature is zero and κ is assumed to be positive, which should in general be true, the shape of lowest energy of such vesicles is spherical. The thermodynamic predictions of average vesicle radii distribu-

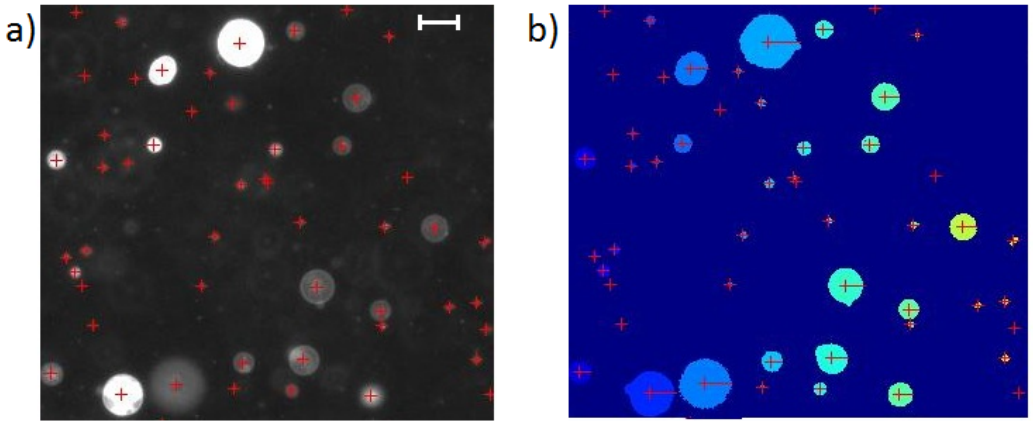

Figure 2.4: *Detection of vesicles in a picture taken by fluorescence microscopy. a) The program identifies the vesicles, and finds their centres (indicated by red crosses). The white bar indicates 20 µm. b) The picture is index-linked fixing a suitable threshold: vesicles are the areas in the pictures brighter than the threshold. The diameter of vesicles is calculated.*

tions in ensembles of vesicles which can freely exchange phospholipids have the form $P(r) \approx r^2 e^{-r^2/r_0^2}$, which is not compatible with the experimental distributions measured in this work. Experiments here occurred on timescales which are too short for the vesicles to be equilibrated. Infact, because of the very low concentration of free phospholipids in solution [107], one can assume that there is no transfer of lipids between vesicles at all, and that the vesicles therefore have the same size distribution as immediately following electroformation.

The distribution of vesicle radii found experimentally here is well fitted by a single exponential function over the full range of observed vesicle radii:

$$P(r) = A \cdot e^{-\frac{2r}{R_0}}, \tag{2.1}$$

where A is a constant, r is the radius of the vesicles of one sample and R_0 is the mean radius.

In figure 2.4 there are some crosses which do not appear to correspond to vesicles. These are small collections of bright pixels, and they were ignored by fitting the exponentials to the size distributions starting from a suitable

size value (3 μm).

2.3.2 Contour analysis

The contour of the vesicle membrane was detected and analysed by an existing algorithm developed in-house and coded as a C++ module called within MatLab [91].
The detection of the contour against a noisy background was performed by using a correlation approach, rather than the typical maximum gradient approach as in [9]. The method treats each frame individually, and can be summarized as follows:

1) the center of the vesicle was determined for each frame;

2) the image was resampled along n equally spaced radial lines diverging from the cell center determined at step (1) (figure 2.5), and each resampled line profile was normalized to make a set of profiles within inner and outer bounds, as shown in figure 2.6(a) and (b). Polar coordinates with the origin in the contour centre were used, so that the contour shape was described by $r(\theta)$;

3) a correlation kernel was created: the profiles of step (2) from the first frame were aligned with each other by matching their maximum gradient points, and these were averaged together to create a kernel for correlation;

4) using the correlation kernel of step (3), a correlation value was calculated for each line profile at each radial position, resulting in a correlation array such as figure 2.6(c) for each frame;

5) the correlation profiles of step (4) shows a well defined peak at the cell boundary, and this was fit to a quadratic function to extract the

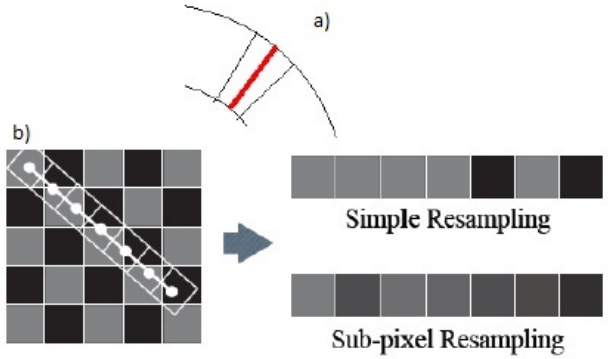

Figure 2.5: *a) The thick line is the radial line within one sector along which the pixels are considered for the contour detection. b) Sub-pixel resampling: the pixels surrounding the ones in the middle of the sector are averaged, obtaining a finest definition of the contour.*

boundary position at sub-pixel resolution, as shown by the dotted line in 2.6(c).

The result of this procedure was a set of n discrete radial positions of the cell boundary $r(\theta(t))$ for each frame. The mean radius of curvature $<r>$ was calculated as the average of $r(\theta(t))$ over all θ and all frames. The fluctuations $h(\theta(t))$ for each time were defined as the deviation of $r(\theta(t))$ from $<r>$: $h(\theta(t)) = r(\theta(t))$-<r>.

For the statics analysis, the discrete amplitudes obtained for each frame, $h(\theta(t))$, were Fourier transformed (using the FFT algorithm in Matlab) to give a set of complex Fourier coefficients c_q.
Experimental spectra were fitted with Eq.(1.14) in a range between the 6th mode and wavevector where noise becomes appreciable ($q_x \approx 2 \cdot 10^6$ m^{-1}). These modes were used to obtain the values of bending modulus κ and surface tension σ, with κ and σ as the only fitting parameters.

The analysis of point decay was performed by Fourier transforming the set of n discrete amplitudes h(θ(t)), as in Eq.(1.29). The PSD was fitted using Eq.(1.32), with κ, σ and η as only fitting parameters (in Eq.(1.27), η_{int} and

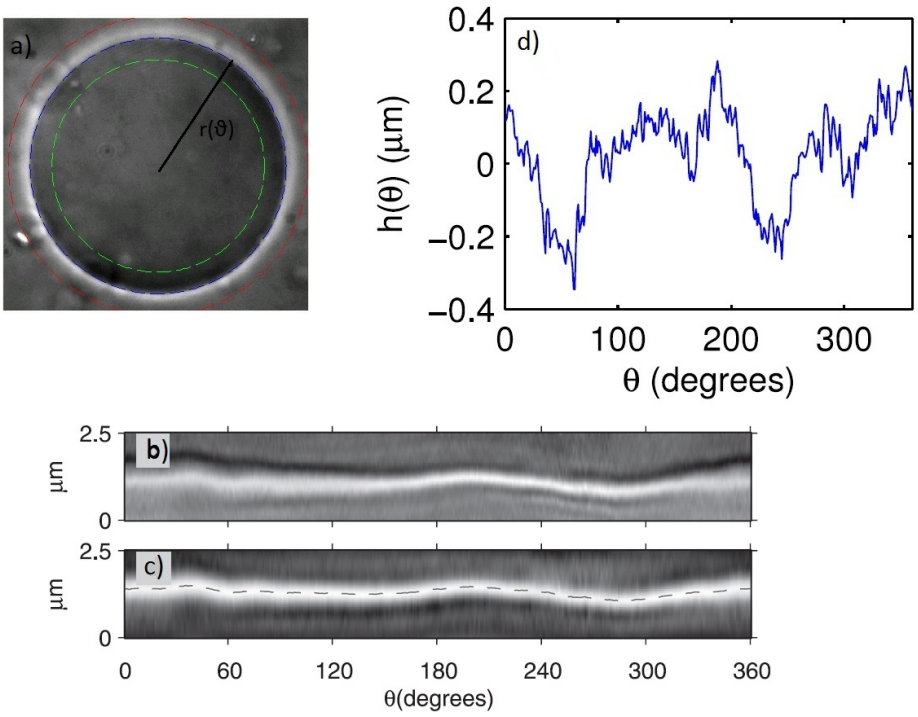

Figure 2.6: *a) Contour of the vesicle (blue dashed line), with inner and outer bounds used in image analysis (red and green dashed lines). b) The line profile array obtained at each radial section of panel a [91]. c) Effect of filtering the array in panel b with an optimized correlation kernel, and locus of maxima in the array (dashed line), which indicate the contour position [91]. d) Fluctuation amplitude h(θ) obtained as the difference between the instantaneous and timeaverage position of the contour at angle θ [91].*

η_{ext} were assumed to be equal to $10^{-3} Pa \cdot s$). The fitting range was 5-50 Hz.

2.3.3 ISR data analysis

At given surface pressure, the instantaneous position of the needle was detected by the CCD camera during all the duration of the stress applied to the film (figure 2.7).

In order to extract the mechanical properties of the film from the needle displacement, we had first to subtract a slow, non periodic, drift in the needle position which may be due to different spurious factors (figure 2.7). To this aim the time evolution of the needle position was reproduced by a slowly varying spline interpolant (of order 12), which was then subtracted, leaving the periodic oscillations as the only displacement. A sine function was used to fit to these periodic oscillations (one sine was used for each single part of the train-wave, known its frequency and calculating its amplitude and phase; figure 2.8); an analogous fit with a sine function was performed on each part of the applied wave. The amplitude ratio AR and phase shift $\delta(\omega)$ were obtained by Eq. (1.43) comparing the two curves. Typical accuracy was $10^{-2} mN/m$.

For the data analysis, frequencies in *Hz* were converted to angular frequencies, expressed in *rad/s*.

It has to be noted that in principle both the real and the imaginary parts G' and G" can simultaneously be obtained. In practice, however, when one of the two parts dominates the response, the other, smaller part, remains poorly determined. Often only an upper limit for the smaller quantity can be determined.

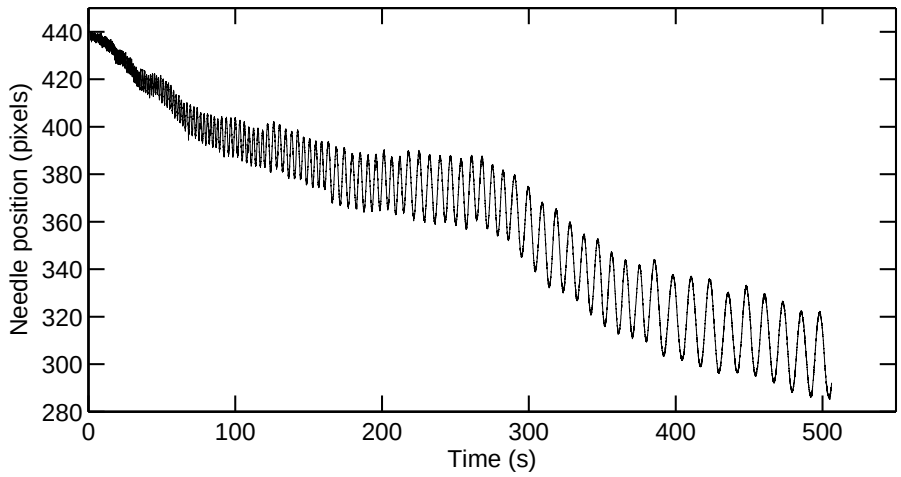

Figure 2.7: *Time evolution of the magnetic needle position by application of a train - wave, before subtracting the non-periodic drift. Pixel size: 1.34 μm.*

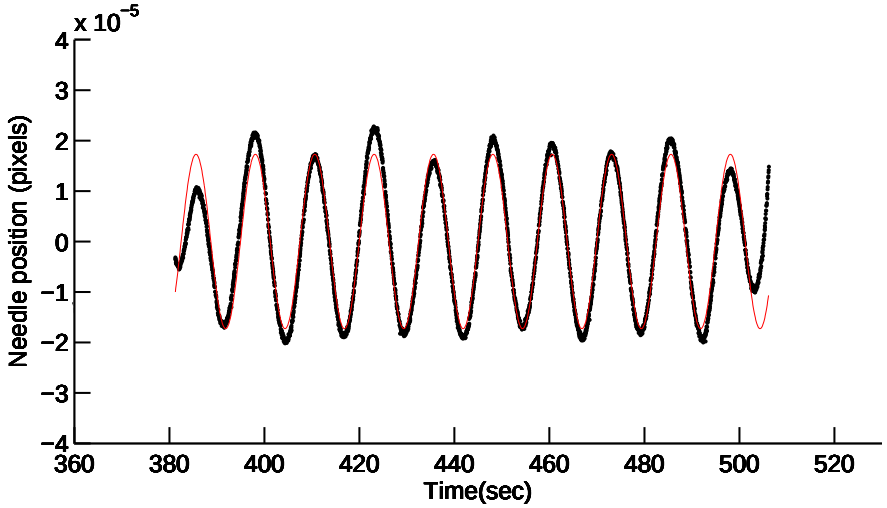

Figure 2.8: *Time evolution of the magnetic needle position by application of a train - wave, after subtracting the non-periodic drift. Thin line fits to the needle position using a sine function. Pixel size: 1.34 μm.*

Chapter 3

Experimental results

In this chapter the results of GUVs size distribution analysis are presented, followed from the results of flickering analysis. Then, rheological analysis on Langmuir lipid monolayers are described. The last two sections deal with the thermotropic studies on lipid monolayers and microfluidics of GUVs.

3.1 Size distributions of GUVs

Samples, prepared as described in section 2.2.2, were analysed by fluorescence microscopy after about 5 hours, 1 day and 2 days of incubation in solution containing each drug (50 μM and 150 μM).
Several thousands of vesicles were detected in each set of 30 pictures (three for each sample) taken at each time of incubation. Direct microscopic examination evidenced that GUVs prepared by electroformation had initial spherical shape with diameters reaching tens of *microns* (figure 3.1 a).
Both addition of 50 μM and 150 μM Azithromycin or Clarithromycin induced an irreversible decrease of the mean number of vesicles per slide within approximately a few hours (figure 3.1 c, d). The same concentrations of Aivlosin

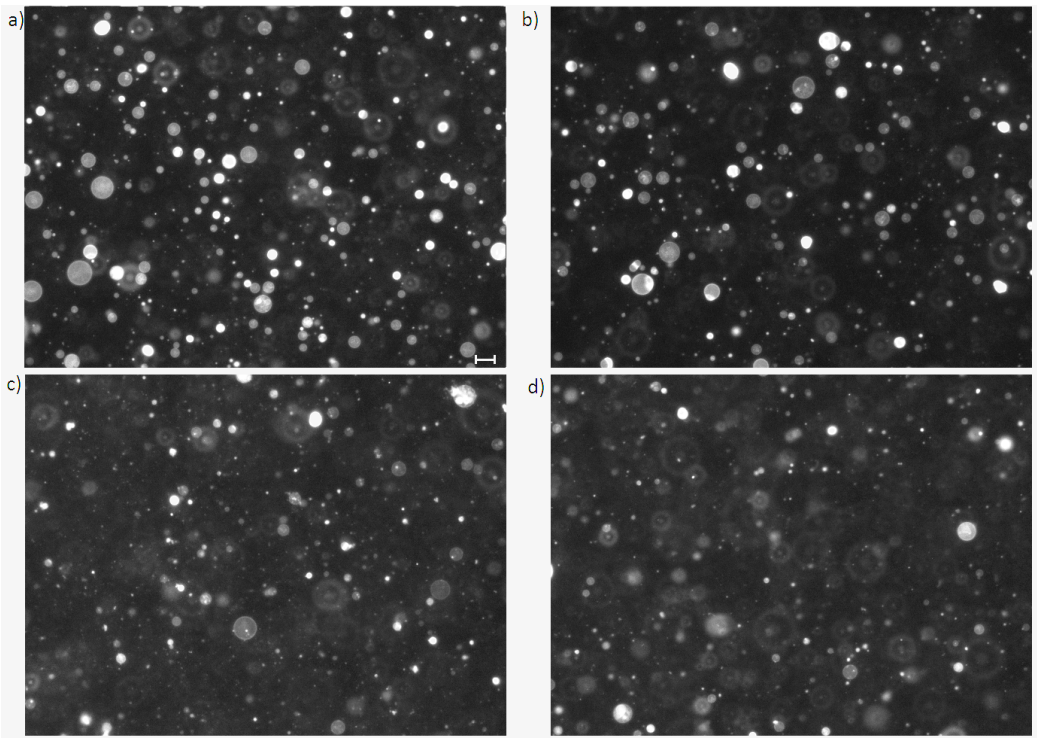

Figure 3.1: *Effect of Aivlosin, Azithromycin, and Clarithromycin on numerical density of GUVs. GUVs in these pictures were incubated for 1 day in a sucrose solution without (a) or with 150 μM Aivlosin (b), Azithromycin (c), and Clarithromycin (d). Scale bar = 20 μm.*

did not induce marked variation in the number of vesicles (figure 3.1 b), and so up to 400 μM. Instead, a clear vesicle number decrease was observed with Aivlosin concentrations of 800 μM (figure 3.2). Another effect of such high concentration of Aivlosin was the formation of clusters made of fluorescent material and small vesicles around normal-sized vesicles (this aspect will be described in detail in section 3.2).

Statistical analysis of size distributions at different incubation times (5 hours, 1 day, and 2 days, figure 3.3) confirmed that Azithromycin and Clarithromycin induced the loss of GUVs larger than 3 μm. The experimental sensitivity in the recognition of vesicles allowed one to reliably detect vesicles from pixels aggregates of $\sim$ 14 pixels^2 and above, that, with the conversion 1 μm = 1.4 pixels (valid for the 10x objective used in this part of work),

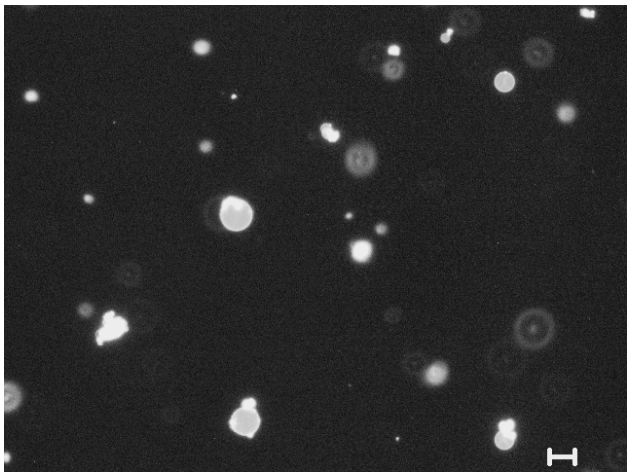

Figure 3.2: *Effect of Aivlosin 800 μM on numerical density of GUVs after one day of incubation in sucrose solution with Aivlosin. Scale bar = 20 μm*

corresponds to a projected area about 7 μm^2. This value of projected area corresponds to vesicles with diameter $\sim$ 3 μm, thus vesicles smaller than this value were not considered in fitting the size distibutions with Eq. (2.1).
Two parameters were calculated fitting Eq. (2.1): A, the prefactor of the exponential decay, and R_0, that can be considered as the characteristic size of each distribution.
Figure 3.3 shows that the effects of Azithromycin and Clarithromycin in reducing the number of vesicles were quantitatively similar, clearly distinct from that of Aivlosin: the normalized size distributions (distributions divided by the number of vesicles found in each sample) of vesicles treated with Azithromycin and Clarithromycin were both lower than control samples and those treated with Aivlosin, in a diameter range between 5 μm and $\sim$ 20 μm. Aivlosin 50 μM and 150 μM appeared not to reduce appreciably the number of vesicles, unless Aivlosin was at high concentration (800 μM). Highly concentrated Aivlosin was tested on a different set of vesicles and the corresponding size distributions are showed in figure 3.4. Two different slopes were found in these distributions, referring to ranges 3-6 μm and 7-20 μm, respectively. The distribution of Aivlosin 800 μM-treated GUVs of diameters larger than 6 μm was higher than that of control GUVs, due to the formation

	Range 1		Range 2	
	A	R_0 (μm)	A	R_0 (μm)
Control	0.38 ±0.09	5.15 ±0.09	0.15 ±0.04	7.5 ±0.6
Aivlosin 400 μM	0.42 ±0.04	4.8 ±0.3	0.14 ±0.08	7.9 ±1
Aivlosin 800 μM	0.21 ±0.05	7.2 ±2	0.14 ±0.08	11.5 ±3

Table 3.1: *Size distribution fitting parameters of control and highly-concentrated Aivlosin GUVs (errors between parenthesis). Range 1 refers to 3-6 μm, range 2 refers to 7-20 μm.*

of clusters. At the same time, the distribution of drug-treated GUVs in the first range was slightly lower, probably due to aggregation of smaller vesicles in clusters. The detection program was not modified to take into account the not-spherical shape of the clusters. Neverthless it was able to recognize the larger size of clusters, even with a little overestimation.

The fitting parameters A and R_0 (see table 3.1) were in agreement between control and Aivlosin 400 μM-treated GUVs, (differences both on A and R_0 within the error). Instead, a clear effect was observable when GUVs were treated with the highest concentration of Aivlosin: the mean size R_0 in both ranges was found to be higher than that of control GUVs, but this apparent size increase was due to the formation of vesicle clusters detected in the pictures.

There did not appear to be any consistent pattern in the size distribution of vesicles as a function of incubation time, and the differences in results between different incubation times were not statistically relevant. In practice the time necessary for the drugs to equilibrate in the phospholipid membranes should be of the order of seconds, depending on the drug molecule size and the thickness of the vesicle membrane. In addition, in [69], the release of small vesicles induced by Azithromycin was seen to occur within a few seconds of contact with the antibiotic (see 1.5.2). For this reason, it was decided to average over the three incubation times to produce more reliable statistics for the parameters of antibiotic type and concentration. The results of this averaging are presented in figure 3.5.

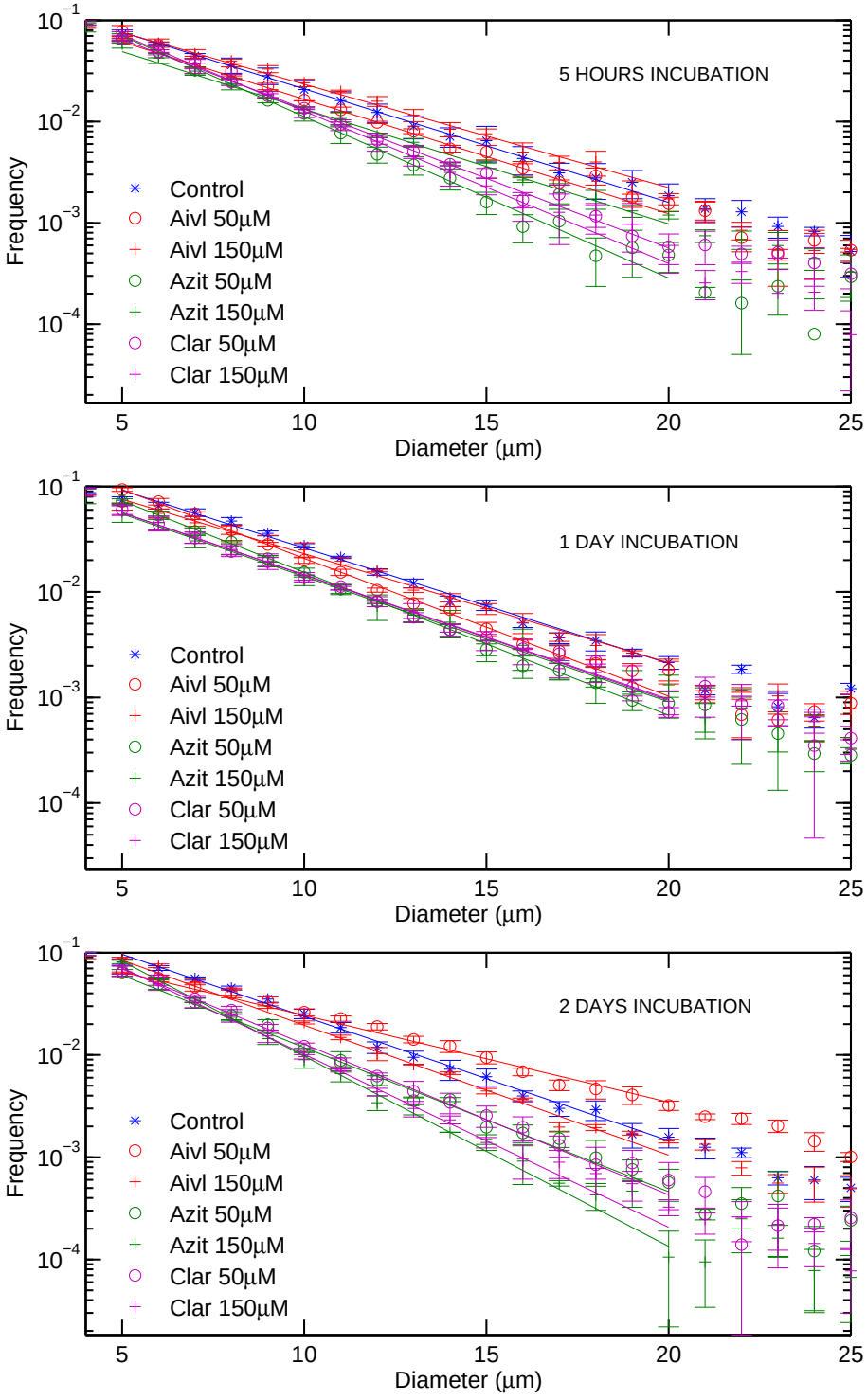

Figure 3.3: *Normalized size distributions of control and drug-treated GUVs at 5 hours (top), 1 day (centre), and 2 days (bottom) incubation in drug solution. Each size distribution was calculated on 90 GUVs. Azithromycin and Clarithromycin significantly altered the GUVs distributions, and the two different concentrations appeared to have the same effect. Aivlosin slightly affected the number of GUVs, and also here the highest concentration appeared to not have a clear effect on GUVs.*

Each distribution was obtained averaging over all the object detected in

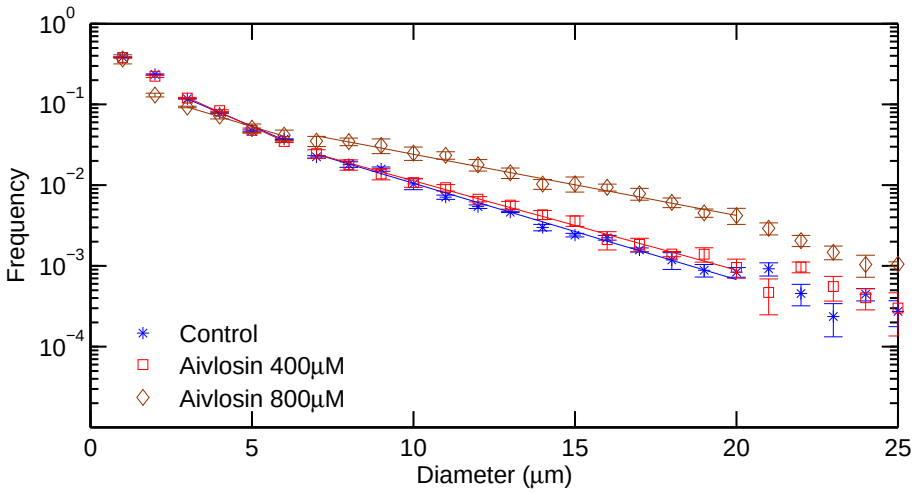

Figure 3.4: *Size distributions of control vesicles and GUVs treated with Aivlosin 400 µM and 800 µ M. Up to 400 µM the effect of Aivlosin on size distributions of GUVs is not accentuated. With 800 µM Aivlosin both a reduction of GUVs smaller than 6 µm and an increase of GUVs larger than 6 µm is observable in comparison with control GUVs. The increase of objects with large diameters is due to clusters formed specifically with high concentrations of Aivlosin (see section 3.2.)*

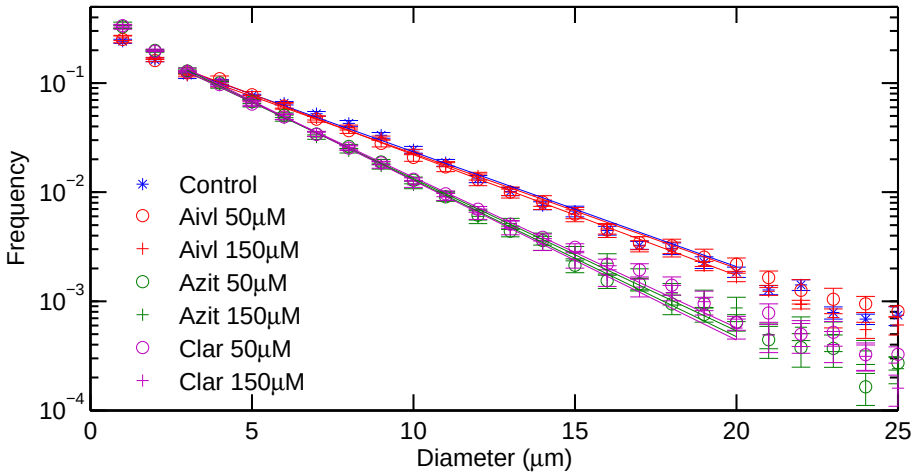

Figure 3.5: *Averaged size ditributions of GUVs treated with 50 µM and 150 µM Aivlosin, Azithromycin, and Clarithromycin. Distributions measured after 5 hours, 1 day, and 2 days incubation in drug solution were averaged together. Aivlosin showed to not have effect used in these concentrations. Azithromycin and Clarithromycin had a clear effect in reducing the distribution of GUVs.*

each sample: 149,000 (control), 116,000 (Aivlosin 50 μM), 97,600 (Aivlosin 150 μM), 84,900 (Azithromycin 50 μM), 101,600 (Azithromycin 150 μM), 92,900 (Clarithromycin 50 μM), 97,800 (Clarithromycin 150 μM). Objects detected with size larger than 3 μm (and, thus, actually associated to vesicles) were: 78,700 (control), 60,839 (Aivlosin 50 μM), 50,829 (Aivlosin 150 μM), 35,025 (Azithromycin 50 μM), 40,443 (Azithromycin 150 μM), 37,418 (Clarithromycin 50 μM), 39,625 (Clarithromycin 150 μM).

Figure 3.5 clearly shows two distinct size distribution behaviours: the mean diameter of vesicles treated with Azithromycin and Clarithromycin (50 μM) decreased by $\sim 20\%$ compared to the control. In addition, only Clarithromycin-treated vesicles showed a drug concentration dependent effect, with a decrease of mean diameter of $\sim 35\%$ in 150 μM Clarithromycin solutions compared to control. Aivlosin did not induce any observable effect at these concentrations.

The fitting parameters calculated from these averaged distributions are showed in table 3.2. Parameter A slightly changed over all the samples: control and Aivlosin-treated vesicles had the same parameter (about 0.26), but Azithromycin and Clarithromycin showed a small increase of A (to about 0.33). Due to the small increase of A and the uncertainty of data in the very first range of size distributions, the parameter A was considered unchanged over all the samples. A variation of parameter R_0 was observable as the drug was varied: the ineffectiveness of Aivlosin was confirmed from R_0, unchanged in comparison with that of control GUVs (about 8 μm). Azithromycin and Clarithromycin induced a reduction of this parameter to a value about 6 μm, so that a smaller characteristic size can be associated with the size distributions of GUVs treated with these two drugs. The drug concentration range studied in this work seemed to not induce effects detectable by this technique.

	A	R_0 (μm)
Control	0.29 ±0.04	7.8 ±0.4
Aivlosin 50 μM	0.27 ±0.04	7.9 ±0.6
Aivlosin 150 μM	0.27 ±0.03	8.0 ±0.4
Azithromycin 50 μM	0.36 ±0.04	6.1 ±0.3
Azithromycin 150 μM	0.32 ±0.07	6.2 ±0.5
Clarithromycin 50 μM	0.32 ±0.03	6.3 ±0.2
Clarithromycin 150 μM	0.36 ±0.06	5.0 ±0.4

Table 3.2: *Fitting parameters of size distributions of GUVs from figure 3.5 obtained by fitting with Eq.* (2.1). *Size distributions were averaged over different incubation times.*

3.2 Other effects of highly concentrated Aivlosin

The effects of high concentrations of Aivlosin on GUVs were also studied in this work.

The first effect (observed under suspension of GUVs in 800 μM Aivlosin solution, and up to 4 mM) was the formation of clusters around some large vesicles. These clusters were observed both by fluorescence and phase contrast microscopy. The first method showed these clusters as very bright areas around vesicles of usual brightness (figure 3.6, left panel). High magnification phase contrast microscopy (40x dry objective) revealed these clusters as made of many small vesicles stuck together around the surface of larger vesicles (figure 3.6, right panel). Combining high magnification with fluorescent mode, images of shining clusters were obtained, showing a round shape (figure 3.7): this confirmed the hypothesis of clusters essentially made of small vesicles. Most probably these structures were both made of small vesicles and phospholipids reassembled in multilayers.

Occasionally vesicles exposed to very high concentration of Aivlosin (4 mM) were found to undergo a kind of explosion. Round-shaped objects with uneven contour were found to stay all within the bottom plane of the observation chamber (figure 3.8m left panel): they were much thinner than normal vesicles of the same diameter, as a small change of focus moved them out

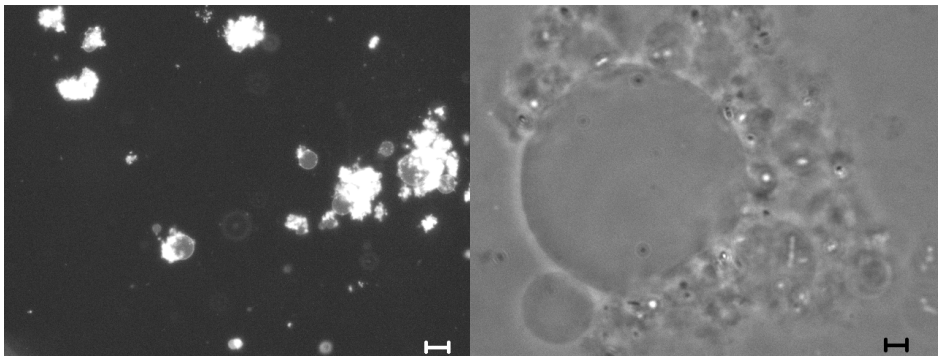

Figure 3.6: *Left panel: epifluorescence image of vesicles incubated in 2 mM Aivlosin solution for 4 days, showing bright clusters around normal-coloured vesicles. Scale bar = 20 μm. Right panel: phase contrast microscopy image at high magnification (40x objective) of vesicles incubated in 4 mM Aivlosin solution for 3 days. Scale bar = 5 μm.*

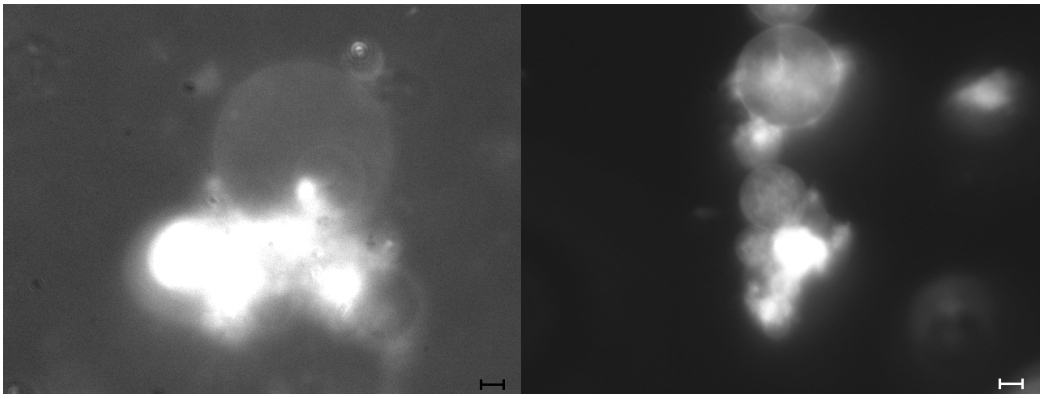

Figure 3.7: *Left panel: high magnification epifluorescence image of vesicles incubated in 4 mM Aivlosin solution for 3 days. Right panel: epifluorescence image of vesicles incubated in 800 μM Aivlosin solution for 1 day. In both the images the clusters are made of small vesicles attached to large vesicles. The clustering is not even around the vesicle. Scale bars = 5 μm*

of the image plane. Not all the vesicles subjected to this treatment showed this behaviour: some of them appeared as exploded, whereas some others maintained their spherical shape (figure 3.8, right panel).

A third effect induced by very concentrated Aivlosin was a loss of contrast. Phase contrast microscopy revealed that some vesicles, exposed for some time to the concentrated drug, progressively lost their contrast with the back-

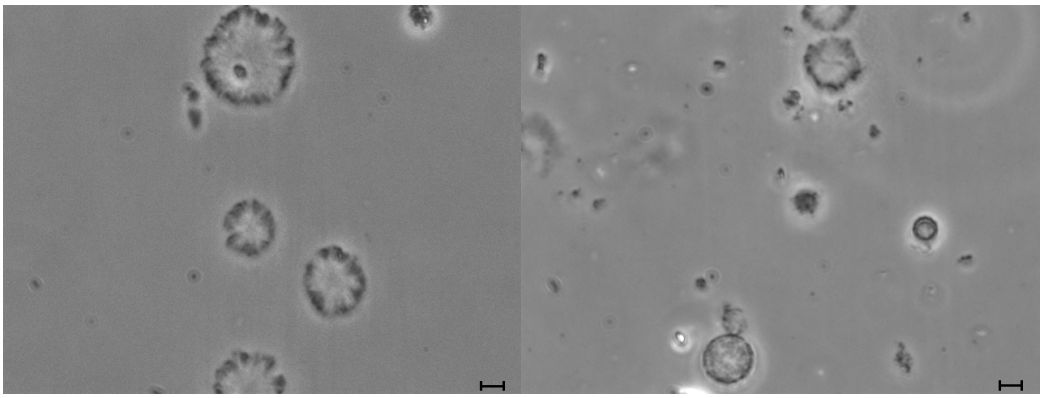

Figure 3.8: *Phase contrast microscopy images of GUVs incubated in 4 mM Aivlosin for 3 days. Left panel: exploded vesicles, showing uneven contour and round shape, indicating the size of the original vesicle. Right panel: not all the vesicles of the sample underwent this phenomenon. Scale bars = 5 μm.*

ground (figure 3.9). Not all the vesicles underwent this modification, and not all at the same time (figure 3.10). Tipical time-scale for loss of contrast observed here was few tens of seconds.

For each sample, pictures were taken at different height-steps from the slide. Small vesicles rising away several microns from the observation plane of the slide were observed. In some extent, this would explain a decrease in vesicle number, and would tie in well with the increased permeability of some vesicles. No quantitative measurements were performed to take into account this phenomenon.

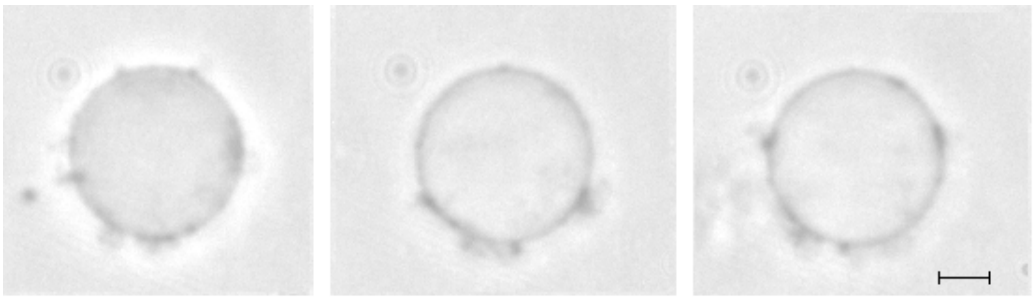

Figure 3.9: *Phase contrast image of vesicles incubated in 4 mM aivlosin solution for 1 day. From left to right, progressive loss of contrast between the internal volume of the vesicle (darker, due to the sucrose inside) and the brighter background (due to the glucose outside). Scale bar = 5 μm.*

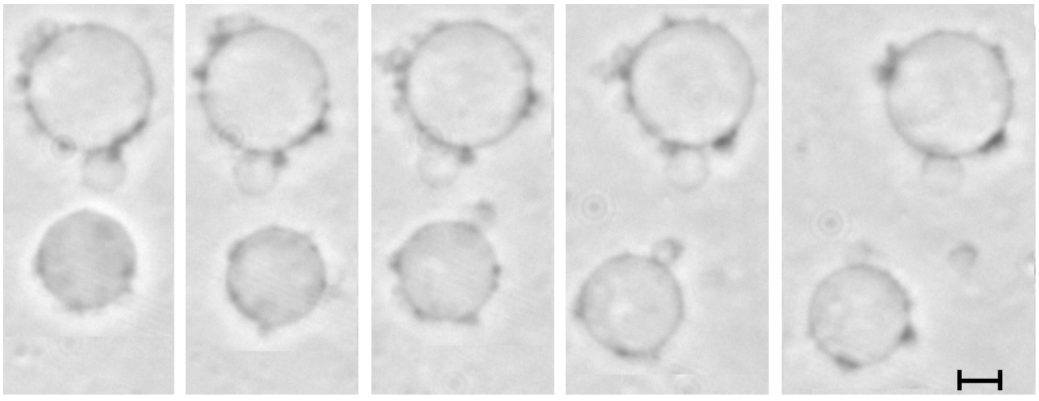

Figure 3.10: *Phase contrast image of vesicles incubated in 4 mM Aivlosin solution for 1 day. From left to right, progressive loss of contrast: it did not happen for all the vesicles, and at the same time for all the vesicles. Scale bar = 5 μm.*

3.3 Flickering analysis of GUVs

3.3.1 Effect of antibiotics on mechanical properties of GUVs

Statics

The bending rigidity modulus κ of vesicles has been measured by analysing fluctuation spectra: Eq. (1.14), based on a fluctuation spectrum in a planar geometry, was used to fit to the experimental mean-square amplitudes of

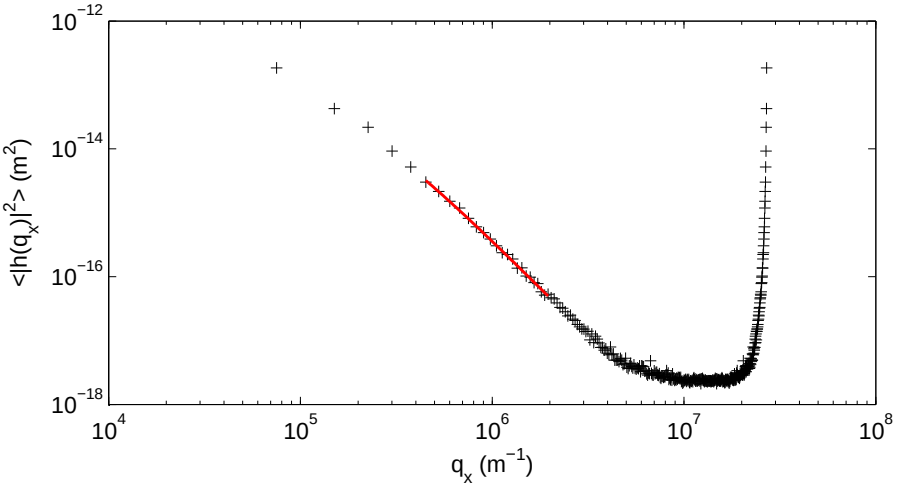

Figure 3.11: *Variation of the mean-square amplitude of contour fluctuations* $< |h(q_x)|^2 >$ *versus the wave vector* q_x *for a DOPC vesicle (radius = 13.3* μm*). The solid line corresponds to the fit of the data using Eq.* (1.14)*, with* $\kappa = 31.64 k_B T = 13.10 \times 10^{-20} J$*, and* $\sigma = 1.07 \times 10^{-8} N/m$*. Fitting range: 4* $\times$ 10^5 m^{-1} *-* 2×10^6 m^{-1} *(6th - 26th mode). The high-q region where the spectrum rises up is due to the sampling frequency and it is not relevant for the analysis purposes.*

contour fluctuations. To evaluate the fluctuation modes, the vesicle contour was discretized in 360 sectors.

Along with the bending rigidity modulus, the surface tension of the vesicles was calculated, these being the only fitting parameters. The fitting range was between the 6th mode and the mode corresponding to q = 2 $\times$ 10^6 m^{-1} (whose mode number therefore depended on vesicle radius a as $m_{max} = q_{max} a$): the first five modes were discarded, as explained in subsection 1.6.2. The fit quality was very good, as displayed in a typical example (figure 3.11).

Eq. (1.14) has limiting behaviours $< |h(q_x)|^2 > \sim q^{-1}$ for modes dominated by membrane tension ($\sigma \gg \kappa\ q_x^2$) and $< |h(q_x)|^2 > \sim q^{-3}$ for modes dominated by bending modulus ($\sigma \ll \kappa\ q_x^2$). The last behaviour is highlighted in figure 3.12, where the mean-square fluctuation amplitude has been multiplied by q^3: this clearly emphasizes the region where the q^{-3} slope exists, corresponding to the flat region in the spectrum. The fitting range is completely contained inside this region. The crossover between the two regimes clearly depends on the physical values of the two parameters, but also on

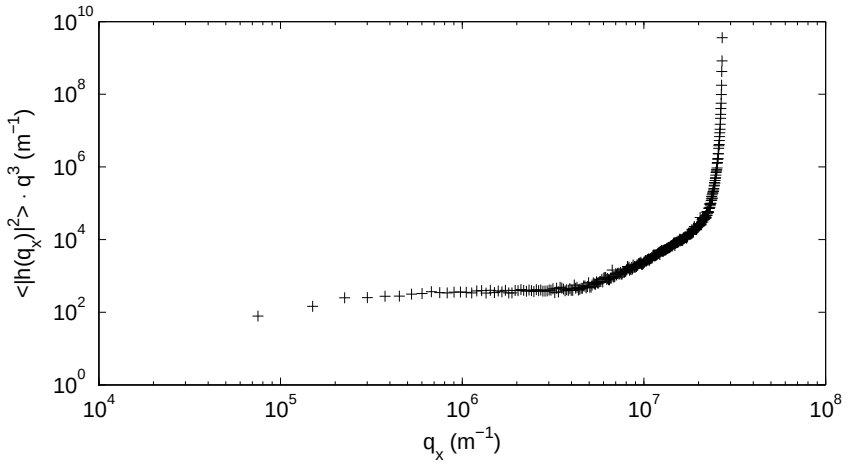

Figure 3.12: *Mean-square fluctuation amplitude multiplied by a q^3 factor for highlighting the q^{-3} limiting behaviour, distinctive of the bending-dominated modes (spectrum referring to the same vesicle of figure 3.11). The fitting range (4×10^5 m^{-1} - 2×10^6 m^{-1}) is all within the flat region and out of the region where data rise up (from 4×10^6 m^{-1}).*

the lengthscale. For sufficiently small wavelength fluctuations (large q) the bending modulus will always be the dominant constraint. The tension dominated regime at low q_x, instead, only extends over a few modes before the limit of $m_{min} = 6$ is reached. Therefore it is difficult to extract an accurate tension in this case, being the tension too small.

The bending modulus κ calculated experimentally for each vesicle were divided depending on the sample analysed from time to time (the same was done in the case of surface tension σ).

For each sample they were first plotted as function of the radius of the vesicle each one referred to. As can be seen in figure 3.13, there seems to be no clear relationship between κ and the vesicles radii. Similarly, no correlation with vesicle size was observed for the surface tension (data not shown). This allowed us to exlude any dependence of the bending modulus and surface tension on the size of the vesicles. This was a check on the consistency of our contour detection method, since mis-detection of contours would be expected to lead to such a dependence of the apparent bending modulus on the vesicle radius. For example, if the pixellation of the images had a significant effect

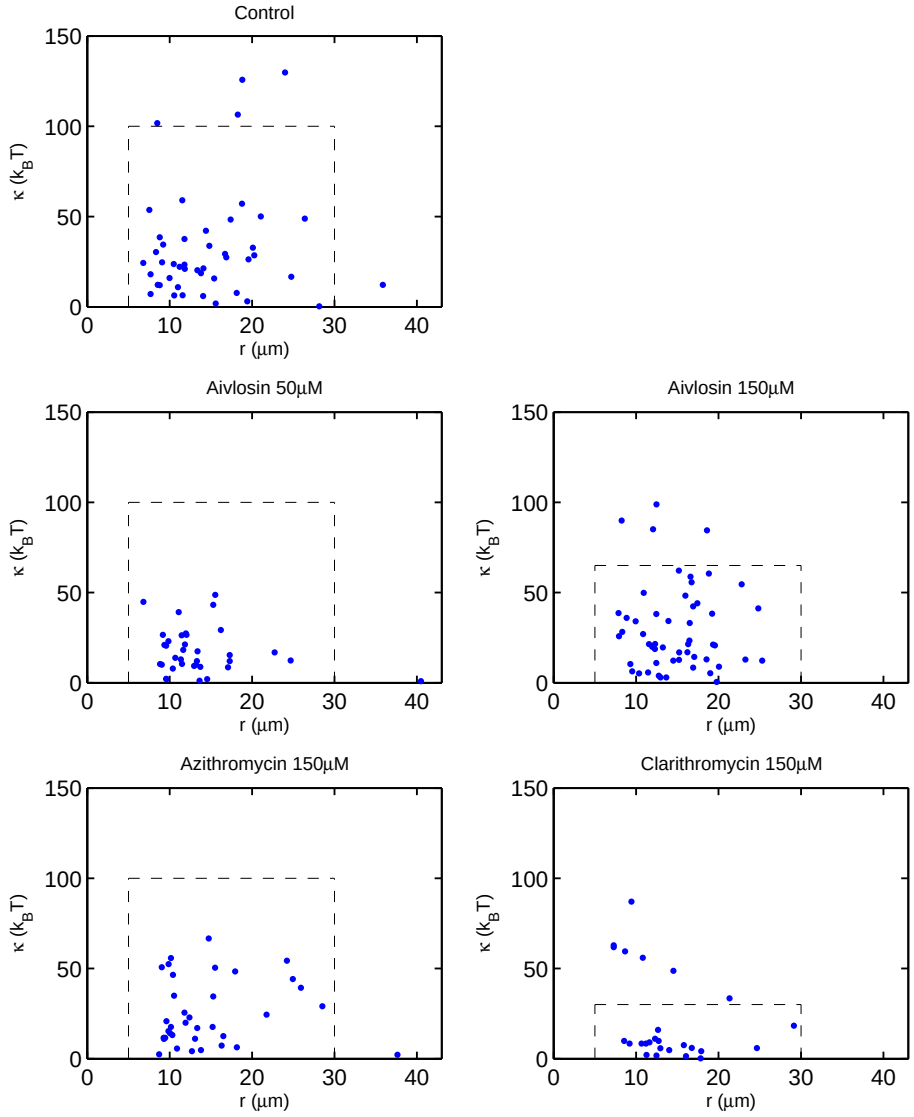

Figure 3.13: *Plot of κ versus radii of vesicles. Each marker corresponds to a different vesicle. The dashed boxes refer to the statistically relevant κ, that were actually used in considering the effect of the drugs on the GUVs membrane oscillations.*

on the apparent bending modulus, this effect would be most pronounced in smaller vesicles (see section 3.3.3).

In figure 3.13 the dashed boxes indicate the limits of the statistically relevant κ's: bending moduli outside the boxes were not used in the following discussion, because they were too high.

The fits of the experimental data produced bending moduli ranging between 0.23 k_BT and 66.67 k_BT, and tensions between 0.6 $\times$ 10^{-8} N/m and 86 $\times$ 10^{-8} N/m. Experimental error on κ of an individual vesicle was estimated to be about 8 k_BT: a single video was divided in three sets of frames, κ was calculated for each one, and their standard deviation was taken as error. The procedure was repeated with 10 vesicles, averaging the standard deviations. A distribution of κ was obtained for each sample: these distributions are shown in figure 3.14, in which the ordinate of the histogram gives the number of vesicles yielding the same κ-value. In general, the histograms show up as multi-peak gaussian distributions: a main peak centred on a minimum κ is followed by minor peaks centred on multiple values of the previous κ (this result was also found in [108]). As the larger values of κ are multiples of the minimum value, this leads to the conclusion that these groups correspond to vesicles with shells composed of multi-bilayers.

The distributions showed in figure 3.14 were fitted with multi-gaussian distributions. Each probability function was centered on the main κ of each distribution and on values two and three times the previous, according to the expressions:

$$G(\mu, \sigma_g) = \frac{1}{\sigma_g\sqrt{2\pi}} e^{\frac{-(x-\mu)^2}{2\sigma_g^2}}, \tag{3.1}$$

$$G_T = A \cdot G(\mu) + B \cdot G(2\mu) + C \cdot G(3\mu), \tag{3.2}$$

with mean μ ($\mu = \kappa_{mean}$), standard deviation σ_g, and weights A, B, C expressed using spherical coordinates (A = $(\sin(\theta) \cdot \cos(\phi))^2$, B = $(\sin(\theta) \cdot \sin(\phi))^2$, C = (1-A-B) = $\cos(\theta)^2$). Total number of free parameters in Eq. (3.2) is 7 (μ, σ_g, A, B, C, θ, ϕ).

In control and Clarithromycin-treated samples peaks at very high values of κ exist. Because the number of elements in these peaks is much lower than that in the main peaks, these values were discarded and a single gaussian function was used to fit to these data (free paramters: μ, σ_g). Discarded data are the same shown out of the dashed boxes in figure 3.13.

Mean values of κ and their standard deviations obtained by multi- (or single-)

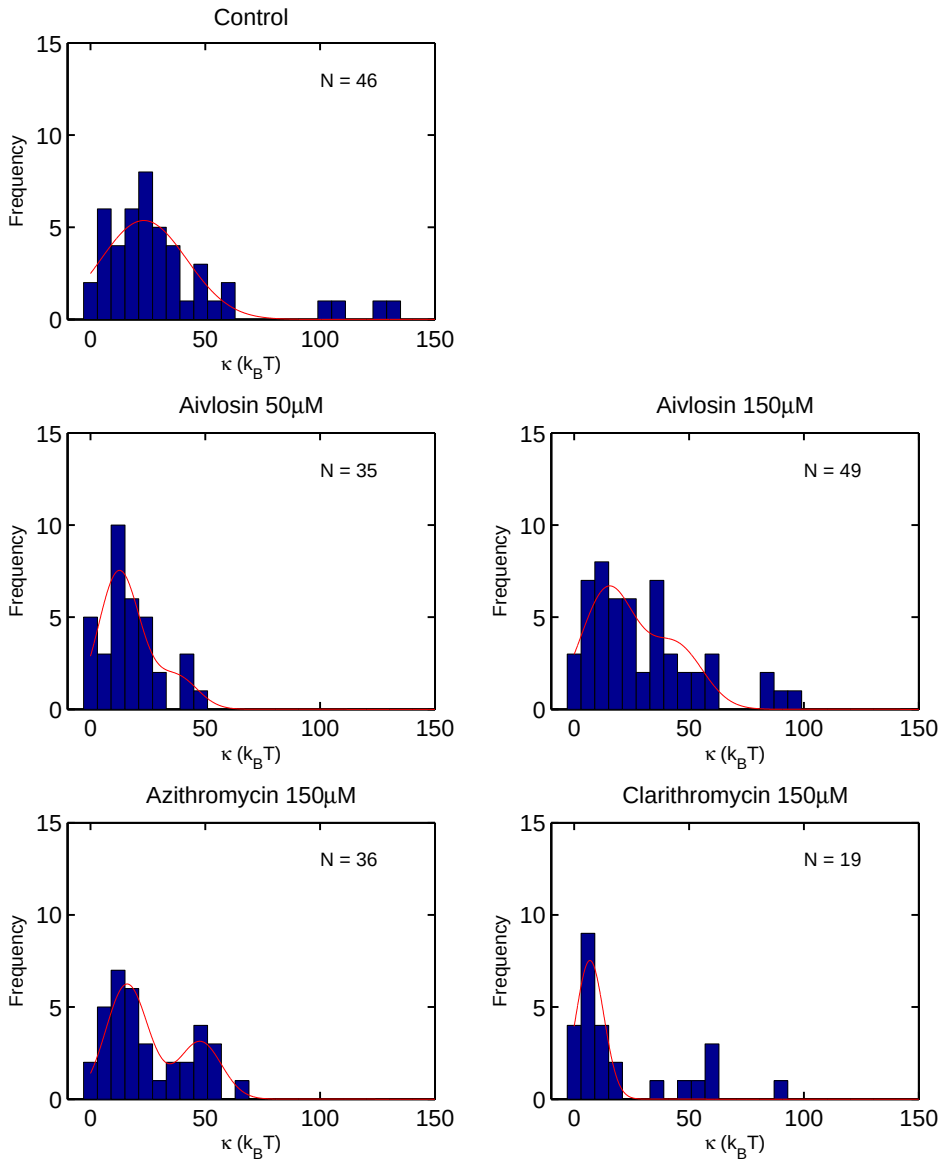

Figure 3.14: *Summary of κ values measured for DOPC GUVs by contour analysis. The ordinate of the histograms give the numbers of vesicles exhibiting the same bending elastic modulus. Red lines are fits of the distribution using Eq.* (3.2)*, showing that, in some cases, groups of κ exist at multiple values of the lowest κ. N is the number of vesicles in each histogram.*

gaussian fittings are shown in table 3.3. In control vesicles the mean value of κ from the only peak considered was found to be 23.2 k_BT, about the double

of those found in vesicles treated with Aivlosin 50 μM and 150 μM (12.5 k_BT and 14.8 k_BT, respectively). Aivlosin 50 μM distribution shows also a minor peak centred on a value of κ three times the main one (37.5 k_BT), and the corresponding weights are A = 0.81, C = 0.19. Aivlosin 150 μM and Azithromycin 150 μM distributions show the same behaviour, with a lower peak centred on a κ three times the main one (44.4 k_BT and 47.7 k_BT), and A = 0.66, C = 0.34, and A = 0.67, C = 0.33, respectively. Clarithromycin 150 μM shows a single narrow peak centred on 6.9 k_BT.

Fitting parameters obtained by Eq. (3.2) are shown in table 3.3. Interestingly, the data seem to suggest that triple-bilayer vesicles are induced after exposition to some drugs (Aivlosin and Azithromycin). Control vesicles and Clarithromycin-treated vesicles seem to show only single-bilayer shells.

It seems to be typical of these studies that the experimental error of the bending rigidity for an individual vesicle (here about 8 k_BT) is smaller than the scatter of the results for different vesicles (here indicated with σ_g). In general, the half width of the distribution is more than a third of its mean value [109][110][111][112].

	κ_{mean} (k_BT)	$\delta\kappa$ (k_BT)	σ_g	A	B	C
Control	23.2	10.5	18.7	1	0	0
Aivlosin 50 μM	12.5	4.3	9	0.81	0	0.19
Aivlosin 150 μM	14.8	4.2	11.8	0.66	0	0.34
Azithromycin 150 μM	15.9	2.8	9.2	0.67	0	0.33
Clarithromycin 150 μM	6.9	3.2	6.0	1	0	0

Table 3.3: *Mean values of κ calculated fitting histograms in fig. 3.14 by Eq.* (3.2). *$\delta\kappa$ is the uncertainty on κ_{mean}, σ_g is the width of main peak. All B parameters come from fitting.*

Dynamics

In this work the mode dynamics was used as an alternative way to get information about the bending modulus of vesicles.
According to section 1.6.4, in the high frequency, planar approximation Eq. (1.33) allows to relate the bending modulus κ of the membrane with the Power Spectral Density (PSD). κ can be obtained as the only fitting parameter of the PSD, assuming constant the viscosity (10^{-3} Pa $\cdot$ s). Figure 3.16 shows a typical example of PSD, fitted with Eq. (1.33). Using the full expression for the PSD, Eq. (1.32), an analogous fit was obtained (not shown).

Unfortunately, the bending modulus calculated with the static approach and that obtained with this procedure are not in agreement. In the last case, in fact, the bending moduli calculated fitting the PSD both by Eqs. (1.33) and (1.32) in the range 3-50 Hz are much lower (80%) than the corresponding values found from the statics, which are more reliable and in agreement with previous work.
A visual test of the actual slope of the PSD is shown in figure 3.16, where the

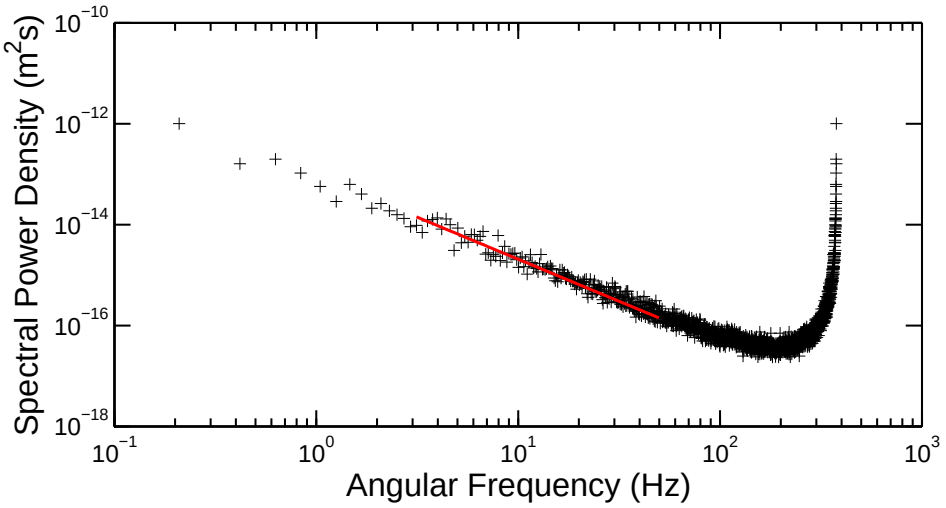

Figure 3.15: *Power Spectral Density (PSD), fitted in the range 3-50 Hz with Eq.* (1.33) *and Eq.* (1.32) *(not shown). In this example the κ's obtained are 5.68 k_BT and 4.69 k_BT, respectively. κ calculated from statics for the same vesiscle was 31.74 k_BT.*

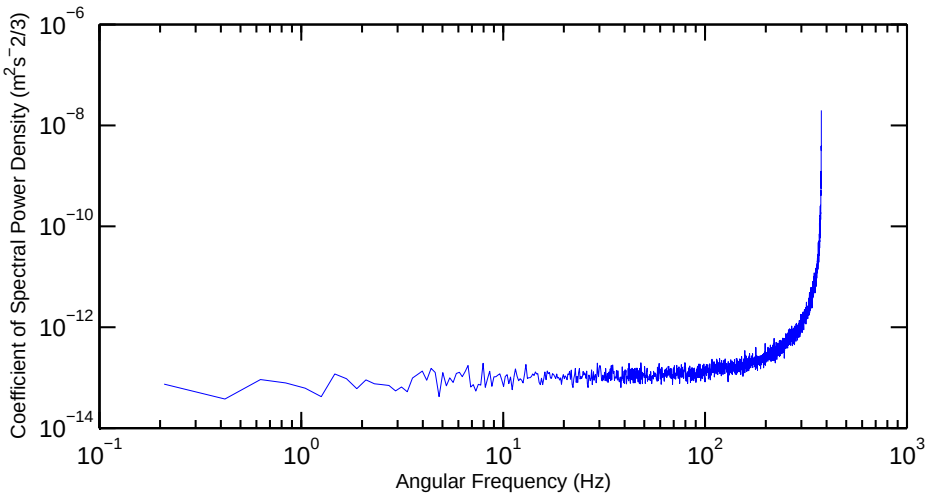

Figure 3.16: *Coefficient of spectral density, obtained multiplying the PSD by the angular frequency raised to 5/3. The flat region, that extends up to 50-70 Hz indicates the area in which the limiting behaviour described by Eq.* (1.33) *is valid.*

PSD has been multiplied by the angular frequency raised to 5/3. This allows to clearly see the region in which the proportionality between the PDS and $\omega^{-5/3}$ is valid: the curve is mostly flat up to 50-70 Hz.

There is no clear explanation on why the dynamic approach does not allow to obtain a reasonable value of κ. More study of this aspect is needed to better understand this phenomenon.

3.3.2 Effect of spatial sampling

The aim of this short paragraph is to justify the number of sectors (360) used to discretize the vesicle contour. Choosing the correct number of sectors involves to take care about oversampling and averaging effects.

A vesicle with radius 25.9 μm was used to test this effect. Eight different numbers of sampling angles were used (92, 120, 160, 200, 280, 360, 400, 480), and one value of κ and σ were calculated at each number of sampling angles using the model described by Eq. (1.14).

Increasing the number of sampling angles allows one to have information

up to higher q values (i.e., it is possible to detect modes with smaller wavelengths). Figure 3.17 shows as the increase of angle number makes measurable modes at q higher and higer. One effect of a short region in which mode amplitudes are accessible, as with low number of angles, is that the fitting range ends in the region where the effect of the limited resolution takes place. This makes the analysis unsuitable and underestimated values of κ and σ (ten times lower than the real value) are obtained. Higher number of angles extend the static spectrum ensuring the fitting range to be out of the region where noise becomes relevant (see figure 3.18).

As the number of angles increases, the values of κ seem to increase, leveling off to a constant value ten times higher than the value at low number of angles. Analogously, also σ showed a dependence from the number of angles, leveling off at a value 15% lower than the value at low number of angles. κ and σ appear to level off above approximately 300 angles (figure 3.19, top panel). A similar behaviour was observed analysing a smaller vesicle (radius

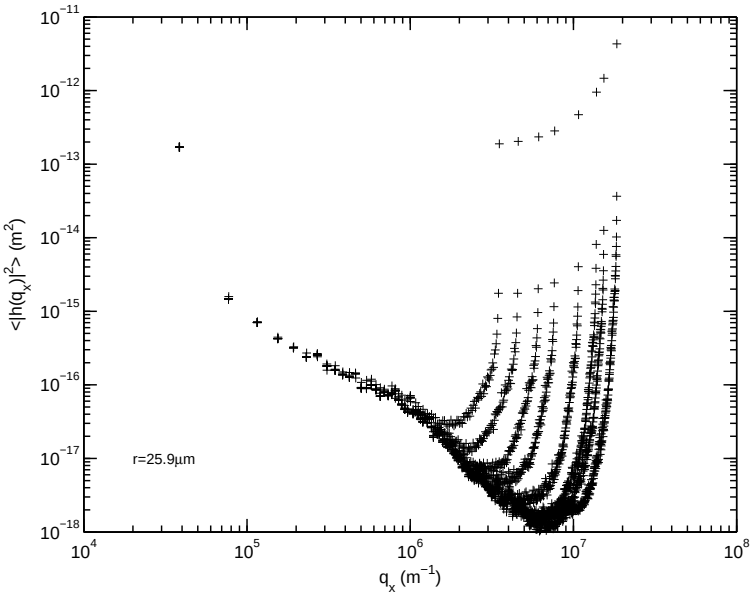

Figure 3.17: *Static spectra calculated for a single vesicle (radius = 25.9 μm) with different numbers of sampling angles (92,120,160,200,280,360,400,480). The image resolution was 0.184 μm/pixel.*

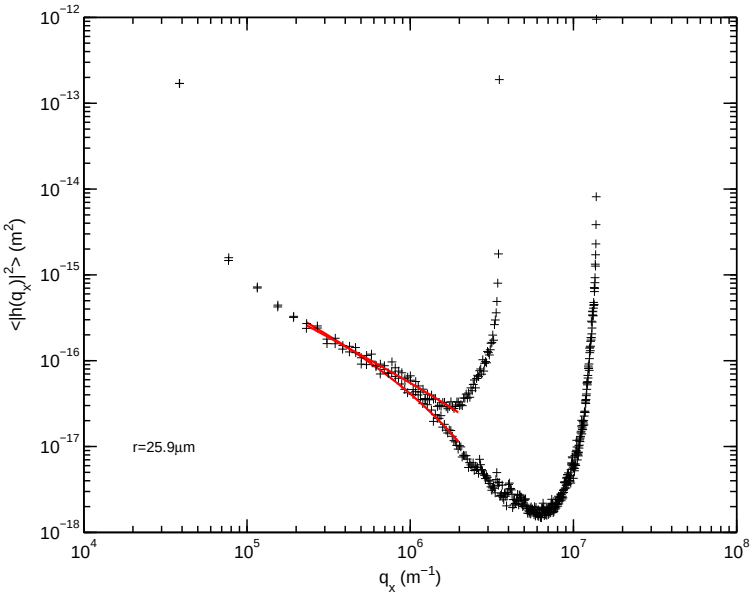

Figure 3.18: *Fitting range for a single vesicle (radius = 25.9 μm) with different numbers of sampling angles (92 360). At low numbers the fitting range falls within the region where the limited resolution is relevant. Higher numbers allow the fitting range to be out of this region, making the calculation of the mechanical parameters of the vesicle more accurated.*

= 9.8 μm), but in this case the plateau already appeared at 120 angles and the differences between mechanical parameters at low and high number of angles was not as high as for the large vesicle (figure 3.19, bottom panel). Thus, to avoid any dependence of κ from the number of angles, 360 was chosen to be the number of sampling sectors.

Sampling the contours with too many angles could lead to oversampling effects. The vertical dashed lines in figure 3.19 indicate the number of angles for which integer numbers of pixels were contained in each sector. For the large vesicle, with 360 angles more than 2 pixels were contained in each sector, 1 pixel corresponding to $\sim$ 850 pixel (top panel). For the small vesicle, with 360 angles about 1 pixel was inside each sector (bottom panel). To avoid oversampling in small vesicles, the contour was sampled ensuring at least on pixel for each sector. Thus, the contour of all vesicles was sampled in 360 sectors.

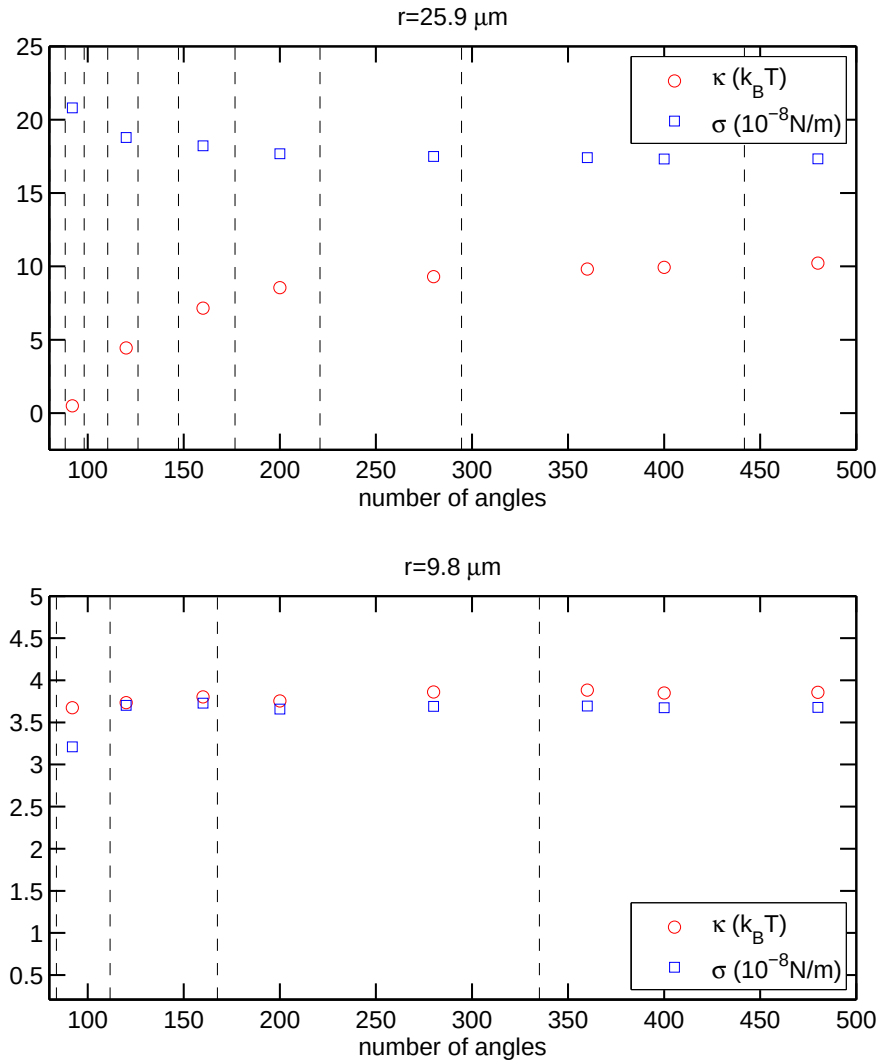

Figure 3.19: *Values of κ and σ calculated from two different vesicles with radii 25.9 µm (top panel) and 9.8 µm (bottom panel), respectively. Number of sampling angles used were 92,120,160,200,280,360,400,480. Vertical dashed lines indicate the number of angles for which integer numbers of pixels are contained in each sector.*

3.3.3 Pixellation effect on the static spectra

As described in section 1.6.5, the mean square amplitudes actually observed are scaled by a $\mathrm{sinc}^6(\frac{qa}{2})$ factor in comparison with the theoretical amplitudes.

The effect of this factor on the spectrum is shown in figure 3.20. The behaviour of the spectra is absolutely similar at low wavevectors, that is the range used to obtain the mechanical parameters of the membrane. Differences rise at high wavevectors.

The mechanical parameters obtained considering the $\mathrm{sinc}^6(\frac{qa}{2})$ factor are listed in table 3.4. The results without the pixellation effect are also reported.

The difference between the mechanical parameters obtained in the two cases was of the order of the 4%. Anyway the pixellation effect was considered in the data analysis.

	vesicle 1		vesicle 2	
	κ	σ	κ	σ
sinc^6 factor	54.3	23.0	16.9	10.2
no sinc^6 factor	56.3	22.8	17.47	10.1

Table 3.4: *Mechanical parameters obtained with and without the* sinc^6 *factor in the observed spectra of two vesicles: vesicle 1, radius = 11 μm (spectrum not shown), and vesicle 2, radius = 17 μm (spectrum in fig. 3.20).*

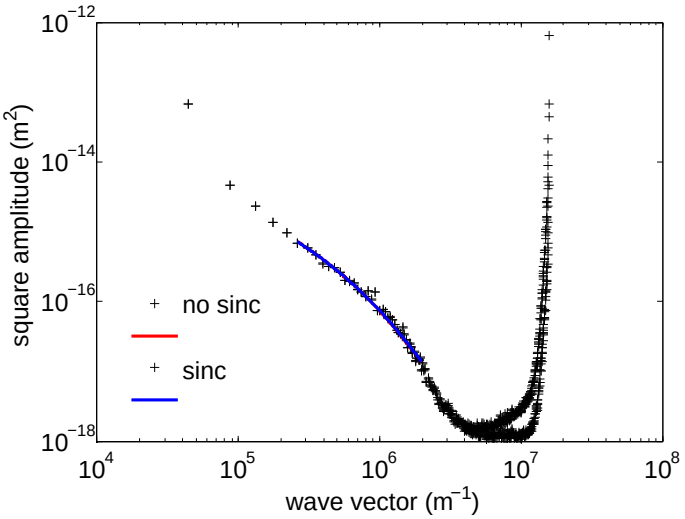

Figure 3.20: *Example of pixellation effect on the shape of static spectrum of a vesicle (radius = 17 μm). The spectrum fitted with red line was obtained without considering the pixellation effect, and that fitted with blue line resulted from considering it. The two fitting lines are completely superimposed and only one (blue) is visible.*

3.4 Langmuir monolayers of phospholipid

3.4.1 DPPC monolayers

3.4.1.1 Π-A isotherm

The isotherm of DPPC monolayer was first measured to find the working limits of surface pressure that can be applied to the film without its rupture. Then the effect of exposition to Aivlosin and Clarithromycin on the isotherm was studied.

For pure DPPC monolayers a structural polymorphism was observed as a function of surface pressure (figure 3.21). The Π-A isotherm presented three distinct regions: a liquid-expanded (LE) phase at low surface pressures, a first-order phase transition - the intermediate region of surface pressures - between LC and LE structures (this structure is observed at $\Pi > 9$mN/m), and the LC structure (at $\Pi > 30$mN/m). Finally, the monolayer collapsed at a surface pressure higher than the collapse pressure ($\Pi_e \approx$ 46-49mN/m).

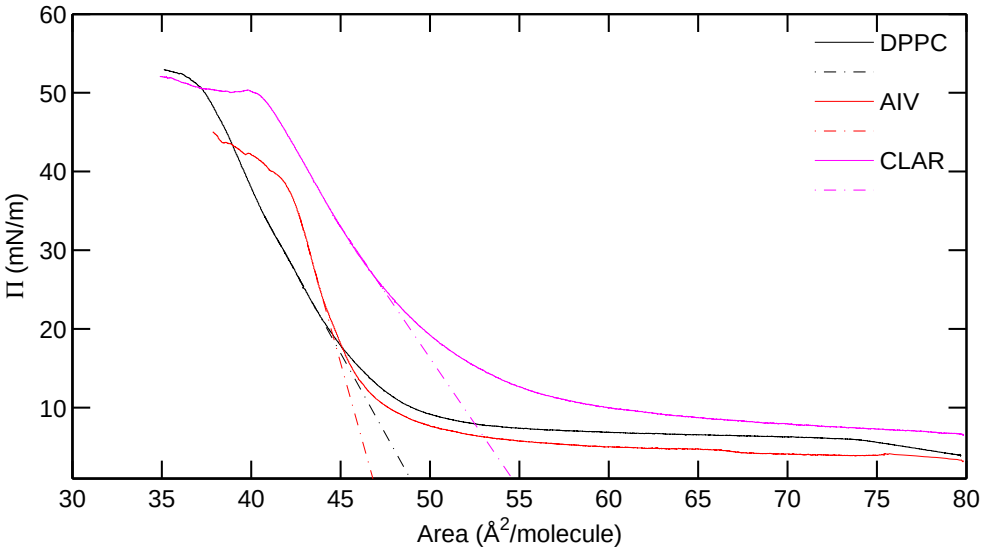

Figure 3.21: Π-*A isotherms of DPPC monolayers: control (DPPC on subphase with no drug) and films exposed to Aivlosin 50 μM and Clarithromycin 50 μM are shown. Limit areas per molecule for LC phase are extrapolated by intersecting the linear region of LC with area-axis (dashed lines).*

The range of surface pressure in which the film is in a condensed phase falls between 20 mN/m and 50 mN/m. At pressures lower than 20 mN/m the film displays a much looser molecular packing than real membranes. This regime is therefore of little interest to the present study. Accordingly, in this work the range 25 - 45 mN/m was chosen for the following ISR measurements with control DPPC monolayers.

Aivlosin reduced the collapse pressure of the monolayer below 40 mN/m. It has been possible to analyse the film in the surface pressure range 15 - 30 mN/m. Clarithromycin did not modify the collapse pressure of the DPPC film. The surface pressure range studied in the ISR experiments for this sample was the same of control film (25 - 45 mN/m). Azithromycin (whose isotherm is not shown here) stabilized the DPPC film up to 50 mN/m. The range studied in this case was 30 - 50 mN/m, because the measurement performed at lower Π (25 mN/m) resulted too noisy for unknown reason.
From the isotherm the mean area per molecule for the LC phase can be calculated, by extrapolation to $\Pi = 0$. Control monolayer shows a limit area around 49 $\mathring{A}^2$/molecule (figure 3.21). Monolayer exposed to Aivlosin

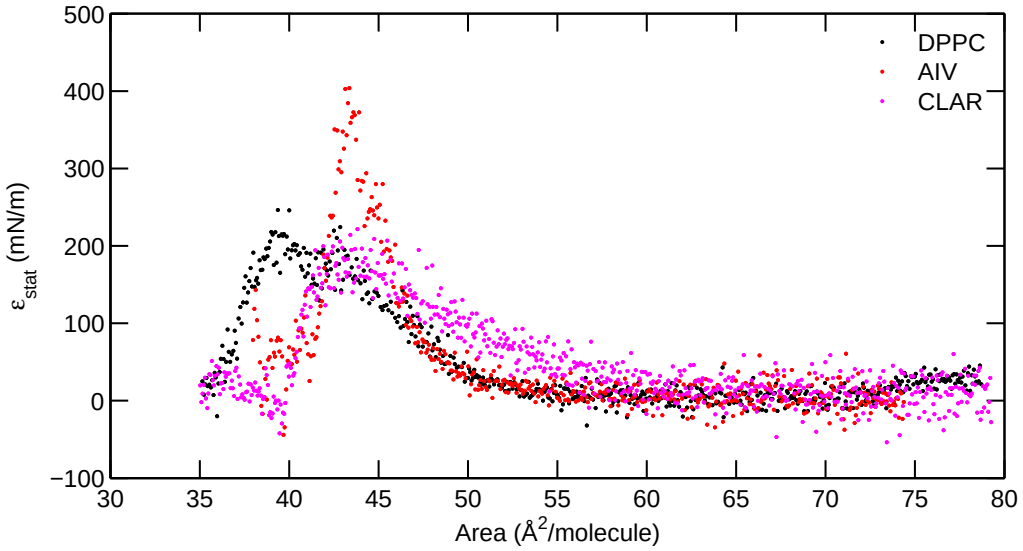

Figure 3.22: *Compressibility moduli of control and antibiotic-treated monolayers.*

50 μM and Clarithromycin 50 μM show limit areas 47 $\AA^2$/molecule and 55 $\AA^2$/molecule, respectively (accuracy about 1-2 $\AA$. Interestingly, after exposition to Clarithromycin the isotherm increases more gently than control, further than showing an increase of the limit area.

3.4.1.2 Compressibility modulus

The Π-A isotherm of DPPC monolayer allows one to calculate the compressibility modulus of the film. The compressibility modulus of the monolayer is a measure of the film resistance to a change in area and can be calculated directly from the slope of the Π-A isotherm at constant temperature as $\epsilon_{stat} = -A \cdot d\Pi/dA$, where A is area per molecule and Π is surface pressure. The monolayer is less compressible in the condensed state than in the liquid expanded state. Upon further compression one typically observes a kink on the isotherm, corresponding to a peak in the compressibility. The compression modulus decreases further after the kink due to film collapse. The kink was first observed and treated as a phase transition by [113].

The compressibility modulus for control and antibiotic-treated film is shown

in figure 3.22. A peak is visible, whose position and height can vary depending on the drug used: control film shows a peak centred around 40 $\mathring{A}^2$/molecule with height 220 mN/m (in quantitative agreement with previous works [114] [115]. Clarithromycin induced a shift of the peak position, which was centred around 44 $\mathring{A}^2$/molecule), but did not vary its height. Aivlosin, instead, substantially left unchanged the peak position but increased its height to 370 mN/m.

3.4.1.3 ISR measurements of pure DPPC

A first set of measurements was performed to check the mechanical properties of pure DPPC monolayer, and to compare with the literature the effect of compression on its rheological properties.
The increase of surface pressure Π in the DPPC monolayer, from 25 mN/m to 45 mN/m, induced a reduction of the stress-strain amplitude ratio (figure 3.23, left panel).
Looking at the frequency dependence for a given value of the surface pressure, at low frequencies the film did not follow very fast the perturbation, with a high phase delay (about 90°), indipendent from the surface pressure. Differences between films at several surface pressures rose at high frequencies. The response to the oscillating stress was more and more faster (i.e, approaching to zero) as the film became more compact (figure 3.23, right panel).

The orders of magnitude of the shear moduli measured in this work are in agreement with literature [117] [118], even if slightly higher values were obtained here (about three times, comparing with previous data at 1 Hz = 6.28 rad/s and 35 mN/m).
As usual, the compression of the film induced its stiffening, as showed by the increasing values of G' and G" at surface pressures higher and higher (figure 3.24).

At given surface pressure the shear moduli showed two distinct regions. At low frequencies (0.5 - 5 rad/s) G" was dominant; at high frequencies a crossover between the two moduli was observable, above which the elastic modulus was dominant.
The effect of raising the surface pressure was the shift of the crossover to lower frequencies. At low surface pressures the crossover was out of the experimentally accessed frequency range and it was not visible. It became accessible at surface pressure 35 mN/m: it shifted from about 22 rad/s to 18 rad/s to 12 rad/s going from 35 mN/m to 45 mN/m (see table 3.6).
The mainly viscous character of DPPC film at low frequencies was first quantitatively studied here by fitting G" in this range with a power law as:

$$G" = A \cdot \omega^{\alpha}. \tag{3.3}$$

The fitting parameters α obtained at each surface pressure are reported in table 3.5. It can be seen as the exponents of the fit reasonably approximate to unity over all the working pressures. This induced us to treat the film as

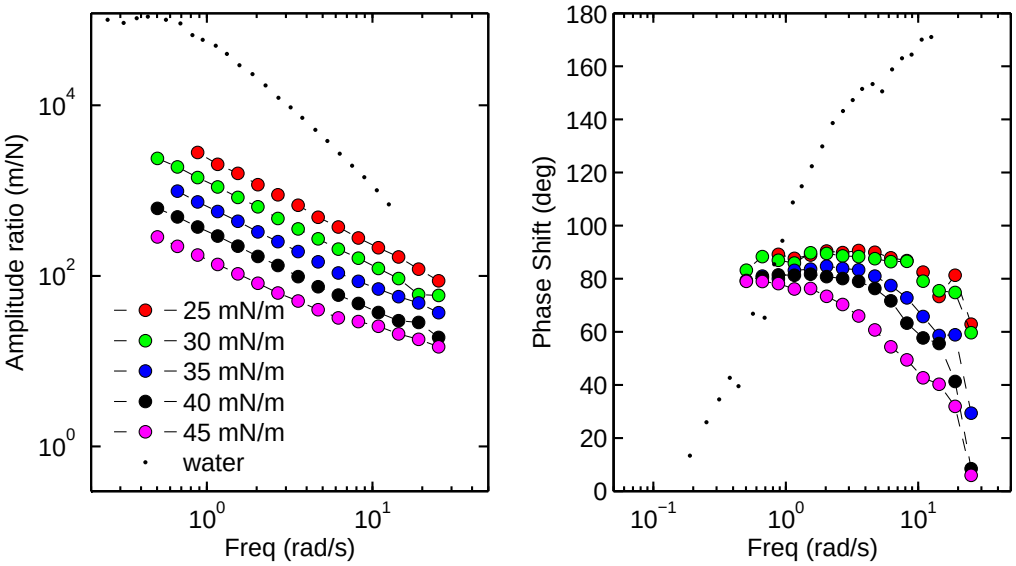

Figure 3.23: *Different behaviours of a DPPC Langmuir film at several surface pressures. Left panel: increasing surface pressure induces a reduction of amplitude ratio. Right panel: phase shift depends on frequency perturbation and film surface pressure. Black curves refer to water signal.*

	25 mN/m	30 mN/m	35 mN/m	40 mN/m	45 mN/m
α	1.02	0.98	0.98	0.95	0.84

Table 3.5: *Summary of exponents α obtained by fitting with Eq.* (3.3) *the low-frequency regime of G" of control monolayer. Being all reasonably close to unity, they show the Newtonian behaviour of DPPC film.*

a Newtonian system. Fits of the low-frequency range of G" with Eq. (1.44) are shown in figure 3.24.
The Newtonian model allows one to obtain information on dynamic viscosity of the monolayer, and on how it is modified by varying the surface pressure of film and interacting with antibiotics. For DPPC control monolayer, dynamic viscosities ranging between 40 - 600 μNs/m were obtained (see table 3.7). Dynamic viscosity was found to lie in the range 40 - 600 μNs/m, in good agreement with data in literature [118] (where data were measured at pH between 5 and 7; pH 6.3 was used for all DPPC monolayers studied in this work). Interestingly, a linear variation of viscosity with surface pressure was found, again in agreement with [118]. In particular, viscosity roughly doubled at each increasing surface pressure analysed.

3.4.1.4 Drug effects on the visco-elasticity of DPPC monolayer

G' and G" versus omega The visco-elastic nature of the DPPC film was preserved after adding drugs to the subphase.

Azithromycin 35 μM stabilized the film up to surface pressure 50 mN/m, and made the measurement at 25 mN/m too noisy to be used. The frequency range analysed was 0.5-25 rad/s (figure 3.25): at 35 mN/m the crossover appeared at about 20 rad/s, being shifted to 15.5 rad/s, 10 rad/s, and 7 rad/s at 40 mN/m, 45 mN/m, 50 mN/m, respectively (table 3.6). At low frequencies the film was well described by the Newtonian model, with a linear dependence from frequency as indicated in figure 3.25. Dynamic viscosity of

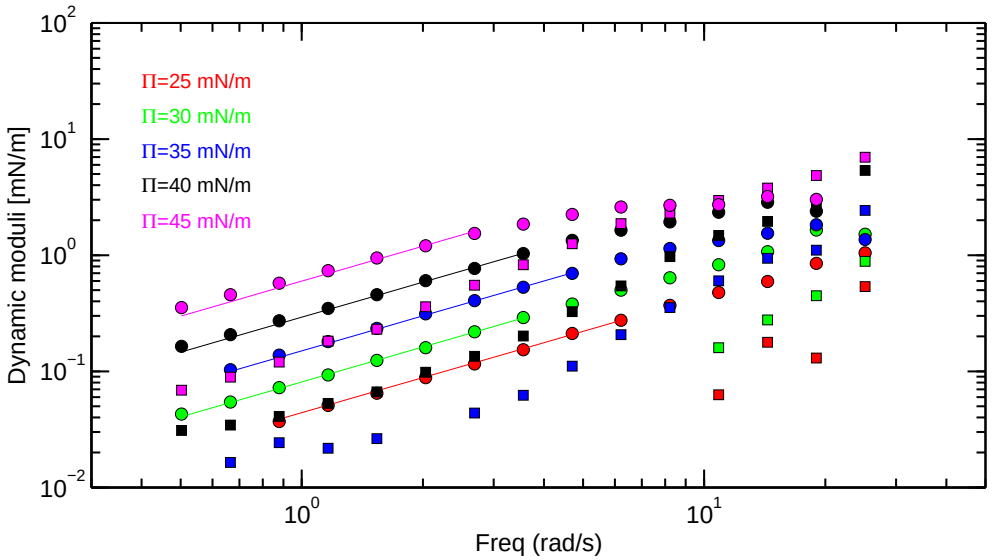

Figure 3.24: *Elastic (squares) and viscous (circles) part of shear modulus in untreated DPPC monolayer. At low frequencies viscous part dominates, with a crossover to the elastic regime at high frequencies. Fits of low-frequency range of G" with Newtonian model are shown.*

Azithromycin-treated film was found to range between 62 - 850 μNs/m (see table 3.7), increasing with pressure. In this sample was also found a doubling of viscosity by increase of 5 mN/m of surface pressure analysed. Very high

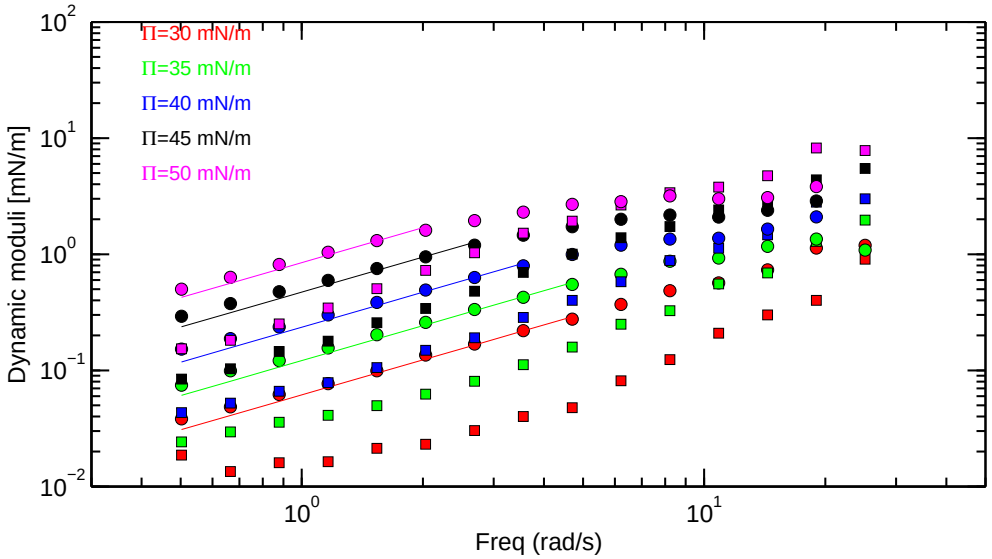

Figure 3.25: *Elastic (squares) and viscous (circles) part of shear modulus of DPPC film after adding Azithromycin 35 μM.*

values of viscosity at high pressures probably indicate a poorer adherence of the Newtonian model to the system.

Similarly, Clarithromycin 50 μM induced a crossover shift to lower frequencies (figure 3.26). The crossover started to be detectable at about 25 rad/s with a surface pressure 30 mN/m. Progressive increase of surface pressure

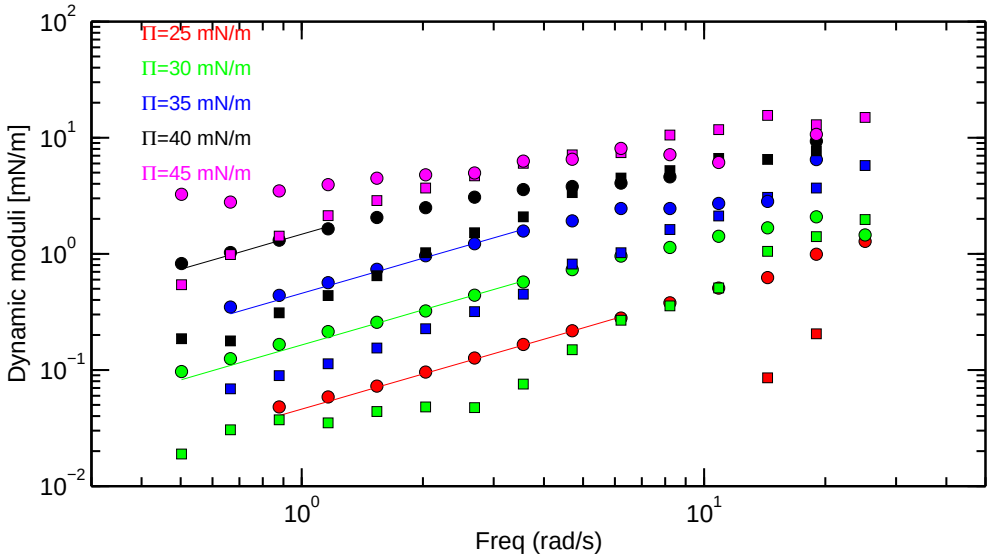

Figure 3.26: *Elastic (squares) and viscous (circles) part of shear modulus of DPPC film after adding Clarithromycin 50 μM.*

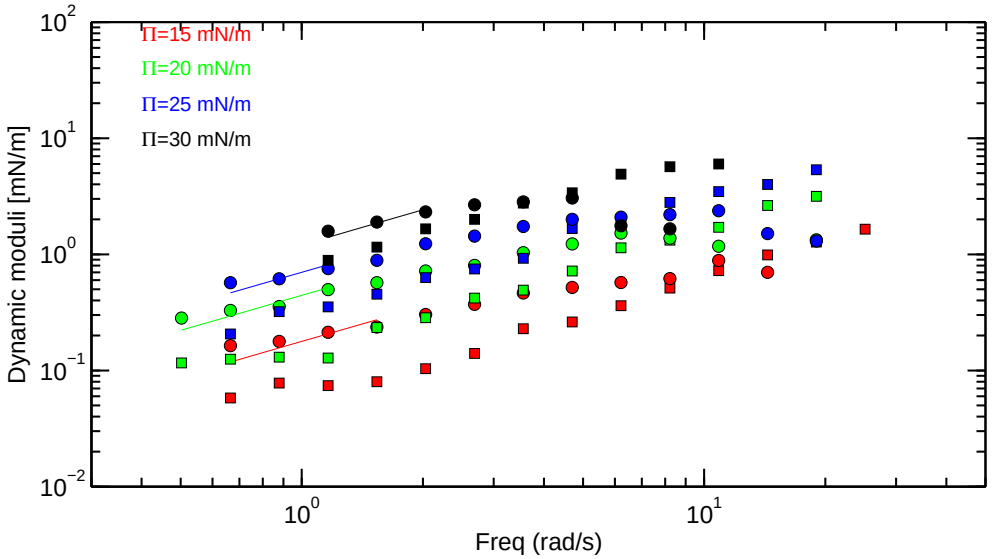

Figure 3.27: *Elastic (squares) and viscous (circles) part of shear modulus of DPPC film after adding Aivlosin 50 μM.*

	Control (rad/s)	Aivlosin (rad/s)	Azithromycin (rad/s)	Clarithromycin (rad/s)
15 mN/m		12.6		
20 mN/m		8.2		
25 mN/m	-	6.6		-
30 mN/m	-	3.6	-	22.0
35 mN/m	21.5		20.1	12.8
40 mN/m	18.0		15.0	5.4
45 mN/m	9.1		9.5	4.7
50 mN/m			7.2	

Table 3.6: *Summary of frequencies at which crossovers in the G'/G" versus ω plot appeared for all the samples at several surface pressures.*

to 35 mN/m, 40 mN/m and 45 mN/m induced a correspondent decrease of the crossover frequency to 14 rad/s, 5.4 rad/s, 4.7 rad/s, respectively (table 3.6). At highest pressure (45 mN/m) a longer cohesistance between viscous and elastic part of the shear modulus appeared to exist, within the range 3.5-6 rad/s. The Newtonian behaviour of the film was again measurable, as confirmed by the proportionality between G" and frequency in figure 3.26. Good matching between Newtonian model and experimental data was found from 25 mN/m to 35 mN/m. Above these pressures, the Newtonian model was no longer suitable to describe the system, as can be seen in figure 3.26. At 40 mN/m the model poorly reproduced the data yielding unphisically large value for the dynamic viscosity, while at 45 mN/m no fit was possible with this model. Interestingly, increasing the surface pressure by step of 5 mN/m appeared to induce quadrupling of viscosity (see table 3.7).

Aivlosin 50 μM-treated monolayer showed the crossover at 12.6 rad/s at the pressure 15 mN/m; the crossover shifted to 8.2 rad/s, 6.6 rad/s, and 3.6 rad/s by increasing surface pressure (table 3.6). Fits in figure 3.27 show that Newtonian model described less adequately the experimental data with Aivlosin than with other antibiotics. Nerverthless, viscosity of Aivlosin-treated film was calculated and ranged between 160 - 1200 μNs/m (see table 3.7). No defined relation between viscosity and surface pressure seemed to exist.

G' and G" versus Π The shear modulus can be usefully considered as a quantity depending on the surface pressure Π of the film, at fixed frequency. The plot, shown in figure 3.28 for two angular frequencies (8.23 rad/s, top panel, and 1.51 rad/s, bottom panel), allows one to clearly observe as the shear properties of the film change varying the surface pressure in a high- and low-frequency regime.

DPPC monolayer showed a G" always higher than G' at the lowest frequency, where, being the film exclusively Newtonian, the viscous regime is always dominant. At the highest frequency, increasing surface pressures allowed the elastic shear modulus G' to become more and more relevant, even without the crossover between the two regimes.

At both frequencies, the shear moduli G' and G" of the Azithromycin-treated film reasonably coincide with those of control.

At the highest frequency, Clarithromycin-treated film showed a viscous shear modulus G" diverging from control, with highest deviation (two times compared to the values of control) at high pressures; G' also showed higher values (about four times) compared to control. The crossover was also shifted to lower pressures, indicating an earlier transition (i.e., at lower pressures, be-

	Control (μNs/m)	Aivlosin (μNs/m)	Azithromycin (μNs/m)	Clarithromycin (μNs/m)
15 mN/m		149.1 ±10		
20 mN/m		427.0 ±15		
25 mN/m	44.3 ±4	577.8 ±11		45.0 ±4
30 mN/m	81.6 ±7	1141.0 ±7	58.7 ±6	161.0 ±7
35 mN/m	148.5 ±6		116.7 ±6	441.6 ±7
40 mN/m	290.9 ±7		223.3 ±7	1409.9 ±15
45 mN/m	572.1 ±9		445.4 ±9	-
50 mN/m			791.5 ±11	

Table 3.7: *Viscosities of DPPC monolayer calculated from the slope of the fitted range of G" in figures 3.24, 3.25, 3.26, 3.27.*

tween 35 mN/m and 40 mN/m) from viscous to elastic behaviour. At the lowest frequency an analogous divergence between G" of Clarithromycin-treated and control film was observable increasing the surface pressure, with G" higher in presence of antibiotic than control. G' was always higher with the drug, up to values four times compared to control.
Aivlosin-treated film showed higher rigidity behaviour than control. The effect of Aivlosin was partially analogous to Clarithromycin, with the difference that in this case Π is lower. At the highest frequency G" of Aivlosin and Clarithromycin were quite similar (a higher value for Aivlosin can be observed only comparing their highest pressures); G' was higher with Aivlosin and converged to Clarithromycin at 30 mN/m. In general, at high frequency the film exposed to Aivlosin showed G' comparable with G" except at 30 mN/m, unlike other samples in which one of the two regimes dominated depending on the pressure. At the lowest frequency G" was higher than Clarithromycin and converged to it at high pressure (30 mN/m). G' with Aivlosin was quite higher than Clarithromycin over all the pressures studied, with higher deviation at low pressures (value with Aivlosin four times compared to Clarithromycin), which gradually decreased with increasing pressure (value with Aivlosin 50% higher than Clarithromycin). Thus, at low frequency the film exposed to Aivlosin showed a rigid behaviour, being both G' and G" higher than control and Clarithromycin-treated film.

Master curves In this work the application of a time-pressure superposition on Langmuir phospholipid monolayers is proposed. The application of this method to Langmuir phospholipid systems can be justified assuming the validity of the free volume theory. Surface pressure was the only thermodynamic variable changed in these experiments. In such systems the surface pressure can play the role of temperature, as a highly compacted monolayer shows a limited conformational freedom, in analogy with a colder material.
G' and G" moduli showed in figures from 3.24 to 3.27 were used to build mas-

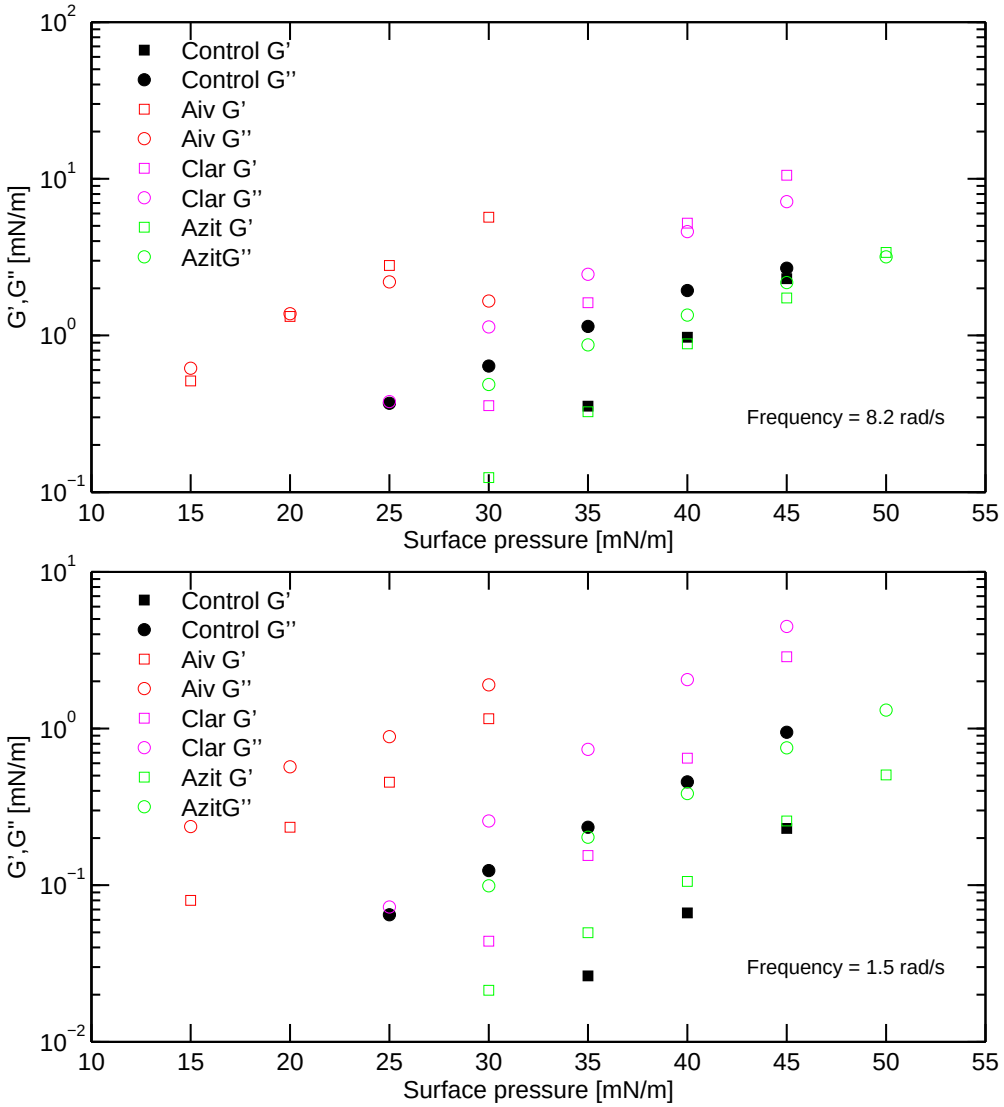

Figure 3.28: *Viscous and elastic shear moduli versus* Π*, in high (8.23 rad/s, top panel) and low (1.51 rad/s, bottom panel) frequency regime.*

ter curves. The moduli were shifted on the frequency axis, and only curves referred to pressure 30 mN/m were left unshifted. Control and Azithromycin-treated DPPC monolayers are plotted together in figure 3.29, top panel; Aivlosin- and Clarithromycin-treated monolayers are compared with control in figure 3.29, bottom panel. G' and G" were fitted by using the Maxwell model with Eqs. (1.45) and (1.46), respectively. The two fitting parameters (G_0 and τ) are reported in table 3.8. Experimental data showed a

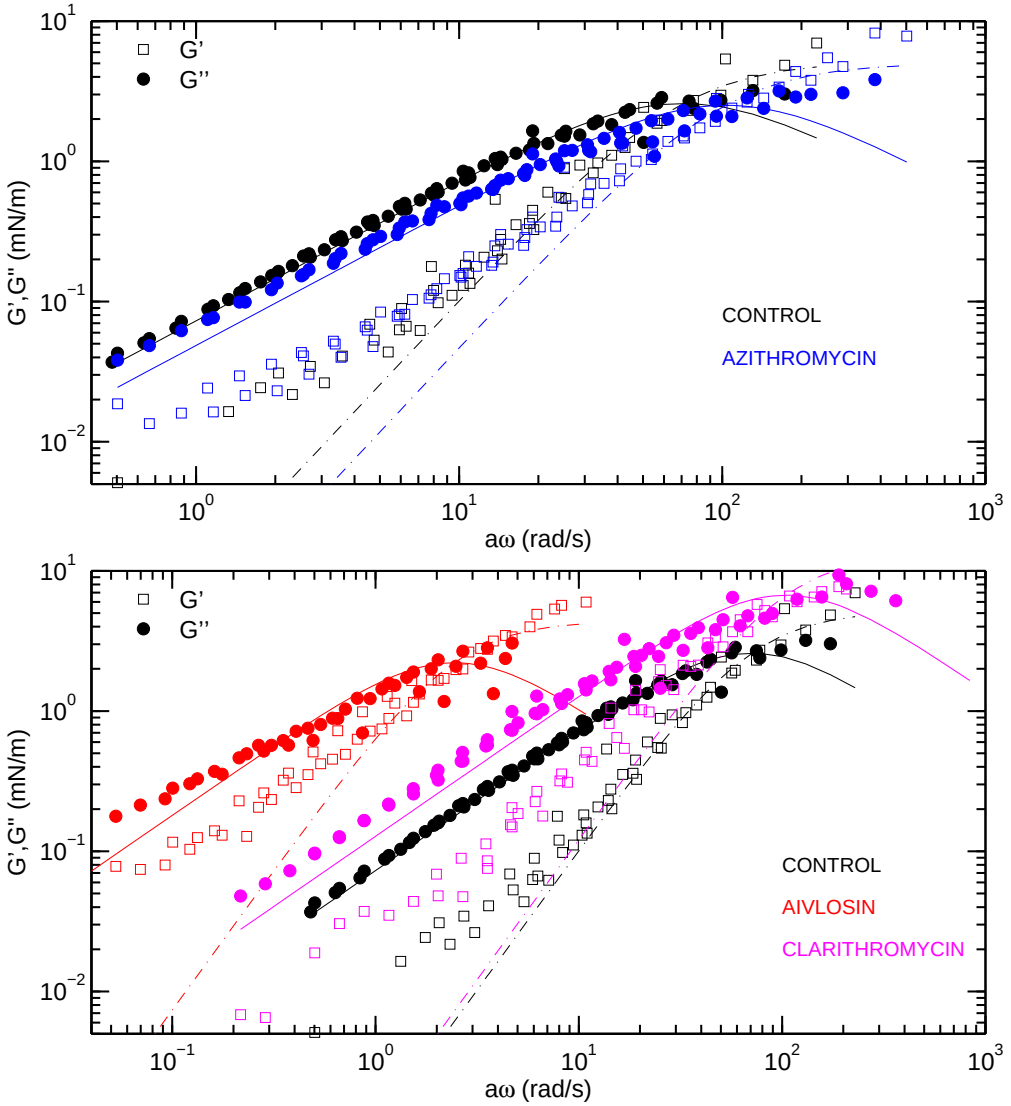

Figure 3.29: *Master curves of control and Azithromycin-treated DPPC monolayers (top panel); master curves of control, Clarithromycin- and Aivlosin-treated DPPC monolayers (bottom panel). Surface pressure 30 mN/m was chosen as reference.*

clear deviation from the Maxwell model in the low frequency region of G': as usual, in this range G' is very low compared to G" and not accurately detectable. Moreover, the higher values of experimental G' in comparison to model could be due to spurious effects (e.g., harmonic potential effects caused by the meniscus orientation in the channel).

The horizontal shift factors used to generate the master curves are shown in figure 3.30 as a function of the surface pressure. Their dimension is that of

a time, and an exponential dependence of a from pressure can be observed. This suggests an interpretation in terms of an activation law

$$a \propto exp(\frac{\Pi A_0}{k_B T}), \tag{3.4}$$

which finds justification by assuming that molecular lateral rearrangement occours only if a minimum free area A_0 is available for the molecules to exchange their position. The energy cost of this free area is obviously $\Pi \cdot A_0$ and therefore Eq. (3.4). Curves in figure 3.30 were fitted by Eq. (3.4); the A_0 parameters are reported in table 3.9.

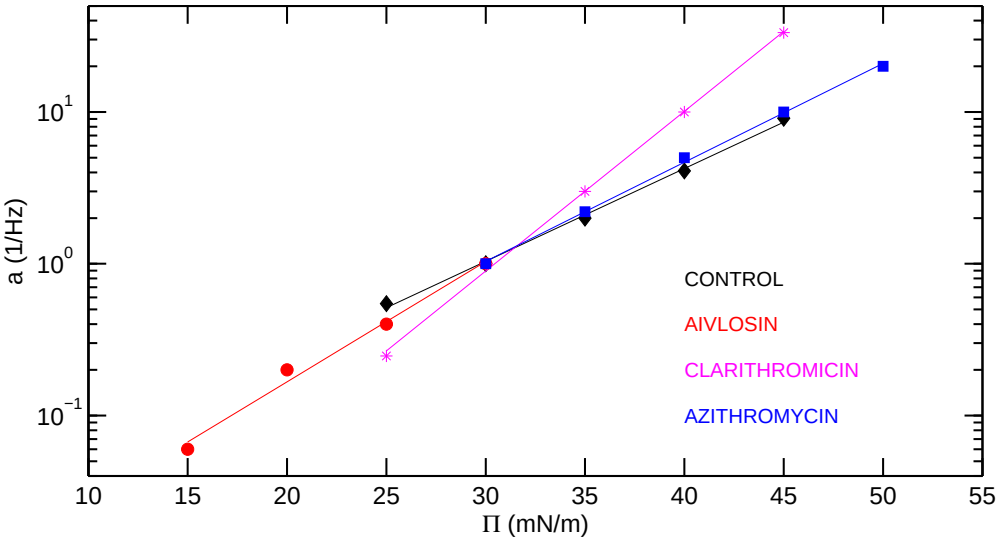

Figure 3.30: *Shift parameters* a *plotted versus surface pressure* Π.

	Control	Aivlosin	Azithromycin	Clarithromycin
G_0 (mN/m)	5.17	4.42	5.02	13.4
τ (s)	0.014	0.409	0.0097	0.0095

Table 3.8: *Parameters* G_0 *and* τ *deduced by fitting the Maxwell model to the master curves of figure 3.29. Values are given for* $\Pi = 30$ *mN/m.*

	Control	Aivlosin	Azithromycin	Clarithromycin
A_0 ($\AA^2$)	58	76	62	100

Table 3.9: *Fitting parameters A_0 of curves* a *versus surface pressure.*

3.4.2 DOPC monolayers

Rheological measurements performed on DOPC monolayers showed that, at room temperature, its behaviour is indistinguishable from that of water. Both amplitude stress-strain ratios and phase shifts were very similar to those of water (figure 3.31, left and right panels). As it was the case for DPPC, the experiments have been performed in the LC phase, which ranges from 20 mN/m to 35 mN/m.

The measurement of the shear modulus revealed that only the viscous part G" of the modulus was experimentally accessible, while the elastic part G' was too small to be detected. G" showed a linear dependence from the

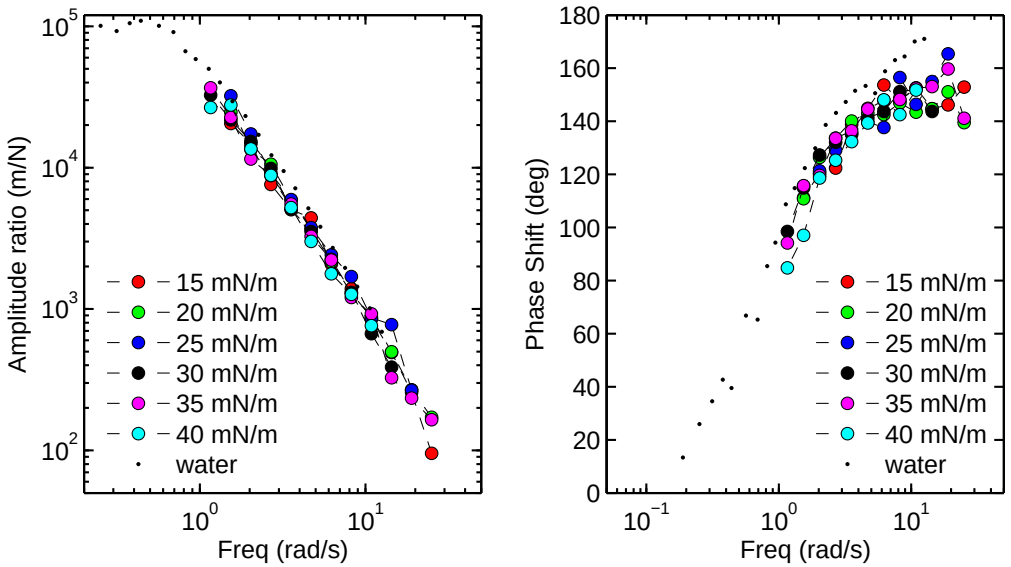

Figure 3.31: *Left panel: amplitude stress-strain ratios of DOPC film at several surface pressures. Right panel: phase shift of the film response to the perturbation at several film surface pressures. In both cases the behaviour was identical to that of water, regardless the compression of the film.*

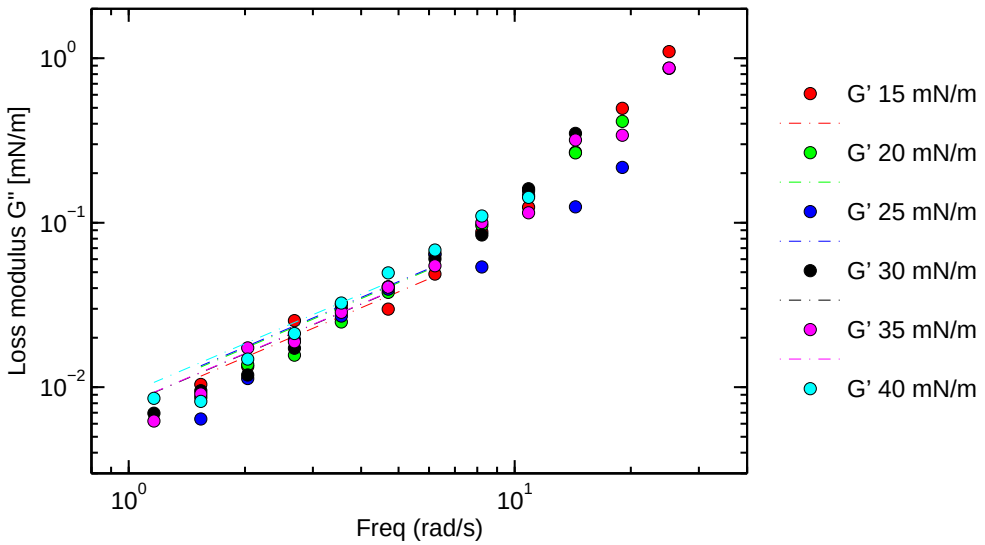

Figure 3.32: *Viscous shear modulus of DOPC film versus frequency. G" reveals the Newtonian character of the DOPC film, with a linear dependence from frequency.*

frequency (figure 3.32), confirming the film to be a Newtonian fluid with dominant viscosity and negligible elasticity over all the frequency range experimentally studied (1-20 rad/s). Mean viscosity was calculated 8.4 μNs/m.

3.5 Microfluidics of GUVs

Stabilization of flows in laminar regime and their addressing towards the outlet of the device were difficult, and they were achieved only for short periods (figure 3.33).

Often flows were not balanced in the main channel, with an asymmetric disposition (figure 3.34). As the drug concentration is related to the amount of drug solution inside the channel, this made the concentration unknown and not reliable.

Driving flows in the right direction was also difficult, and it was not achieved in some parts of the experiment. Mixing of drug and vesicle solutions took

place also before stopping, in the arms of the channel and not in the main channel.
Finally, observation of instantaneous drug effect on vesicles was difficult: stopping flows was not as rapid as desired.

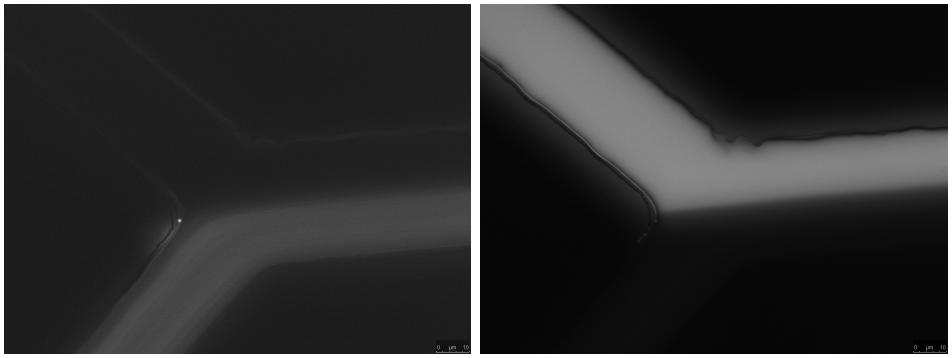

Figure 3.33: *Laminar flows of solutions containing DOPC GUVs and Clarithromycin. The solution with drug was mixed with fluorescein to enhance the fluorescent signal. Left panel: vesicle flow (on the bottom), visualized using a red filter. Right panel: drug flow (on the top), whose visibility was enhanced by a green filter. A 10x oil immersion objective was used.*

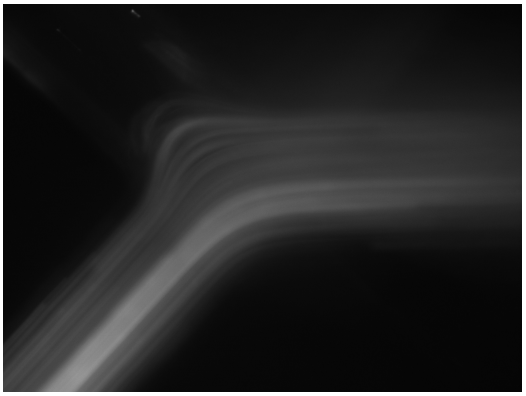

Figure 3.34: *Unbalanced flows in microfluidic channels.*

3.6 Thermotropic behaviour of DOPC bilayers

DSC measurements on DOPC multilayers allowed us to measure the temperature of the main transition ($L_\beta - L_\alpha$) of DOPC. It was found to be about -18°C, in good agreement with literature.

DSC measurements performed on DOPC multilayers treated with Aivlosin showed that no drug effect was detectable on the main transition, over a wide range of drug concentrations (5 μM, 50 μM, 500 μM). Transition peak temperatures were not modified within the experimental accuracy.

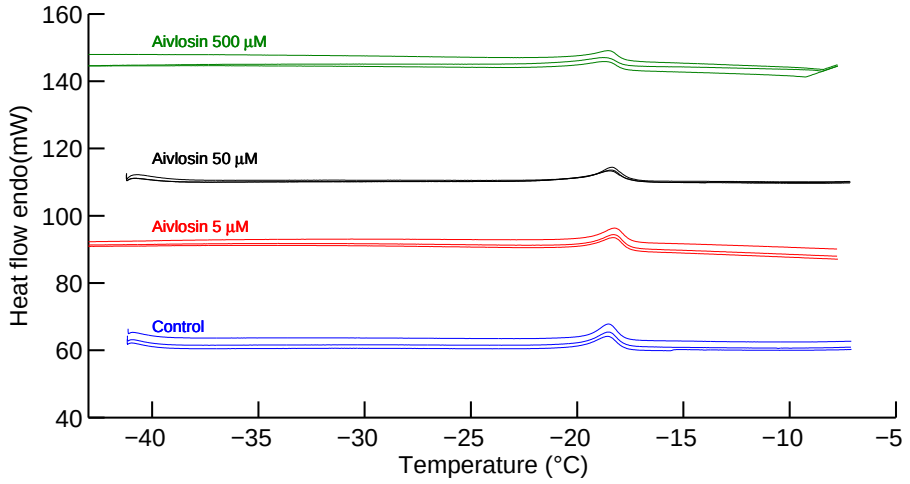

Figure 3.35: *Thermograms of pure and 5 μM, 50 μM,500 μM Aivlosin- treated DOPC multilayers. Main transition peak is visible at -18°C. No effect of drug is observable on its position.*

Chapter 4

Discussion

4.1 Morphological alterations of DOPC GUVs

Vesicles are very important in many different areas of science and technology. In basic research they serve as models for cell membranes and their fusion, transport studies and investigations of membrane proteins that can be reconstituted in vesicles (i.e. 'proteoliposomes'). They also serve as delivery vehicles for drugs, genetic material, enzymes and other (macro)molecules into living cells and through other hydrophobic barriers in pharmacology, medicine, genetic engineering, cosmetic industry and food industry [119]. They are also used as a support for semiconductor particles, in applications such as the photoconversion of solar energy [120].

The major force holding membrane lipid molecules together are the London-Van der Waals forces, which, in general, are attractive forces. These forces, together with the configurational entropy of the hydrogen bond networks, are involved along the acyl chains and are responsible for the organization of phospholipids into various lyotropic structures. In addition to this global organization, lipid bilayers can be characterized by their dynamic equilibrium thermal fluctuations including stretching and bending deformations.

Lipid:lipid interactions and mechanical properties of membranes, especially bending rigidity, can be affected by incorporation of amphiphilic molecules,

such as drug molecules, which perturbs the lipid packing. At low curvature, as in the case of GUVs, stochastic fluctuations should enhance penetration of exogenous molecules [121], making easy the study of the interaction between these molecules and phospholipid membranes.

4.1.1 Microfluidics

In previous work [69] addition of Azithromycin immediately triggered visible GUVs fluctuations and the vesicle started budding (the mechanism that controls the budding remains uncertain). In this work no budding was observed after addition of drugs, probably because the microscopy experimental setup did not allow to follow such fast vesicle dynamics.
To better understand the budding phenomenon and to test if it can be observed using also different drugs from Azithromycin, microfluidic channels were used. In particular, to monitor the instantaneous effect of mixing vesicles with drug, Clarithromycin was used given its higher effect on phospholipid membranes found in this work. Unfortunately, measurements of drug-vesicle mixing effect by microfluidics were performed unsuccessfully. Some technical problems did not allow to obtain the required information about the fast interactions between vesicle membrane and drug.

4.1.2 Antibiotics affect size distributions of GUVs

Vesicles not exposed to antibiotic showed spherical initial shape with sizes ranging from few μm to tens of μm. This demonstrated the efficiency of electroformation method in preparing μm-sized vesicles.
After time intervals (few hours, one day, two days), largest GUVs disappeared in samples treated with Azithromycin and Clarithromycin. It is likely that

these drugs, added outside GUVs, are unable to cross the membrane bilayer, thus preferentially insert into the outer membrane layer (at the phospholipid acyl chain/polar headgroup interface) and affect the bilayer couple [122]. Let us suppose a vesicle at given area, A, given volume, V, and given area difference between the two monolayers in the bilayer membrane area, ΔA. In the presence of Azithromycin or Clarithromycin, the increase in the area difference between the two leaflets of the bilayer, ΔA, without change of V, would lead to a rearrangement of the lipid molecules until destruction of the vesicle. Since fluctuations of the largest vesicles should lead to considerable movement of the membrane, a high proportion of foreign molecules should be entrapped in the external monolayer and affect the equilibrium of the entire bilayer, explaining the disappearance of the large vesicles [69].
The ineffectiveness on numerical density of large GUVs found with Aivlosin could be explained by a higher hydrophobicity of this antibiotic than Clarithromycin and Azithromycin. This would induce a high solubility in the hydrophobic region of phospholipid membrane: a relevant absorption could take place deep inside the membrane, close to the bilayer centre. This could not cause immediately a large area difference between the two leaflets of the vesicle bilayer, explaining the ineffectiveness of this drug on the size distributions at relatively low concentrations (50 and 150 μM). Very high concentrations of Aivlosin could induce instability of membranes, causing destruction of vesicles and reduction of number of large vesicles.

4.1.3 Clusters

The formation of clusters, triggered by very high concentrations of Aivlosin, could be explained by aggregates of separate vesicles or single vesicles which have exploded into smaller vesicles.
One example of force which would draw vesicles together could be depletion forces. The drug could cause very small (invisible nm-μm sized) vesicles to

bud off from larger vesicles, which then cause short range attraction by depletion forces between the larger vesicles which form the aggregates (very short range effect).
The vesicles could be exploding instead, and the large amounts of lipid present in some collections could be accounted for by the explosion of multilamellar vesicles.
Exploded vesicles in figure 3.8 could indicate some kind of attraction to the surface, which would be consistent with an attraction between vesicles leading to aggregates. On the other hand, the fact that these vesicles seem to have exploded suggests that the aggregates formed by explosion also.

4.1.4 Loss of contrast: a possible variation of the membrane permeability

When the untreated vesicles were sucked into a pipette and transferred to a different medium (glucose) in the observation chamber the stability of the optical contrast (in phase contrast microscopy) proved that the vesicles remained sealed after transfer.
A change of contrast is most likely caused by a variation of permeability of the GUVs phospholipid membrane. The existence of permeability is very interesting biologically, since breaching the bilayer would be dangerous to all kinds of cells.

4.2 Antibiotics affect flickering of GUVs

4.2.1 Triggering of thermal undulations

The absence of visible thermal undulations in untreated, just prepared vesicles suggests a surface tension that is probably responsible for the sphericity of the vesicles. As Angelova et al. [26], here the vesicles relaxed and fluctuated after a few hours. Partial lipid degradation, as already noted by Faucon and al. [110], may help to relax the vesicle tension.
The application of a small osmotic pressure appeared to be sufficient to trigger large-scale surface undulations in untreated vesicles. Undulations in vesicles containing 100 mM sucrose were typically triggered by an external concentration of 125 mM glucose without complete modification of the overall vesicle shape. The progressive evaporation of water in unsealed samples achieved a similar result.

4.2.2 Bending modulus of control vesicles

Thermal fluctuations of GUVs constitute a useful tool to quantify the bending elasticity of lipid bilayers. Fluctuation amplitudes being random variables, the precision is directly related to the number of analysed contours. Determination of the bending modulus κ requires several hundreds (up to thousands) vesicle contours to be digitized and analysed to obtain a significant statistics and a good accuracy.
The bending modulus κ of untreated DOPC GUVs was measured as 23.2 ± 10.5 k_BT, in excellent agreement with the literature [69] [109] [38]. It should be taken into consideration that differences in the mode of preparation of GUVs, in the temperature during the formation of GUVs, and in the composition of the buffer can all induce strong discrepancies in the measured elastic parameters. It is not clear whether the spreading of κ values within the same

sample resulted from the change in experimental methods or from differences in bilayer composition. Natural lipids are variable and even one-component lipids, mostly used as purchased, need not be completely pure. Additional impurities may enter during sample preparation, in particular from glues and other materials that seal the sample cell, or may appear gradually as a consequence of chemical degradation.

4.2.3 Decrease of κ and formation of groups of κ-values

In several cases the measured κ values formed groups clearly distinguished. The differences between the average κ values of adjacent groups were equal to the lowest values of κ. Therefore each group corresponds to a vesicle composed of a fixed number of bilayers. The lowest values can be attributed to single bilayer vesicles. Interestingly, Aivlosin- and Azithromycin-treated vesicles showed groups centred on values three times the fundamental κ, indicating the presence of triple bilayers. Untreated vesicles showed no groups further than the main one. In Clarithromycin-treated vesicles a short group was visible centred on κ value six times the lowest: this group was statistically negligible, given its low population.

The bending modulus κ decreased by 30% in presence of Azithromycin (15.9 $\pm$ 2.8 k_BT), indicating that insertion of the antibiotic in the DOPC bilayer reduces the energy requirements for thermal fluctuations. This decrease could be due to a modification of the spontaneous curvature and/or to a higher lateral diffusion of the constituents of the bilayer [38]. An even more accentuated reduction of the bending modulus was observed in presence of Clarithromycin, where κ was measured as 6.9 $\pm$ 3.2 k_BT. This could be due to a similar but more effective insertion of the Clarithromycin in the DOPC bilayer.

Aivlosin reduced two times the bending modulus (12.5 $\pm$ 4.3 k_BT and 14.8 $\pm$ 4.2 k_BT at 50 and 150 μM, respectively). The two concentrations induced substantially the same reduction, indicating that at concentrations higher

than 50 μM saturation is reached and no further effects are observable on vesicle membranes. The reduction of κ value could be again related to a reduced energy requirement for thermal fluctuations, induced by insertion of the antibiotic in the bilayer (even if in a deeper region than Azithromycin and Clarithromycin).
The same reduction effect on the bending modulus seems to be induced by insertion of antibiotics in the bilayer, regardless their exact position but more depending on the specific characteristics of the antibiotic molecule.

4.3 Effect of antibiotics on phospholipid monolayer rheology

4.3.1 Thermotropic phases of DPPC monolayer and compression modulus

Aivlosin and Clarithromycin did not affect the general phase bahaviour of DPPC monolayer: coexistance between LE-LC phase, transition to LC phase and solid (or untilted compressed) phase were all present in the Π-A isotherms measured in this work.
All the antibiotics studied in this work, except Aivlosin, did not affect the stability of the film outside the range of control sample (20-50 mN/m).
The increase of limit area in Clarithromycin-treated DPPC monolayer (from 49 $\AA^2$/molecule of control to 55 $\AA^2$/molecule) could be due to a kind of interaction between drug and phospholipid molecules, with formation of non-soluble drug-phospholipid complexes with higher area than phospholipid alone. In this case, assuming an average diameter for the drug of 1 nm, one can extrapolate a surface concentration of one drug molecule per 5-7 phospholipids units. This could be independently checked, e.g., by FT-IR

spectroscopy in ATR mode. The hypothesis of drug-phospholipid complexes was corroborated by the effect of Clarithromycin on the compressibility modulus of the DPPC monolayer. The peak was shifted about 10% to higher area/molecule, being this shift comparable with that of the limit area found in the corresponding isotherm.
Only Aivlosin reduced the pressure of the film (15-30 mN/m). The stability at lower pressures could be explained by some loss of sample due to formation of water-soluble macromolecular complexes between the higly hydrophobic Aivlosin and phospholipids. Thus, these complexes would seize part of phospholipids from the air/water interface. If the hypothesis of soluble Aivlosin-phospholipid complex was correct, it would indicate a higher hydrophobicity of Aivlosin compared to Clarithromycin. In the latter, in fact, the interaction between drug and phospholipid would not be strong enough to induce a solubilization in water of phospholipids; differently, another mechanism of interaction between Clarithromycin and phospholipids could exist. The limited variation of limit area induced by Aivlosin (47 $\AA^2$/molecule) in comparison with control could be the result of the equilibration of two opposite phenomena: the formation of macromolecular complexes described above would tend to reduce the limit area of the film, while a partial intercalation of Aivlosin in the monolayer would induce an increase of limit area. Finally, the increased maximun value of compression modulus (about 400 mN/m) could be related to a stiffening of the monolayer, as confirmed by the higher values of shear moduli found for Aivlosin-treated monolayers (see figure 3.28).

4.3.2 Rheology of pure DPPC monolayer

The reduction of the amplitude ratio is related to the compaction of the film when Π increases.
In the low frequency regime, where a phase shift between stress and strain about 90° was observable, the film behaved as a viscous system, regard-

less the surface pressure and, hence, its structure. High frequencies applied stresses induced a faster response in the film, that is a lower phase shift. The correlation rapidity of the two oscillations grew when the film become more compressed. At high compressions the film was more elastic than an expandend one: it ceased to behave as a viscous Newtonian fluid and became a elastic system.

The variation of the elastic G' and viscous G" part of shear modulus versus angular frequency showed well the visco-elasticity of the Langmuir films studied here. According to the frequency of the applied stress the monolayer responded differently, indicating the existence of a high-frequency regime in which the film behaves as a mainly elastic system, and a low-frequency regime in which the film is a mainly viscous system. The transition from one regime to the other is represented by the crossover between G' and G". Surface pressure influences this property as shown by the reduction of the crossover frequency; this is due to the rigidity of the film that increases with pressure: more rigid films are likely to show an elastic response to a stress in a wider frequency range than soft ones, shifting the onset of the viscous regime to lower frequencies.

The Newtonian model fitted well to the experimental data at low frequencies, comfirming that DPPC monolayer behaves as a Newtonian system in this frequency range. The validity of the Newtonian model held for higher frequency ranges at lowest surface pressures (0.5 - 5 rad/s at 25 mN/m), where the elastic modulus affected less the viscous behaviour of the film. As the surface pressure increased, the influence of G' on G" also increased and the fit had to be performed on a shorter frequency range.

4.3.3 Influence of antibiotics on the rheology of DPPC monolayer

Rhelogical measurements of DPPC monolayer showed that its shear moduli G' and G" undergo an increase of magnitude after exposition to Clar-

ithromycin 50 μM, indicating an increased compaction of the film. The monolayer treated with Clarithromycin showed Newtonian behaviour over almost all the pressures analysed (except the highest pressure), at low frequencies. Dynamic viscosities higher than control were obtained (5 mN/m increase of surface pressure induced quadruplication of viscosity): this indicated a very rapid loss of fluidity by the system with increase of surface pressure. Crossover positions reported in table 3.6 showed a general lowering of the onset frequency of the elastic regime: again, this could be related to a higher rigidity of this system. Here it has been phenomenologically demonstrated that it is possible to apply the time-pressure superposition to phospholipid systems, such as Langmuir phospholipid monolayers: surface pressure of the film played the role of temperature, giving appreciable results. Interesting conclusions were drew by application of the Maxwell model to master curves: although no variation of τ was found in comparison to control, G_0 was definitely larger in the Clarithromycin-treated film. Moreover, fitting the curve a versus Π with an activation law allowed us to calculate a A_0 parameter much higher (double) than control; if this parameter was associated to a conformational area to be moved to modify the conformation of the film, this last result would tie in with results from isotherms, indicating the formation of non-soluble drug-phospholipid complexes, with size larger than phospholipid alone. Being A_0 and the limit area from isotherm different, they could refer to different physical quantities.

Aivlosin 50 μM showed to have partially different effects on the DPPC monolayer in comparison to Clarithromycin. Comparable magnitudes of shear moduli G' and G" at high frequency (figure 3.28) indicated that the Aivlosin-treated monolayer is very visc-oelastic. At low frequency, the higher magnitudes of G' and G" in comparison to control showed a higher rigidity of the film exposed to Aivlosin, with a mainly viscous behaviour. Viscosities calculated by Newtonian model were about 15 times higher than control (where comparation was possible), indicating a very low fluidity of the Aivlosin-treated monolayer. The accuracy of Maxwell model in describing this film

was not very high. Neverthless, a rough estimation of the parameters G_0, τ, and A_0 was performed. This analysis indicated that the Aivlosin-treated monolayer is described by a much higher characteristic relaxation time τ than control: this could be related to the formation of macromolecular complexes differently arranged, in such a way to induce their intercalation in the monolayer. The intercalation of these large complexes in the monolayer would induce an increase of the rigidity of the monolayer. The value of A_0 in this case, slightly higher than control, could support the idea of a complex, even if from τ one would expect a value of A_0 much higher.

According to table 3.6 in the case of Azithromycin-treated DPPC monolayer, at corresponding surface pressures the crossover between viscous and elastic regime appeared at angular frequencies very similar to those of control DPPC monolayer; this indicated that the visco-elastic behaviour of the DPPC monolayer is unaffected by interaction with Azithromycin. Analogously, according to table 3.7, the dynamic viscosity was also comparable to that of control at corresponding surface pressures. Moreover, after exposition to Azithromycin, magnitudes of viscous and elastic shear moduli were found to be completely similar to control over all the surface pressures analysed, both at low and high angular frequency. Finally, both the Maxwell model and the horizontal shift factors a from master curves showed that Azithromycin-treated monolayer had characteristic values (G_0, τ and A_0) very close to those of control. According to the results presented above, Azithromycin showed to not influence the rheology of Langmuir DPPC monolayers. In particular, the unmodified values of τ and A_0 would indicate that no formation of drug-phospholipid complexes takes place. On the basis of this conclusion, the Π-A isotherm of DPPC monolayer treated with Azithromycin 35 μM should resemble that of pure DPPC, without modifications of limit area in the LC phase.

Interestingly, it can be noted as only the pure DPPC monolayer was correctly described by the Maxwell model. All monolayers exposed to the drugs showed a discrepancy with the model. This could be explained by the fact that the control monolayer is homogeneous and it can be really described

by a Maxwell model with one single characteristic time. On the contrary, the lack of adherence of experimental data to the model in the case of interaction with antibiotics could be due to the formation of complexes: this would reduce the homogeneity of the film, introducing more characteristic times than in the simple Maxwell model. Thus, it is likely that a generalized Maxwell model is suitable to describe such systems, containing two or several characteristic relaxation times.
From the τ's in table 3.8 a viscosity η can be obtained by considering that $\eta \propto G"/\omega \rightarrow \eta \propto G"\tau$. For each sample, this quantity appeared to be roughly consistent with viscosity in table 3.7, obtained fitting experimental data with Newtonian model. The two approaches show that Aivlosin induced a high increase of viscosity of the phospholipid monolayer: this could be related to the drug-phospholipid complexes intercalated in the monolayer that would increase both its rigidity and its viscosity.

4.3.4 Rheology of DOPC monolayer

As mentioned in section 1.4, DOPC at room temperature is well above its main transition temperature ($T_C = -18°C$), unlike DPPC that is still below its main transition ($T_C = +41°C$). As the experiments were performed at room conditions, the fluidity of DOPC was very high. This made its signal indistinguishable from that of water, within the experimental accuracy: the measured behaviour of DOPC was that of a Newtonian fluid, with viscous part of shear modulus proportional to the frequency over all the range experimentally analysed.
At room temperature DOPC is not a suitable system for ISR measurements, in which films with high shear modulus are required. An identical signal to that of water is obtained, with no information on the DOPC monolayer. Instead, good ISR measurements were obtained with DPPC films.

4.4 Possible mechanism of antibiotic-phospholipid interaction proposed

A possible mechanism of interaction between the macrolide antibiotics studied and phospholipid model membranes is proposed in the last part of this work.

Data in literature show that all three antibiotics studied here are characterized by a hydrophobic behaviour. Hydrophobic interaction could be the main interaction between antibiotics and phospholipids. However, despite the common hydrophobic character, the antibiotics studied showed different effects on phospholipid model membranes.

Aivlosin was found to be more hydrophobic than other macrolides [56], even if no previous work comparing the three antibiotics studied here. It is likely Aivlosin inserts deep inside the phospholipid bilayer, due to its high hydrophobic interaction with phospholipids. Recalling the ADE model, this would not induce an area difference between the inner and the outer leaflet of the bilayer, avoiding rupture or instability of larger GUVs. The very hydrophobic character of Aivlosin could induce the formation of macromolecular drug-phospholipid complexes, in interacting with phospholipid monolayers. These complexes could intercalate in the monolayer; successive solubilization in the bulk subphase could take place, as the formation of these complexes at the air-water interface would be an out-of-equilibrium process. In this case, phospholipids could arrange around the hydrophobic Aivlosin molecule with hydrophobic tails inwards and hydrophilic heads outwards, shielding the drug molecule from the water subphase and contemporarly favouring the transferring of the complex in the bulk subphase. The effect of Aivlosin-phospholipid complexes could be seizing part of the phospholipids from the monolayer and, during the intercalation into the monolayer, increasing its rigidity and viscosity.

Both Azithromycin and Clarithromycin could bind to the phospholipid bilayer, inserting into the outer membrane layer (at the phospholipid acyl

chain/polar headgroup interface). Neverthless, their hydrophobic interaction with phospholipid membrane would not be strong enough to allow them to penetrate deeper in the bilayer. Data in literature show that Clarithromycin has higher hydrophobic behaviour than its parent compound Erythromycin [123]; as Azithromycin and Erythromycin are quite similar compounds, it was suggested that Clarithromycin also has higher hydrophobicity than Azithromycin. Due to its hydrophobicity, Clarithromycin-phospholipid complexes would form: these complexes could be more strongly intercalated into the monolayer, without subsequent solubilization in the bulk subphase. Presumably, the lower hydrophobicity of Azithromycin avoids the formation of drug-phospholipid complexes.

Chapter 5

Conclusions and outlook

5.1 Results obtained in this work

Object of this study is the interaction of macrolide antibiotics with phospholipid model membranes. The properties investigated included the stability of some of their aggregation forms (Giant Unilamellar Vesicles, GUV) and the effects of the drugs on the mechanical moduli of the model membranes.
The techniques involved are video-image analysis for the GUVs and interfacial shear rheometry for the Langmuir monolayers.

5.1.1 Effect of Macrolide antibiotics on size distributions of GUVs

Azithromycin and Clarithromycin had analogous effect in reducing the fraction of larger GUVs and therefore reducing also the average size. Noteworthy, this effect was found to be at saturation even at the lowest concentration studied(50 μM). Thus, it could be useful to extend the present study to lower concentration. No saturation effect was observed here with Clarithromycin, where further reduction of mean size of GUVs took place at the highest concentration (150 μM).
Aivlosin did not induce any relevant effect on the fraction of GUVs at low

concentrations (from 50 μM 400 μM). Extremely high concentrations (800 μM and 4 mM) induced several effects on GUVs (clusters, occacional explosion and permeability variation).

5.1.2 Bending modulus of bilayers

Bending modulus κ of bilayer control vesicles was found to be in very good agreement with literature [69]. Macrolide antibiotics reduced, in some extent, this value, depending on the drug used: Clarithromycin showed the strongest effect among the drug studied here, with analogous effect between Aivlosin and Azithromycin. In some cases (Aivlosin and Azithromycin) a multimodal distribution of κ was found: multiple values of κ would be related to multilamellar vesicles, with the lowest κ referring to unilamellar vesicles.

5.1.3 Visco-elasticity of Langmuir phospholipid monolayers

Langmuir monolayers of DPPC showed a visco-elastic behaviour, very well described by the Maxwell model over all the frequency range experimentally analysed. This allowed us to plot master curves. Several properties of the monolayer were studied: compressibility modulus, dynamic viscosity, viscous G" and elastic G' shear moduli. The Newtonian model described adequately the system at low frequencies (viscous regime). All the properties studied were in very good agreement with literature.

5.1.4 Drug-phospholipid macromolecular complexes

Several results obtained in this work showed that macromolecular complexes are likely to form by interaction of antibiotic molecules with phospholipids.

The driving force leading to these complexes is likely to be the hydrophobicity of the antibiotic: this would cause the formation of complexes that can intercalate in the monolayer (Aivlosin and Clarithromycin). Several results showed that Azithromycin does not affect the shear properties of the DPPC monolayer, and, presumably, no drug-phospholipid complexes are formed with this antibiotic.

Visco-elasticity of monolayer was preserved after interaction with antibiotics. Nerverthless, discrepancies between data and the Maxwell model appeared by interaction with Azithromycin, Clarithromycin, and Aivlosin (in increasing effect order). To take into account the possible structural inhomogeneity of the monolayer exposed to the drug, a more generalized model could be used, characterized by a distribution of relaxation times τ and instantaneous moduli G_0.

Bibliography

[1] McConnell, H.M., Watts, T.H., Weis, R.M., Brian, A.A., Supported planar membranes in studies of cell-cell recognition in the immune system, Biochim. Biophys. Acta 864 (1986) 95-106.

[2] Thompson, N.L., Palmer, A.G., Model cell membranes on planar substrates, Comments Mol. Cell. Biophys. 5 (1988) 39-56.

[3] Sackmann, E., Supported membranes: scientific and practical applications,Science 271 (1996) 43-48.

[4] Seydel, J.K., Wiese, M. (Eds.), Drug-Membrane Interactions, Wiley-VCH, Weinheim, 2002.

[5] Seydel J.K., Coats E.A., Cordes H.P., Wiese M., Drug membrane interaction and the importance for drug transport, distribution, accumulation, efficacy and resistance, Arch. Pharm. 327 (1994) 601610.

[6] Helfrich, W., Elastic properties of lipid bilayers: theory and possible experiments, Z Naturforsch C 28 (1973) 693-703.

[7] Helfrich, W., and Servuss R. M., Undulations, steric interaction and cohesion of fuid membranes, Nuovo Cimento D 3 (1984) 137-151.

[8] Yoon, Y.Z., Hale, J.P., Petrov, P.G., and Cicuta, P., Mechanical properties of ternary lipid membranes near a liquidliquid phase separation boundary, J. Phys.: Condens. Matter 22 (2010) 062-101.

[9] Pecreaux J., Dobereiner H. G., Prost J., Joanny J. F. and Bassereau P., Refined contour analysis of giant unilamellar vesicles, Eur. Phys. J. E 13 (2004) 27790.

[10] Betz, T., Lenz, M., Joanny, J-F. and Sykes, C., Atp-dependent mechanics of red blood cells, Proc. Natl. Acad. Sci., 106 (2009) 15312-15317.

[11] Voet, D., Voet, J.G., Biochemistry, Wiley, 1995.

[12] University of Florida Agricultural and Biological Engineering, Web site of David P. Chynoweth MSPH, Ph.D.

[13] Avanti Polar Lipids website.

[14] Berg, J.M., Tymoczko, J.L., Stryer, L., Biochemistry, W. H. Freeman and Co., New York (U.S.A.), 2002.

[15] Zachowski, A., Devaux, P.F., Transmembrane movements of lipids, Experientia, 46 (1990) 644656.

[16] http://www.colorado.edu/intphys/Class/IPHY3730/image/membrane.jpg.

[17] Cullis, P.R., Hope, M.J., Tilcock, C.P.S., Lipid Polymorphism and the Roles of Lipids in Membranes, Chemistry and Physics of Lipids, 40 (1986) 127-144.

[18] de Gennes, P.G. (1974) The Physics of Liquid Crystals, Oxford University Press, Oxford.

[19] Luzzati, V., Biological Membranes (Chapman, D., ed.), vol. 1, pp. 71-123, (1968) Academic Press, London.

[20] Lewis, B.A., Engelman, D.M., Lipid Bilayer Thickness Varies Linearly with Acyl Chain Length in Fluid Phosphatidylcholine Vesicles, J. Mol. Biol., 166 (1983) 211-217.

[21] Bangham, A.D., Home, R. W., J. Mol. Biol. 8, (1964) 660-668.

[22] Papahadjopoulos, D. (ed.), Ann. N.Y. Acad. Sci. 308, (1978) 1-412.

[23] Reusch, W., Virtual Textbook of Organic Chemistry, Michigan State university, 1999.

[24] Angelova, M.I., Dimitrov, D.S., Liposome electroformation, Faraday Discuss. Chem. Soc., 81 (1986) 303311.

[25] Needham, D., Evans, E., Structure and mechanical properties of giant lipid (dmpc) vesicles bilayers from 20c below to 10c above the liquid crystalcrystalline phase transition at 24c, Biochemistry, 27 (1988) 8261-8269.

[26] Angelova, M.I., Soleau, S., Meleard, Ph., Faucon, J.F., Bothorel, P., Preparation of giant vesicles by external ac electric fields. Kinetics and applications. Progr. Colloid Polym. Sci., 89 (1992) 127-131.

[27] Montes, L.R., Alonso, A., Goni, F.M., Bagatolli, L.A., Giant unilamellar vesicles electroformed from native membranes and organic lipid mixtures under physiological conditions, Biophys. J., 93 (2007) 35483554.

[28] Hub, H.H., Zimmermann, U., Ringsdorf, H., Preparation of large unilamellar vesicles, FEBS Lett., 140 (1982) 254256.

[29] Baumgart, T., Hammond, A.T., Sengupta, P., Hess, S.T., Holowka, D.A., Baird, B.A., Proc. Natl. Acad. Sci. U.S.A., 104 (2007) 31653170.

[30] Holowka, D., Baird, B., Structural studies on the membrane-bound immunoglobulin E-receptor complex. 1. Characterization of large plasma membrane vesicles from rat basophilic leukemia cells and insertion of amphipathic fluorescent probes, Biochemistry, 22 (1983) 34663474.

[31] Shimanouchi, T., Umakoshi, H., Kuboi, R., In Giant Vesicles, Walde, P., Luisi, P. L., Eds., John Wiley Sons: New York, 2000; pp 369-377.

[32] Kuroiwa, T., Nakajima, M., Sato, S, Mukataka, S., Ichikawa, S., Maku (Membrane) 32 (2007) 229233.

[33] University of Texas, Houston Medicine website, http://www.uth.tmc.edu/med/comm/alumniMag/2007-Fall/articles/cover-00e-heart.html.

[34] V.I. Troitsky, Methods of deposition of molecular organized thin films.

[35] Ma, G., Allen, H.C., DPPC Langmuir Monolayer at the Air-Water Interface: Probing the Tail and Head Groups by Vibrational Sum Frequency Generation Spectroscopy, Langmuir, 22 (2006) 5341-5349.

[36] Kaganer, V.M., Structure and phase transitions in Langmuir monolayers, Reviews of Modern Physics, Vol. 71, No. 3, 1999.

[37] KSV INSTRUMENTS LTD, Application note, Langmuir and Langmuir-Blodgett Films: WHAT and HOW ?

[38] Rawicz W, Olbrich KC, McIntosh T, Needham D, Evans E., Effect of chain length and unsaturation on elasticity of lipid bilayers, Biophys. J., 79 (2000) 32839.

[39] Berg, H.C., Random walks in biology (Extended Paperback ed.). Princeton, N.J: Princeton University Press (1993).

[40] Tenchov, B., Koynova, R., Rapp, G., New Ordered Metastable Phases between the Gel and Subgel Phases in Hydrated Phospholipids, Bioph. J., 80 (2001) 18731890

[41] Janiak, M.J., Small, D.M., Shipley, G.G., Nature of the thermal pretransition of synthetic phospholipids: dimyristoyl- and dipalmitoyllecithin, Biochemistry, 15 (1976) 45754580.

[42] H.W. Meyer et al., Hydration of DMPC and DPPC at 4°C produces a novel subgel phase with convexconcave bilayer curvatures, Chemistry and Physics of Lipids, 105 (2000) 149166.

[43] Laggner, P., Nonequilibrium phenomena in lipid membrane phase transitions, Colloque C1 (supplement au Journal de Physique 11), 3 (1993).

[44] Leonenko,Z.V., Finot, E., Ma, H., Dahms, T.E.S., Cramb, D.T., Investigation of Temperature-Induced Phase Transitions in DOPC and DPPC Phospholipid Bilayers Using Temperature-Controlled Scanning Force Microscopy, Bioph. J., 86 (2004) 37833793.

[45] Dr. Silvius, J.R., Thermotropic Phase Transitions of Pure Lipids in Model Membranes and Their Modifications by Membrane Proteins, *Lipid-Protein Interactions*, John Wiley Sons, Inc., New York, 1982.

[46] Dobereiner, H.G., Evans, E., Kraus, M., Seifert, U., Wortis, M., Mapping vesicle shapes into the phase diagram: A comparison of experiment and theory, Phys. Rev. E 55 (1997) 4458-4474.

[47] Jorgensen, K., Ipsen, J. H., Mouritsen, O. G., Zuckermann, M. J., The effect of anaesthetics on the dynamic heterogeneity of lipid membranes. Chem. Phys. Lipids 65 (1993) 205216.

[48] Jorgensen, K., Ipsen, J. H., Mouritsen, O. G., Bennett, D., Zuckermann, M. J., The effects of density fluctuations on the partitioning of foreign molecules into lipid bilayers: application to anaesthetics and insecticides, Biochim. Biophys. Acta, 1067 (1991) 241253.

[49] Wenz, J. J., Barrantes, F. J.. Steroid structural requirements for stabilizing or disrupting lipid domains. Biochemistry 42 (2003) 1426714276.

[50] Agasosler, A.V., Tungodden, L.M., Cejka, D.,Bakstad, E., Sydnes, L.K., Holmsen H., Chlorpromazine-induced increase in dipalmitoylphosphatidylserine surface area in monolayers at room temperature. Biochem. Pharmacol. 61 (2001) 817-825.

[51] Saint-Laurent, A., Boudreau, N., Lariviere, D., Legault, J., Gaudreault, R.C., Auger, M., Membrane interactions of a new class of anticancer agents derived from arylchloroethylurea: a FTIR spectroscopic study. Chem. Phys. Lipids 111 (2001) 163 175.

[52] Mingeot-Leclercq, M.P., Tulkens, P.M., Aminoglycosides: nephrotoxicity. Antimicrob. Agents Chemother. 43 (1999) 1003-1012

[53] A. Schanck, M. P. Mingeot-Leclercq, P. M. Tulkens, D. Carrier, I. C. Smith, and H. C. Jarrell. Interactions of aminoglycoside antibiotics with phospholipids. A deuterium nuclear magnetic resonance study. Chem. Phys. Lipids 62 (1992) 153163.

[54] D. Tyteca, A. Schanck, Y. F. Dufrene, M. Deleu, P. J. Courtoy, P. M. Tulkens, and M. P. Mingeot-Leclercq. The macrolide antibiotic azithromycin interacts with lipids and affects membrane organization and fluidity: studies on Langmuir-Blodgett monolayers, liposomes and J774 macrophages. J. Membr. Biol. 192 (2003) 203215.

[55] G. Kaiser, Protein synthesis inhibitors: macrolides mechanism of action animation. Classification of agents, The Community College of Baltimore County, Retrieved on July 31, 2009.

[56] Stuart, A.D., Brown, T.D.K., Imrie, G., Tasker, J.B., Mockett, A.P.A., Intra-cellular accumulation and trans-epithelial transport of aivlosin, tylosin and tilmicosin, The Pig Journal, 60 (2007) 2635.

[57] Eco Animal Health website, http://www.ecoanimalhealth.com/.

[58] Personal communication, Dr David Brown, Dept of Viriology, Cambridge University.

[59] Pagine Sanitarie, Health care network web site (http://www.paginesanitarie.com/euromedia/veterinari.nsf/0e5ded19dfd64caa41256d2e003cc6cc/06cb52d7ea6c6ae8c125763400381d8a?OpenDocument).

[60] http://www.rxlist.com/zithromax-drug.htm.

[61] U.S. Food and Drug Administration prescribing information.

[62] http://en.wikipedia.org/wiki/Azithromycin.

[63] http://www.rxlist.com/biaxin-drug.htm.

[64] U.S. Food and Drug Administration prescribing information.

[65] http://en.wikipedia.org/wiki/Clarithromycin.

[66] Tyteca, D., Der Smissen, P., Van Bambeke, F., Leys, K., Tulkens, P.M., Courtoy, P.J., Mingeot-Leclercq, M.-P., Azithromycin, a lysosomotropic antibiotic, impairs fluid-phase pinocytosis in cultured fibroblasts, Eur. J. Cell Bio., 80 (2001) 466 -478.

[67] Berquand, A., Fa, N., Dufrêne, Y.F., Mingeot-Leclercq, M.-P., Interaction of the Macrolide Antibiotic Azithromycin with Lipid Bilayers: Effect on Membrane Organization, Fluidity, and Permeability, Pharm. Res., Vol. 22, No. 3, 2005.

[68] Tyteca, D., Schanck, A., Dufrene, Y.F., Deleu, M., Courtoy, P.J., Tulkens, P.M., Mingeot-Leclercq, M.P., The Macrolide Antibiotic Azithromycin Interacts with Lipids and Affects Membrane Organization and Fluidity: Studies on Langmuir-Blodgett Monolayers, Liposomes and J774 Macrophages, J. Membrane Biol. 192 (2003) 203-215.

[69] Fa, N., Lins, L., Courtoy, P.J., Dufrêne, Y., Van Der Smissen, P., Brasseur, R., Tyteca, D., Mingeot-Leclercq, M.-P., Decrease of elastic moduli of DOPC bilayers induced by a macrolide antibiotic, azithromycin, Bioch. et Bioph. Acta, 1768 (2007) 18301838.

[70] Fa, N., Ronkart, S., Schanck, A., Deleu, M., Gaigneaux, A., Goormaghtigh, E., Mingeot-Leclercq, M.-P., Effect of the antibiotic azithromycin on thermotropic behavior of DOPC or DPPC bilayers, Chem. and Phys. of Lip., 144 (2006) 108116.

[71] Brochard, F., and Lennon, J. F., Frequency spectrum of the flicker phenomenon in erythrocytes, J. Physique, 36 (1975) 1035-1047.

[72] Bao, G., Suresh, S., Cell and molecular mechanics of biological materials, Nat Mater 2 (2003) 715725.

[73] Park, Y.K., Best, C.A., Badizadegan, K., Dasari, R.R., Feld, M.S., Kuriabova, T., Henle, M.L., Levine, A.J., Popescu, G., Measurement of red blood cell mechanics during morphological changes, PNAS 107, 15 (2010) 6731-6736.

[74] Popescu, G., Ikeda, T., Goda, K., Best-Popescu, C.A., Laposata, M., Manley, S., Dasari, R.R., Badizadegan, K., Feld, M.S., Optical Measurement of Cell Membrane Tension, PRL 97, 218101 (2006).

[75] Helfrich, W., Z. Naturforsch. 30c (1975) 841.

[76] Brochard, F., De Gennes, P. G., and Pfeuty, P., J. Physique 37 (1976) 1099.

[77] Zilker, A., Engelhardt, H. and Sackmann, E., Dynamic reflection interference contrast (RIC-) microscopy a new method to study surface excitations of cells and to measure membrane bending elasticmoduli, J. Phys. (Fr.). 48 (1987) 21392151.

[78] Evans, E.A., Structure and deformation properties of red blood cells: concepts and quantitative methods, Methods Enzymol., 173 (1989) 335.

[79] Hènon, S., Lenormand, G., Richert, A., and F. Gallet, A new determination of the shear modulus of the human erythrocyte membrane using optical tweezers, Biophys. J., 76 (1999) 11451151.

[80] Lee, W. G., Bang, H., Lee, J., Yun, H., Han, D. C., Combined microchannel-type erythrocyte deformability test with optical tweezers. I. Basic principles. J. Kor. Phys. Soc. 50 (2007) 1163.

[81] Zilker, A., Ziegler, M. and Sackmann E., Spectral analysis of erythrocyte flickering in the 0.34 mm1 regime by microinterferometry combined with fast image processing, Phys. Rev. A, 46 (1992) 79988001.

[82] Evans, J., Gratzer, W., Mohandas, N., Parker, K., and Sleep, J., Fluctuations of the red blood cell membrane: relation to mechanical properties and lack of ATP dependence, Biophys. J., 94 (2008) 41344144.

[83] Bo, L., Waugh, R.E., Determination of bilayer membrane bending stiffness by tether formation from giant, thin-walled vesicles, Biophys. J., 55 (1989) 509-517.

[84] Kummrow, M., Helfrich, W., Phys. Rev. A, Deformation of giant lipid vesicles by electric fields, 44 (1991) 8356.

[85] Farago, O., Pincus, P., Statistical mechanics of bilayer membrane with a fixed projected area, Cond. Mat. Stat. Mech., (2008).

[86] Deserno, M., Notes on Differential Geometry, (2004) p.35, http://www.cmu.edu/biolphys/deserno/Deserno_science.html.

[87] Milner, S.T., Safran, S.A., Dynamical fluctuations of droplets microemulsions and vesicles, Phys. Rew. A, 36 (1987) 4371-4379.

[88] Riley, K.F., Hobson, M.P. and Bence, S.J., Mathematical Methods for Physics and Engineering, Cambridge University Press, Cambridge (U.K.), 2nd edition, 2004.

[89] Seifert, U., Configurations of fluid membranes and vesicles, Adv. Phys. 46 (1997) 13137.

[90] Peterson, M.A., Shape dynamics of nearly spherical membrane bounded fluid cells, Mol. Cryst. Liq. Cryst., 127 (1985) 257.

[91] Yoon, Y.Z., Hong, H., Brown, A., Kim, D.C., Kang, D.J., Lew, V.L., Cicuta, P., Flickering Analysis of Erythrocyte Mechanical Properties: Dependence on Oxygenation Level, Cell Shape, and Hydration Level, Bioph. J., 97 (2009) 1606-1615.

[92] Brooks, C.F., Fuller, G.G., Frank, C.W., Robertson, C.R., An Interfacial Stress Rheometer To Study Rheological Transitions in Monolayers at the Air-Water Interface, Langmuir, 15 (1999) 2450-2459.

[93] Orsi, D., Cristofolini, L., Fontana, M.P., Equilibrium and out-of-equilibrium dynamics in a molecular layer of azopolymer floating on water studied by Interfacial Shear Rheology, Journal of Non-Crystalline Solids, article in press.

[94] Reynaert, S., Brooks, C.F., Moldenaers, P., Vermant, J., Fuller, G.G., Analysis of the magnetic rod interfacial stress rheometer, Journal of Rheology, 52 (2008) 261-285.

[95] Larson, R.G., The structure and rheology of complex fluids, Oxford University Press, New York, 1999.

[96] Ferry, J.D., Viscoelastic properties of polymers, 3rd ed., Wiley, New York.

[97] Nakagawa, Y., Itai, S., Yoshida, T., Nagai, T., Physicochemical properties and stability in the acidic solution of a new macrolide antibiotic, Clarithromycin, in comparison with Erythromycin, Chem. Pharm. Bull, 40 (1992) 725-728.

[98] Berndl, K., Kas, J., Lipowsky, R., Sackmann, E., Seifert, U., Shape Transformations of Giant Vesicles: Extreme Sensitivity to Bilayer Asymmetry, Europhys. Lett., 13 (1990) 659-664.

[99] Miao, L., Seifert, U., Wortis, M., Dobereiner, H.-G., Budding transitions of fluid-bilayer vesicles: The effect of area-difference elasticity, Phys. Rev. E 49 (1994) 5389, which contains additional references.

[100] Mathivet, L., Cribier, S., Devaux, P.F., Shape Change and Physical Properties of Giant Phospholipid Vesicles Prepared in the Presence of an AC Electric Field, Biophys. J. 70 (1996) 1112-1121.

[101] Angelova, M.I., Soléau, S., Méléard, Ph., Faucon, F., Bothorel, P., Progress in Colloid and Polymer Science, 89 (1992) 127-131.

[102] Shimanouchi, T., Umakoshi, H., Kuboi, R., Kinetic Study on Giant Vesicle Formation with Electroformation Method, Langmuir Letter, 25 (2009) 4835-4840.

[103] Borochov, N., Wachtel, E.J., Bach, D., Phase behavior of mixtures of cholesterol and saturated phosphatidylglycerols, Chemistry and Physics of Lipids 76 (1995) 85-92.

[104] Videira, R.A., Antunes-Madeira, M.C., Madeira, V.M., Biophysical perturbations induced by ethylazinphos in lipid membranes, Chem. Phys. Lipids 97 (1999) 139153.

[105] Whitesides, G.M., The origins and the future of microfluidics, Nature, 442 (2006) 368-373.

[106] Helfrich, W., Size distributions of vesicles: the role of the effective rigidity of membranes, J. Physique, 47 (1986) 321-329.

[107] Marsh, D., Handbook of Lipid Bilayers, CRC Press, Boca Raton, Florida, USA, 1990.

[108] Duwe, H.P., Sackmann, E., Bending elasticity and Thermal excitations of lipid bilayer vesicles: modulation by solutes, Physica A, 163 (1990) 410-428.

[109] Niggemann, G., Kummrow, M., Helfrich, W., The Bending Rigidity of Phosphatidylcholine Bilayers: Dependences on Experimental Method, Sample Cell Sealing and Temperature, J. Phys. II France, 5 (1995) 413-425.

[110] Faucon, J.F., Mitov, M.D., Méléard, P., Bivas, I., Bothorel, P., Bending elasticity and thermal fluctuations of lipid membranes. Theoretical and experimental requirements, J. Phys. France, 50 (1989) 2389-2414.

[111] Schneider, M.B., Jenkins, J.T., Webb, W. W., Thermal fluctuations of large quasi-spherical bimolecular phospholipid vesicles, J. Physique, 45 (1984) 1457-1472.

[112] Engelhardt, H., Duwe, H.P., Sackmann, E., Bilayer bending elasticity measured by Fourier analysis of thermally excited surface undulations of flaccid vesicles, J. Physique Lett., 46 (1985) L-395 - L-400.

[113] Adam, N.K., Proc. R. Soc. London, Ser. A 101, 516, 1922.

[114] Matyszewska, D., Bilewicz, R., DPPC monolayers as simple models of biological membranes for studies of interactions with perfluorinated compounds, Annales UMCS, Chemistry, vol. 63, Jan. 2008, pp. 201-210.

[115] Wustneck, R., Wustneck, N., Moser, B., Karageorgieva, V., Pison, U., Surface Dilatational Behavior of Pulmonary Surfactant Components Spread on the Surface of a Pendant Drop. 1. Dipalmitoyl Phosphatidylcholine and Surfactant Protein C, Langmuir, vol. 18, Feb. 2002, pp. 1119-1124.

[116] Kragel, J., Li, J.B., Miller, R., Bree, M., Kretzschmar, G., Mohwald, H., Surface viscoelasticity of phospholipid monolayers at the air/water interface, Colloid Polym. Sci., 274 (1996) 1183-1187.

[117] Ding, J., Warriner, H.E., Zasadzinski, J.A., Schwartz, D.K., Magnetic needle viscometer for Langmuir monolayers, Langmuir, 18 (2002) 2800-2806.

[118] Lucero Caro, A., Rodriguez Nino, M., Rodriguez Patino, J., The effect of pH on surface dilatational and shear properties of phospholipid monolayers, Colloids and Surfaces A: Physicochemical and Engineering Aspects, 327 (2008) 79-89.

[119] Gregoriadis, G.,(1984) Liposome Technology, CRC Press, Boca Raton, FL.

[120] Zhago, X.K., Baral, S., Rolandi, R., Fendler, J.H., J. Am. Chem. Soc., 110 (1988) 1012-1024.

[121] Lentz, B.R., McIntyre, G.F., Parks, D.J., Yates, J.C., Massenburg, D., Bilayer curvature and certain amphipaths promote poly(ethylene glycol)-induced fusion of dipalmitoylphosphatidylcholine unilamellar vesicles, Biochemistry, 31 (1992) 26432653.

[122] Svetina, S., Zeks, B., Membrane bending energy and shape determination of phospholipid vesicles and red blood cells, Eur. Biophys. J., 17 (1989) 101111.

[123] Goldman, R.C., Zakula, D., Flamm, R., Beyer, J., Capobianco, J., Tight Binding of Clarithromycin, Its 14-(R)-Hydroxy Metabolite, and Erythromycin to Helicobacter pylori Ribosomes, ANTIMICROBIAL AGENTS AND CHEMOTHERAPY, Vol. 38, No. 7, 1994, 1496-1500.

Acknowledgements

I would like to thank Prof. Luigi Cristofolini and Dr. Pietro Cicuta. This work was made possible thanks to their efforts, and they allowed me to live an extraordinary professional and personal experience, such as the period spent in Cambridge.

A hearty thank also to Aidan Brown, who have shared his work and ideas with me over all the duration of my work, making a decisive contribution to the success of this work.

Thanks also to Davide Orsi for his professional and human support during the experiments performed in Parma.

A special thank to Dr. David T.K. Brown for his scientific support regarding biological and pharmacological aspects of this work.

Thanks to all the members of the BSS group for the help received during the weekly group meetings and throughout my working days at the Cavendish Laboratory. Particular thank to Debjani Paul, for her kindness and helpfulness in preparing the microfluidics devices used in this work.

Finally, I would like to thank my family for the support received during all my university career. In every moment they believed in my abilities, helping me to overcome the difficult moments and sharing the joy for every small goal achieved.